Beyond patterning: *Hox* Genes Function in the Adult Mammalian Skeleton

by

Jane Song

A dissertation submitted in partial fulfillment
of the requirements for the degree of
Doctor of Philosophy
(Cellular and Molecular Biology)
in The University of Michigan
2020

Doctoral Committee:

Associate Professor Benjamin L. Allen, Co-Chair
Professor Deneen M. Wellik, Co-Chair
Assistant Professor Noriaki Ono
Associate Professor Jason R. Spence

Jane Song

janeys@umich.edu

ORCID iD: 0000-0002-2021-8184

DEDICATION

To my family, for their unconditional love and endless support. To my dad, for encouraging and inspiring the scientist in me. To my mom, for always believing in me. To my little brother, for being the best friend and always making me laugh. To my husband Jason, for being my rock and always being supportive of my career. To my son Aiden, for being my baby. To my best friends, Susan and Grace, for always being there when I need someone to talk to. And finally, to my best friends from graduate school, Martha and Molly, for making grad school bearable and sharing all the ups and downs going through this Ph.D. journey together.

ACKNOWLEDGEMENTS

First and foremost, I thank my Ph.D. mentor Deneen Wellik. You have taught me how to be a careful and rigorous scientist; I have grown so much. Thank you for pushing and motivating me so that I always discover a new and improved version of myself. The fierceness and dedication you bring to science is truly inspiring. Thank you for your encouragement and support.

To all the past and present members of the Wellik lab, thank you for creating an amazing lab environment. To Danielle, for pioneering the MSC work and always willing to help me through email whenever I have a question. To Kyriel, I enjoyed collaborating on the MSC project with you and I will fondly look back at our Friday morning chats with coffee about random things. To Steve, I really enjoyed being part of our desk neighbor trio with Kyriel. We motivated each other to work hard and I always appreciated your funny jokes and stories. To Leilani, your bright and warm personality always made my day better. Thank you for the all the bubble tea and coffee runs. To Lauren, I am so happy to have found another person to share my passion for cosmetics. Thank you for your contagious bubbly-ness. To Elise, for your encouragement and fun stories about the animals from your farm. To Julia, for allowing me to be your mentor and for your hard work and dedication. I treasure the friendship we have developed. To Emma, thank you for sticking around until the very end to help me with my project. To all the undergraduate researchers, Andrew,

Christina, Noah, and Ella thank you for your hard work. Thank you all for the great time and I wish you all the best in your endeavors.

To the members of my thesis committee, thank you for all the valuable feedback and guidance you have provided for me through my Ph.D. training. To Ben, it is not an exaggeration if I said that I would not be in science if it wasn't for you. Thank you for taking a chance and hiring me as a technician in your lab and teaching me all the basics to scientific research. I also thank you for providing space in your lab allowing me to finish my work when Deneen left for Wisconsin. I hold special meaning to finishing my Ph.D. in your lab (even though I'm just squatting). To Jason, for your positive demeanor and enthusiasm for this project. To Noriaki, for your calming presence and helpful advice for future experiments. To Daniel, for all your help and guidance in the MSC project.

To Sherry, thank you for all the help and support you have provided. I was able to solely focus on science because you took care of everything else for me. To Irene, thank you for teaching me all the basic lab techniques when I was starting in Ben's lab. I appreciated your patience and I cherish the friendship we have developed. I wish you both the best in your retirement.

Lab life would have been dull without my lab friends from the Spence lab. I enjoyed our occasional happy hours and appreciated your encouragement and bright spirits. To the CMB student body, thank you for the positive and collaborative environment you fostered. To the members of the Developmental Genetics meetings, thank you for the constructive feedback and general enthusiasm for my project.

To the Cellular and Molecular Biology faculty and staff, thank you for your support. Margarita, Pat, and Lauren thank you for all the help and support you have provided through the years and your willingness to help no matter how big or small the problem.

A special thank you to the Michigan Core facilities and staff: the flow cytometry core, the transgenic animal model core and the microscope and imaging analysis core. This research would not have been possible or successful without your assistance and expertise. Thank you for your help.

To all the researchers and staff in the orthopedic research laboratories at Michigan, I thank you for your support. To Christophe, thank you for always willing to help me with any bone-related questions, training me on all the equipment, and always sharing reagents. To Carol, for teaching me techniques, providing me with protocols, and generously allowing me to use the core's reagents to do my experiments. To Chris, Bonnie, and Ken thank you for all your technical support during the fracture surgeries.

To my funding sources, thank you for providing the financial support that made this work possible. Thank you to the National Institutes of Health R01 AR061402 awarded to Deneen Wellik. Thank you to the Tissue Engineering at Michigan (T32 DE00007057-40 & DE00007057-41) training grants for the outstanding training programs. To Rackham Graduate school, for the Pre-Candidate Graduate Student Research Grant and Travel Grants. Thank you to the American Society for Bone and Mineral Research (ASBMR) for granting me the Young Investigator Travel Award. And thank you to the Cellular and Molecular Biology program for the Warner Lambert Fellowship.

TABLE OF CONTENTS

LIST OF FIGURES

ABSTRACT

Hox genes encode transcription factors that play essential roles in the correct establishment of skeletal morphology of the axial and limb skeleton during embryonic development. Despite continuous expression throughout the life of an animal, *Hox* genes have largely been studied in the context of embryogenesis and there continues to be a dearth of information regarding their functional significance at adult stages after the skeleton has been established. Here, I have used *Hox11* as a model to investigate outstanding questions regarding *Hox* gene function in the adult mammalian skeleton.

Hox11 expression within the limb skeleton is restricted to the zeugopod of the forelimb (radius/ulna) and hindlimb (tibia/fibula). It is indispensable for the proper development of the zeugopod as the loss of *Hox11* function results in the complete malformation of those skeletal elements. In the adult, *Hox11* expression is exclusive to a progenitor-enriched mesenchymal stem/stromal cell (MSC) population in the adult bone. Lineage analysis revealed that the *Hox11*-expressing MSC population establishes during embryonic development, exhibits self-renewal, and gives rise to all mesenchymal lineages within the skeleton—osteoblasts, osteocytes, chondrocytes, and bone marrow adipocytes—throughout the life of an animal. While these studies provided information regarding the cellular contribution of *Hox*-expressing cells, they do not address whether *Hox* function is required at later stages. Continuing functions for *Hox* beyond embryonic development have been suggested by studies examining *Hox11* compound mutants (animals in which only one of the four paralogs is functional). *Hox11* compound mutants

develop normally, but skeletal growth defects begin to manifest at postnatal stages and adults are not able to execute proper fracture injury repair. However, results from these studies are complicated by the fact that three of the four *Hox11* alleles are absent during skeletal development, making it challenging to distinguish between embryonic and postnatal roles. Using a novel *Hoxd11* conditional allele to delete *Hox* function in a temporally and spatially regulated manner, I provide evidence that conditional loss of *Hox11* function in the adult skeleton results in the progressive replacement of normal lamellar bone with an abnormal woven bone-like matrix with highly disorganized collagen fibers. Lineage analyses of the *Hox*-expressing cells demonstrate that while the stem cell population is maintained, osteoblast differentiation is perturbed and osteocytes embedded in the abnormal matrix display abnormal morphology as well as differentiation defects. Collectively, this research provides strong genetic and functional evidence for a continued role for *Hox* genes in the adult skeleton by regulating the differentiation of regional *Hox*-expressing skeletal stem cells.

CHAPTER I

Introduction

Hox genes are patterning factors of the developing embryo

The *Hox* genes are a family of homeo-domain containing transcription factors that are best known for their role in providing axial positional information along the antero-posterior (AP) axis, from the hindbrain down to the tail end of a developing embryo. *Hox* genes are highly conserved across species and the cluster organization has also been conserved throughout evolution[1]. Tandem duplication within the cluster followed by multiple gene duplication events that occurred during evolution ultimately led to mammalians having a total of 39 *Hox* genes. These genes are divided among four chromosomal clusters (*Hox A-D*) and further sub-divided into 13 paralogous groups defined by sequence similarity and position within the cluster[2] (Figure 1.1). The paralogous groups are additionally clustered in anterior (*Hox1-4*), central (*Hox 5-8*), and posterior (*Hox9-13*) classes, mirroring their domains of expression and action, but also correlating with their sequence conservation in the homeodomain (HD).

Hox genes were first discovered in fruit flies, *Drosophila melanogaster*, as two gene clusters: the Antennapedia (ANT-C) and Bithorax (BX-C) complexes[3–5]. Genetic studies in *Drosophila melanogaster* demonstrated that *Hox* genes play a key role in

assigning distinct morphological identities to each body segment[6]. Pioneering work by E.B. Lewis demonstrated that mutations to one end of the BX-C complex resulted in abnormal morphology of anterior structures while mutations to the other end of the BX-C complex affected posterior structures of larvae[3]. Molecular cloning of the BX-C complex and subsequent expression studies revealed that *Hox* genes are expressed in a region-specific manner along the head-to-tail axis[7,8]. Results from these studies also unveiled that

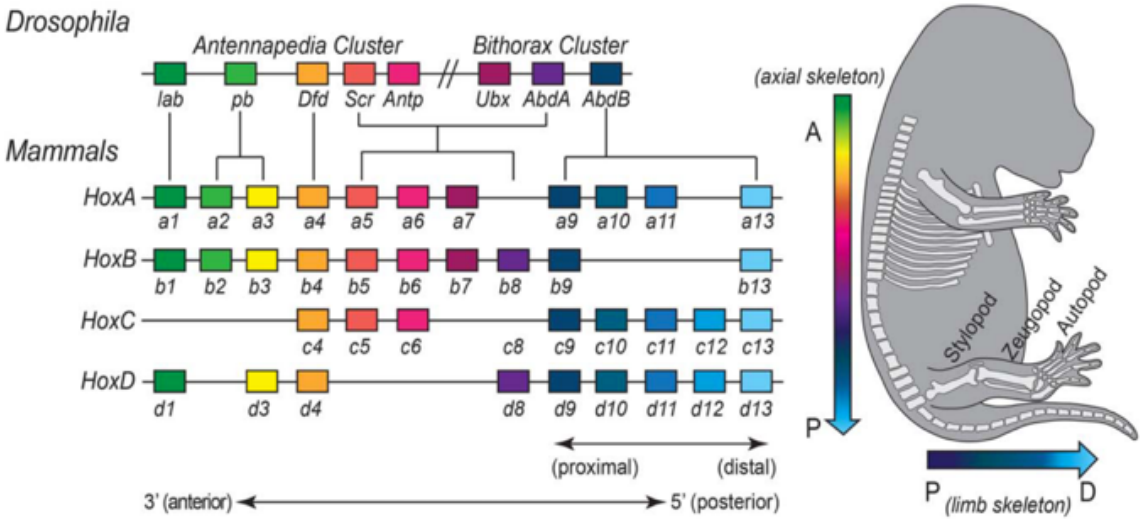

Figure 1.1. The Hox complex and its regional expression pattern along the AP and PD axis. A cartoon schematic of the Hox clusters in Drosophila and mammals. Hox genes that belong to the same paralogous group are color coded and the gradient scale along the AP and PD axis represent the nested, region-specific expression pattern of the paralogous groups along those axes (Figure from Rux, 2016 [9]).

the physiological order of the *Hox* gene cluster along the chromosome closely coincides with their expression pattern along the head-to-tail axis, referred to as spatial collinearity[7,8]. This collinear expression of *Hox* genes is suggested to be regulated by the combination of distance, enhancer tropism, and competition for promoters upstream of the clusters that is refined primarily through a sequence-specific mechanism assisting in establishing a

preferential interaction[10]. During early stages of development, *Hox* genes are kept globally silent and then progressively become activated from the anterior to posterior end of the embryo[11]. As development progresses, *Hox* genes establish an expression pattern along the anteroposterior (AP) axis with an anterior limit creating some overlapping expression between *Hox* genes that are adjacent to each other[12–15]. As a result, each region along the AP axis expresses a unique combination of *Hox* genes referred to as "*Hox* code" which correlates with changes of the vertebral morphology[12–15]. Therefore, the skeletal organization and morphology is regulated by the genomic topography of *Hox* genes[16,17].

Hox genes organize the correct skeletal morphology in the axial and limb skeleton axes

Coinciding with their region-specific expression pattern along the AP axis, *Hox* genes exhibit regionally restricted functions as well. Mutations to a particular paralogous group of *Hox* genes specifically affect the region those genes are expressed in. The high sequence similarity among *Hox* genes within the same paralogous group results in functional redundancy[18–21]. Mutations in a single *Hox* paralog generally leads to a mild or absence of phenotype. Therefore, in order for a discernable phenotype to manifest, multiple or all members from a paralog need to be mutated[18,19,28–33,20–27]. Loss-of-function (LOF) mutations of *Hox* genes result in what is classically referred to as anterior homeotic transformation. This is when the body segment where a particular paralogous group is expressed in is abnormally converted into the next most anterior segment[3,18–20,30]. For example, *Hox10* is expressed within the lumbar region of the axial skeleton. Upon loss-of-function mutations to the *Hox10* paralogous group, the lumbar region usually devoid of floating rib structures now assume the phenotype of the thoractic region with rib structures

protruding from the lumbar vertebrae[20] (Fig 1.2, far-left panel). Similarly, the loss of *Hox11* paralogs expressed in the sacral region, leads to vertebrae that display the same morphological characteristics of those in the lumbar region[20] (Fig 1.2, far-right panel).

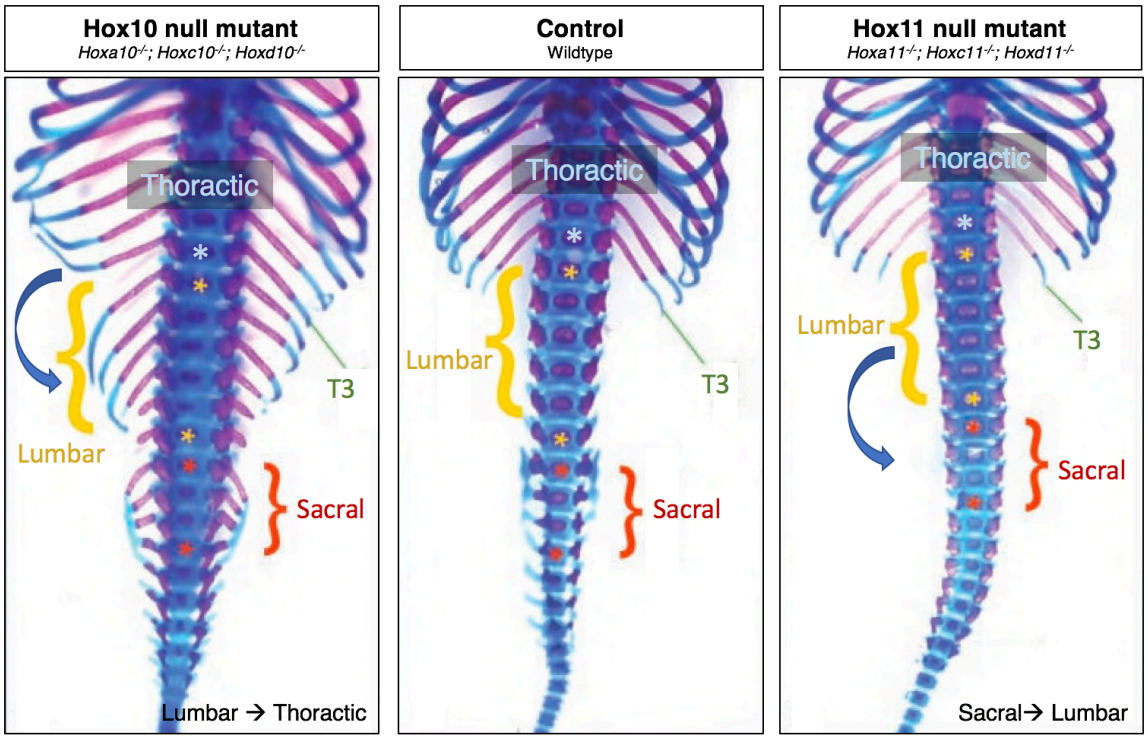

Figure 1.2. *Hox* gene loss-of-function lead to homeotic transformation of axial skeletal morphology. (A) LOF mutation in the *Hox10* paralogous group results in the transformation of the lumbar vertebrae to adopt the thoracic region phenotype identifiable by the floating rib structures (far left panel). *Hox11* LOF leads to the sacral vertebrae to assume lumbar phenotype (far right panel). T13 indicates last rib structure within the thoractic region. (Figure adapted from Wellik, 2003[20]).

In addition to their role in axial skeleton development, the posterior *Hox* genes (*Hox9* through *Hox13*) were co-opted to pattern the proximodistal (PD) axis of the appendicular limb skeleton. The vertebrate limb skeleton is subdivided into three regions along the PD axis; stylopod (humerus and femur), zeugopod (radius/unla and tibia/fibula), and autopod (digits of the forelimb and hindlimb)[20,25–27] (Fig 1.3A). In the early limb bud,

the 5' *Hox* genes are progressively expressed in distally-restricted but overlapping domains[34–37]. As the cartilage anlage for the limb skeleton elements appears, the expression domains of the *Hox* paralogs resolve such that *Hox9* and *Hox10* genes are primarily restricted to the stylopod, *Hox11* genes to the zeugopod, and the *Hox13* genes to the autopod[20,25–27] (Fig 1.3A). Of note, the posterior *HoxA* and *HoxD* clusters are expressed in both the forelimb and hindlimb, whereas the *HoxC* cluster is additionally

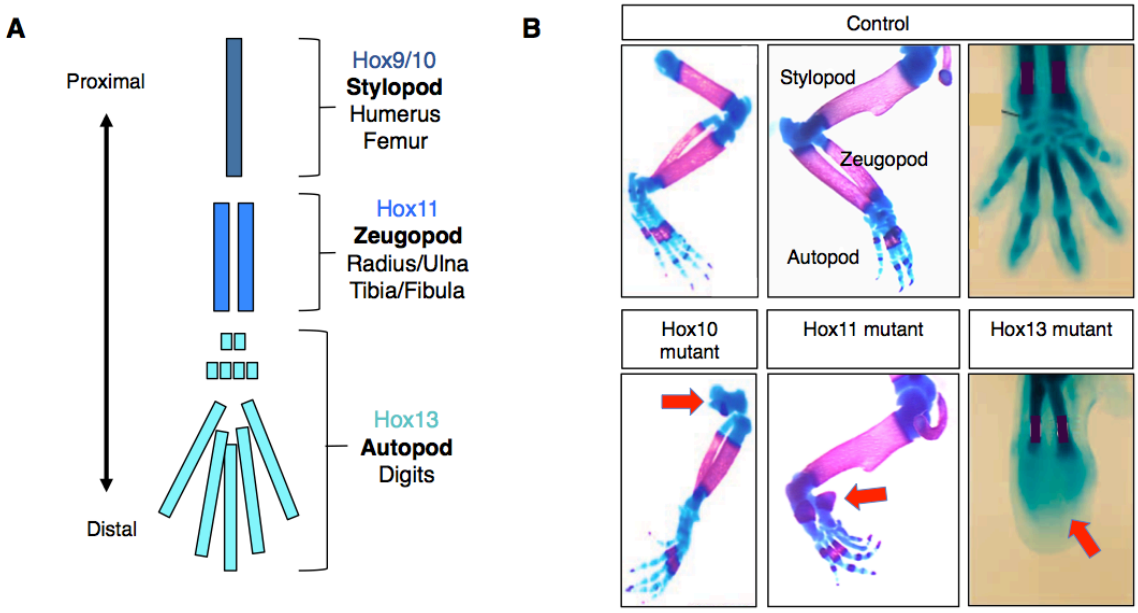

Figure 1.3. Posterior *Hox* genes display nested expression pattern along PD axis and mutations lead to region-specific defects in skeletal morphology. (A) Similar to the axial skeleton, the posterior *Hox* genes are expressed regionally along the PD axis of the vertebrate limb. **(B)** Loss-of-function mutations to posterior *Hox* genes within the limb lead to regional malformation of the appendicular skeleton. *Hox10* mutants (Hoxa10$^{-/-}$;Hoxc10$^{-/-}$;Hoxd10$^{-/-}$) exhibit stylopod-specific malformation, *Hox11* mutants (Hoxa11$^{-/-}$;Hoxc11$^{-/-}$; Hoxd11$^{-/-}$) have zeugopod-specific defects, and *Hox13* mutants (Hoxa13$^{-/-}$; Hoxd13$^{-/-}$) show agenesis of the autopod (Figure adapted from Wellik and Capecchi, 2003 [20] and Fromental-Ramain *et al.,* 1996 [26]).

expressed in the hindlimb[20,25,38]. Similar to the axial skeleton, specific loss-of-function mutations to particular *Hox* paralogs lead to severe defects in skeletal morphology.

However, unlike the axial skeleton where loss of *Hox* function results in homeotic transformation of vertebral morphology, in the limb skeleton, *Hox* mutants display near-complete regional agenesis of the skeleton. For example, *Hox11* triple mutants (Hoxa11$^{-/-}$; Hoxd11$^{-/-}$;Hoxc11$^{-/-}$) exhibit a severe malformation of the zeugopod skeleton while the stylopod and autopod region mostly develop normally[20,25] (Fig 1.3B). Similar regional defects in patterning are observed in *Hox9* or *Hox10* paralog mutants, and a complete loss of the autopod region is observed in *Hox13* null mutants[26,27] (Fig 1.3B).

Hox gene function is required in early limb formation as the loss of all paralogs in the *Hox9* group leads to the loss of *Shh* expression in the ZPA resulting in severe malformation of posterior skeletal elements[39]. Additionally, the *Hox5* paralogous groups is necessary for proper anterior forelimb development as the loss of all three *Hox5* genes result in anterior forelimb skeletal defects attributed to the de-repression of *Shh* expression[40]. Large deletions of the entire *HoxA* and *HoxD* clusters lead to truncation of the skeletal elements as well as abnormality in the specification of the correct number of skeletal anlages in the developing limb[41]. Taken together, the requirement for *Hox* activity in the proper formation and development of the appendicular skeleton is indisputable. However, despite ample evidence establishing the importance of *Hox* genes in skeletal patterning, there is a lack of understanding regarding the specific cellular and molecular mechanisms of *Hox* gene function.

Limb skeletal development and adult bone maintenance

Mesenchymal condensations that preconfigure the limb skeletal elements initiate formation in a proximal to distal fashion beginning at E10.5 in the forelimb. These pre-

chondrogenic mesenchymal cells are derived from the lateral plate mesoderm and are first observed as morphologically dense, compacted groups of mesenchymal cells within the limb bud[42]. The earliest marker of pre-chondrogenic cells is the transcription factor, *Sox9*[43,44]. *Sox9*-expressing cells are found scattered in the limb bud mesenchyme prior to condensation. These chondrogenic precursors subsequently aggregate in a proximal (stylopod, ~E10.5) to distal (autopod, ~E11.5) fashion to form the cartilage anlage that will become the skeletal elements of the limb[43–46].

Subsequent longitudinal bone growth is fueled by the regulated proliferation and differentiation of chondrocytes at the distal ends of the bone. Chondrocytes within the growth plate are organized into distinct cellular zones with specific proliferative and maturity characteristics. The reserve zone, at the distal-most end of the bone, contains slow dividing chondrocyte progenitors, which give rise to all growth plate chondrocytes[47]. Chondrocytes in the proliferative zone are oriented into columns of cells, parallel to the long axis of the bone, and undergo significant proliferation to increase the number of cells within the growth plate[48]. The proliferative zone is characterized by the expression of a type II collagen and other cartilaginous matrix proteins such as aggrecan. At the central metaphyseal side of each growth plate, the hypertrophic zone is observed. Chondrocytes exit the cell cycle undergo hypertrophy, and transition into secreting a type X collagen matrix[49]. The hypertrophic transition zone provides the bulk of the longitudinal expansion of the bone[50].

Concomitant to condensation of the pre-chondrogenic skeletal mesenchyme, a dense connective tissue layer forms surrounding the skeletal anlage termed the perichondrium. It has been suggested that the perichondrium functions to constrain the

radial growth and promote longitudinal growth of the developing skeletal anlage[51]. The perichondrium, and later periosteum, additional serves as a primary site of osteogenesis in the central bone shaft region. Osteogenesis initiates at E13.5 in the mouse, and it can be visualized at its earliest stages by expression of the osteogenic markers *Runx2* and *Osterix* (*Osx*). Osteoblasts are first observed at E14.5 at the medial aspect of the anlage[46]. Starting around E14.5, Osx-expressing pre-osteoblasts enter the bone marrow space concurrent with vascular invasion into the medial region of the developing bone, which is mostly made up of hypertrophic chondrocytes[52]. Osteoclasts erode the hypertrophic matrix and allow invasion of endothelial cells into the cartilage[53,54]. Osteoblasts and other stromal populations invade the developing bone marrow space concurrent with the vasculature and begin depositing bony matrix that make up the primary ossification center[52].

During rapid bone development and growth that occurs during embryogenesis and early postnatal growth, the skeleton is primarily composed of woven bone. Woven bone is characterized as a bony matrix composed of haphazardly organized collagen fibers. Through unclear mechanisms, this woven bone is eventually remodeled into mature lamellar bone that contain collagen fibers arranged in tightly organized parallel sheets or layers that makes up the adult bone[55]. Once skeletal maturity is achieved and bone growth has largely ceased, the bone tissue maintains its integrity and responds to functional demands by continuously turning over through a process termed bone remodeling[56–58]. Bone remodeling involves the removal of the old mineralized matrix by osteoclasts followed by the formation of new bony matrix by osteoblasts that is subsequently mineralized. The resorption and formation of bone during bone remodeling are tightly coupled to maintain a normal bone mass. Initiation of bone remodeling begins with the

recruitment of hematopoietic progenitors and their differentiation into osteoclasts, induced by osteoblast lineage cells that express receptor activator of nuclear factor-κB ligand (RANKL) and macrophage-colony stimulating factor (M-CSF)[59,60]. Multiple cells fuse and further mature to produce a functional multi-nucleated osteoclast. Osteoclasts create a tight seal on the bone surface and release protons and proteolytic enzymes into the resorption compartment dissolving minerals and degrade bone matrix proteins, respectively[58,61]. The release of growth factors that were embedded in the bone matrix (e.g. TGF-β, IGFs, VEGF, PDGF etc.), soluble signals, and membrane-bound proteins (e.g. ephrins, semaphorins etc.) all work in concert to then recruit osteoblast precursors to the resorption site. The recruited osteoblasts differentiate and mature to deposit new bone matrix that is eventually mineralized[60,62]. Terminally differentiated osteoblasts become embedded in the matrix they secrete and eventually become entrapped in the mineralized matrix becoming osteocytes. Osteocytes possess long dendritic processes that are enclosed by canalicular walls, forming a network termed the lacuna-canalicular network that connect neighboring osteocytes as well as bone surface cells including osteoblasts and osteoclasts[63,64]. This connection between cells play a critical role in bone homoestasis[65].

Considering *Hox* genes beyond embryogenesis

Detailed analyses of *Hox* genes have mostly been restricted to embryonic development and largely unexplored at later stages. However, there is growing evidence for their expression extending beyond embryonic development into postnatal and adult stages as well as implications for their continued function. Expression profiles generated from multiple adult human organs show that the expression of *Hox* genes are maintained,

reflecting the regional expression pattern established during embryonic development[66]. Similarly, using human epidermal fibroblasts, it was shown that site-specific *Hox* expression was maintained in a cell-autonomous manner[67]. Cells isolated from various organs and anatomical sites also revealed characteristic *Hox* expression fingerprints highly specific for their anatomical origin[68]. Interestingly, expression of specific *Hox* paralogous groups could be used to distinguish between bone marrow-derived mesenchymal stem cells and cord blood-derived mesenchymal stem cells suggesting that distinct *Hox* paralog expression could be used to identify different cell populations[69].

Deregulation of *Hox* gene expression has been widely implicated as the driving force in tumorigenesis[70]. Upregulation or downregulation of *Hox* genes has been recognized to contribute to all aspects of cancer initiation and progression that include angiogenesis, autophagy, differentiation, apoptosis, proliferation, invasion and metastasis, and metabolism. *HOXA9* has been found to be overexpressed in leukemia and is considered to be an initiating factor of leukemogenesis by epigenetic reprogramming of hematopoietic cells[71,72]. A mutation that affects the auto-regulatory enhancer of the *HOXD4* gene leading to reduced transcriptional activity has been associated with a higher risk of acute lymphoblastic leukemia (ALL)[73]. Missense mutations in *HOXB13* have been correlated with increased prostate cancer susceptibility and an elevated risk of leukemia, bladder, breast, and kidney cancers[74–77]. In Ewing's sarcoma, an abnormal upregulation of the posterior *HOXD* paralogs is observed[78,79]. As the EWS-FLI1 fusion protein—a hallmark of Ewing's sarcoma—recruits epigenetic regulators to reprogram the epigenome, studies have concluded that the aberrant expression of *HOX* genes maintains and facilitates the progression of this cancer[78]. Not only are deregulated *HOX* expression implicated in

tumorigenesis but were also found to have tumor-suppressive roles in distinct contexts. The *p53* gene protects cells from malignant transformation and *HOXA5* was found to transcriptionally regulate *p53* in breast cancer tumor cells by directly binding to the *p53* promoter[80–83]. Additionally, *HOXA5* expression in breast cancer cells induced apoptosis mediated by caspase 2 and 8[84]. Together, whether *HOX* genes are associated with the progression or suppression of malignancies, it is evident that the transcription of *HOX* genes continue to be actively regulated in these malignancies after birth.

Coinciding with the continued expression of *Hox* genes in various organs and tissues, their continuous function after embryogenesis have been implicated. The loss of any complete set of *Hox* paralogous group results in embryonic lethality. Therefore, much of the insight in the continuing function of *Hox* genes have been gained by examining compound mutants that have only one functional paralog allele. The zeugopod forelimb of *Hox11* compound mutants develop normally but start to show phenotypes at postnatal stages with an overall shortened ulna and bowing of the radius[85]. At adult stages, these compound mutants are unable to execute normal fracture repair[86,87]. At the early stages of fracture repair, compound mutants are incapable of generating cartilage within the fracture callus leading to an incomplete bridging of the fracture gap[87]. This gap is never resolved in the *Hox11* compound mutants even out to 12 weeks-post-fracture and the skeleton fails to resume its original structure[86]. Together, these findings are consistent with the possibility of a continuing function of *Hox* genes that extend beyond their embryonic role.

In order to further understand the cellular mechanisms of *Hox* function in the adult skeleton, efforts were devoted to establishing the identity of adult *Hoxa11eGFP*-expressing cells during bone homeostasis and fracture repair. Importantly, the expression

of *Hox11* remains regionally-restricted to the zeugopod skeleton through postnatal and adult stages (Figure 1.4 and [86]). During fracture repair, its expression increases in response to injury and is highly expressed in cells within the fracture callus[86,87]. Extensive co-expression analyses revealed that during both fracture repair as well as normal, un-injured adult bone, Hoxa11eGFP is not expressed in mature osteoblasts, cartilage cells, fat cells, neurons, blood cells, or blood vessels[86]. Flow cytometry analyses demonstrated that *Hox11*-expressing cells are restricted to the non-hematopoietic, non-endothelial stromal compartment of the bone marrow and perichondrium[86]. Cell surface marker analyses and genetic lineage-tracing models determined that *Hox11*-expressing cells are a population of mesenchymal stem cells (MSCs) that co-express PDGFRα/CD51 and Leptin-receptor (LepR)[86].

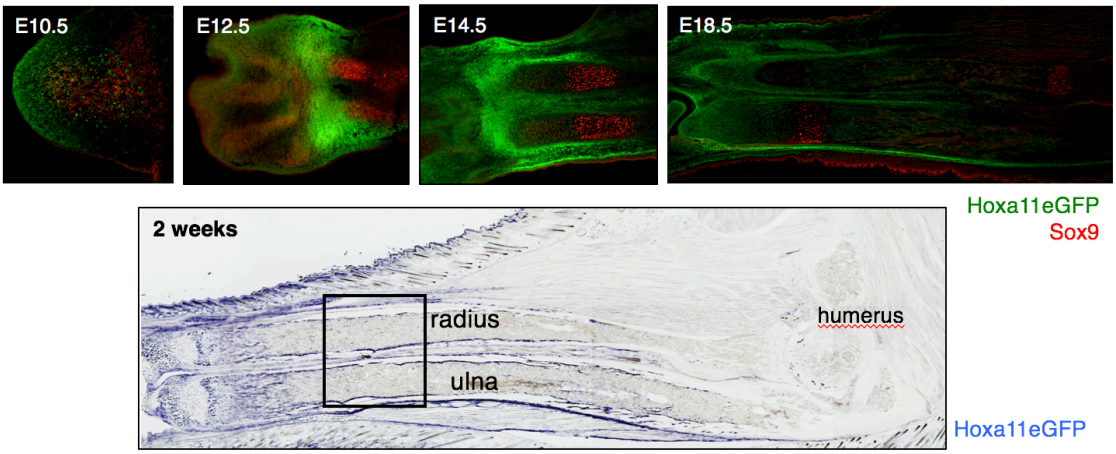

Figure 1.4. Hoxa11eGFP expression in the developing limb bud and maintenance of its expression beyond embryogenesis. Expression of Hoxa11eGFP is observed by the cells expressing GFP (green) in real-time during limb bud development while the condensing skeletal anlage is observed by an early chondrocyte marker, Sox9 (red). Hox11 expression initiates at ~E9.5 with it becoming restricted to the zeugopod region by E11.5 and continues through postnatal and adult stages. Bottom panel shows Hoxa11eGFP

expression (blue) that remains restricted to the zeugopod region 2-weeks after birth (Figure adapted from Swinehart *et al.,* 2013 [88] and Rux *et al.,* 2016 [86]).

While there is mounting evidence that imply a continuing role for *Hox* genes at adult stages, there are several caveats that must be taken into consideration when assessing these results. The interpretation of the phenotypes of compound mutants are complicated by the fact that three alleles are absent throughout embryonic development as well as postnatal and adult stages. Therefore, it is challenging to separate developmental defects that manifest later in life from the adult stage functions. *Hox* expression continues in multiple adult cell types, however it remains to be shown whether this expression confers any significant functional meaning. Further, it is difficult to establish a cause and effect relationship between the differential expression of *Hox* genes and various diseases. Therefore, whether *Hox* genes continue to function in whichever organ or tissue it is expressed in after birth remains an open question.

Mesenchymal stem cells (MSCs) or skeletal stem cells

The existence of adult stem cells was first described by Till and McCulloch when they showed that cells from the bone marrow are capable of giving rise to mesenchymal cell types (osteoblasts, chondrocytes, and adipocytes) and maintain self-renewal[89–91]. Subsequently, Friedenstein and colleagues demonstrated that the rodent bone marrow contained cells capable of forming fibroblastoid colonies (CFU-F), were plastic adherent, gave rise to bone, and could reconstitute a hematopoietic microenvironment when transplanted subcutanesouly[92–95]. When similar cells were identified in human bone marrow aspirates, these cells were given the name “mesenchymal stem/stromal cells (MSCs)”[96].

The identification and characterization of MSCs were primarily fueled by the fact that they were in close proximity to hematopoietic stem cell (HSC) niches associated with blood vessels in the bone marrow and were regarded as critical regulators of the HSC niche. Bone marrow stromal cells adjacent to blood vessels express crucial HSC niche factors such as C-X-C motif chemokine 12 (CXCL-12), stem cell factor (SCF), Angiopoietin-1 (Ang-1), interleukin-7, vascular cell adhesion molecule-1 (VCAM-1) among others[97,98]. Manipulation of these perivascular MSCs by genetic ablation led to disruption of hematopoietic lineages and HSC maintenance. For example, the ablation of *Nestin*-GFP+ cells that primarily localize around bone marrow blood vessels resulted in a significant reduction in hematopoietic stem/progenitor cells[99]. Genetic ablation of CXCL12-abundant reticular (CAR) perisinusoidal cells led to premature differentiation of hematopoietic myeloid cells[100,101]. Additionally, removing fibroblast activation protein (FAP)-expressing bone marrow stromal cells resulted in bone marrow hypocellularity and anemia[102]. The deletion of LepR-expressing MSCs from the bone marrow compartment also led to the depletion of hematopoietic stem/progenitor cells[103,104]. Together with other findings, these results indicated that MSCs are a crucial constituent of the HSC niche.

Due to the close proximity and intimate regulation, studies ensued to dissect the lineage relationship between HSCs and MSCs. Results determined that the two population of stem cells are derived from individual, distinct lineages[105]. Further, the discovery of cell surface markers for the specific identification of MSCs was demonstrated. At this point, the primary focus of MSCs as constituents of the HSC niche shifted. MSCs began to be recognized as a potential skeletal stem cell population that provides a reservoir of stem cells continuously supplying appropriate skeletal lineage cells. Plastic adherence,

expression of specific cell surface antigen, and multipotent differentiation potential became the official defining characteristics of MSCs[106]. Additionally, MSCs are required to exhibit self-renewal in order to be characterized as a stem cell[107].

Genetic mouse models have proven extremely useful in characterizing MSC subpopulations *in vivo.* The *Nestin*-GFP transgenic mouse model was the first to be rigorously interrogated. *Nestin*-GFP+ cells identified rare perivascular stromal cells[99]. These cells were shown to be capable of multi-lineage differentiation *in vitro* giving rise to osteoblasts, chondrocytes, and adipocytes. Self-renewal was demonstrated by serial transplantation of mesenspheres supporting the stem cell properties of this population[99]. While the discovery of the *Nestin*-GFP-expressing cells provided valuable insight in MSC biology, the intracellular location of the Nestin protein precluded prospective live cell isolation for additional characterization. In a follow-up study, Pinho *et al*. identified the cell surface markers, PDGFRα/CD51 (integrinαV), to encompass a large fraction of the *Nestin*-GFP-expressing cells[108]. The PDGFRα+/CD51+ subset of *Nestin*-expressing cells further enriched for MSCs as they contained almost all CFU-F and mesensphere-forming activity and displayed robust tri-lineage differentiation (osteoblast, chondrocyte, and adipocyte) *in vitro*[108]. *In vivo* confirmation of the multi-lineage capacity of the *Nestin*-expressing cells was further interrogated by the use of an inducible *Nestin-CreER.* Postnatal stage induction of recombination followed by lineage-tracing of the *Nestin* lineage revealed that these progenitor cells gave rise to osteoblasts and chondrocytes, but not adipocytes *in vivo*[109]. Intriguingly, neither adult nor postnatal induction led to adipocytes marked by the *Nestin*-CreER lineage. Discrepancies between *in vitro* lineage contribution and *in vivo* multi-lineage potential demonstrated that *in vitro* assays do not

faithfully illustrate the differentiation capacity of MSCs *in vivo* highlighting the importance of careful examination of MSCs in their endogenous environment. The absence of *Nestin* -CreER labeled adipocytes additionally suggested the potential existence of other populations of MSCs that contribute to distinct skeletal cell types[99,109].

Additional progenitor populations identified include *Myxovirus resistance-1(Mx1)-Cre* lineage labeled cells that were strictly comprised of osteoblasts with little to no contribution to chondrocytes or adipocytes *in vivo*[110]. *Gremlin-1 (Grem1)-CreERT* induction at both postnatal and adult stages led to lineage-labeled chondrocytes and some contribution to the osteolineage[111]. A mouse model where *in vivo* adipocyte contribution was observed was in the *Leptin Receptor-Cre* mouse model. This genetic marker identified the broadest MSC population containing the majority of CFU-F activity of bone marrow cells in the adult[112]. Fate-mapping of the *LepR-Cre* cells revealed that contribution to the adult bone begins at 15-weeks of age and that most of the osteoblasts in the adult bone were *LepR*-lineage labeled[112]. Adipocytes were also found to be lineage labeled with *LepR.* However *LepR*-lineage marked chondrocytes were only found during fracture repair, but not homeostasis[112]. An important fact to consider is that this model harbor a ubiquitous *Cre* allele with no temporal control. Therefore, it cannot be excluded that LepR expression initiated in the differentiated osteoblasts and adipocytes to subsequently mark them. Thus, the lineage relationship between *LepR*-expressing MSCs and mature osteoblasts or adipocytes cannot be determined. Additionally, while expression of LepR initiates during late embryogenesis (~E17.5), *LepR*-lineage-labeled cell contribution to bone is not observed until 15 weeks of age[112]. This indicates that a distinct population of MSCs must contribute to the development and growth of the skeleton.

MSC populations that support early skeletal development and growth were demonstrated by the *Prx1-Cre* model that labels the entire limb bud mesenchyme derived from the lateral plate mesoderm[113]. Embryonic and postnatal induction of *Osx-CreERT* and *Osx-CreERT2* models demonstrated a robust contribution to early skeletal development and growth[114,115]. These lineage-labeled cells exhibited multi-lineage potential as well. Interestingly, embryonic induction of the *Osx-CreERT2* model demonstrated the existence of a transient source of skeletal progenitors. Virtually no embryonically induced lineage-labeled cells were found in the adult bone; however, postnatal induction of the same model exhibited a life-long contribution to bone[115]. This led to the notion of the 'waves of progenitors' where distinct, age-dependent MSC populations arise to separately support the development, growth, and maintenance of bone. It is important to note that many of the genes used in these mouse models are known to be expressed in mature cell types. Osterix is expressed in osteoblasts, nestin is expressed in endothelial cells, and LepR is expressed in neurons[116–118]. Therefore, this raises the possibility of these models marking downstream progenitor populations rather than a true skeletal stem cell.

As more subsets of MSCs were identified in the skeleton, the heterogeneous nature of MSCs was increasingly evident. *Nestin*-CreER lineage-labels two subsets: one found closely associated with endothelial cells, co-expressing CD31, predominantly found in the perichondrium while the other does not express CD31 and is found to encompass the early osteoblast lineage during limb skeletal development[109]. The heterogenous nature of MSCs was further reinforced by the *Nestin*-GFP-expressing population as one subset expresses high levels of *Nestin*-GFP (*Nestin*-GFP^{high}) that mainly localized around arterioles and the other expresses low levels of *Nestin*-GFP (*Nestin*-GFP^{low}) primarily found near

sinusoids[119]. Bone marrow stromal cells marked by *Leptin-receptor (LepR)-Cre* only label a subset of the *Nestin*-GFP-expressing cells while virtually all (>95%) *LepR*-lineage labeled cells express PDGFRα, CD51, PDGFRβ, and a high proportion (68%) expresses CD105[112]. PDGFRα+/Sca1+ was one of the earlier MSC subsets to be isolated by cell surface markers[120] and minimal overlap was observed between Sca1+ and LepR+ cells. Mouse skeletal stem cells (mSSCs) that are CD51+/CD200+ was demonstrated to give rise to multiple downstream progenitor populations *ex vivo* in ectopic transplantation models into the kidney capsule[121]. During development, mSSCs and PDGFRα+/Sca1+ arise as mutually distinct populations encompassed within the PDGFRα+/CD51+ population[122]. Moreover, based on expression of CD73 and CD90 four sub-populations within PDGFRα+/Sca1+ was identified with distinct differentiation potentials *in vitro*[122].

In addition to the heterogeneity identified by cell surface marker expression, the existence of regionally distinct MSCs are beginning to emerge adding another layer of complexity. A *Cathepsin K-Cre (CatK-Cre*) model was shown to label periosteal stem cells that are largely excluded from the mesenchymal cells within the bone marrow or endosteal compartment[123]. Coinciding with this finding, the behavior of stem/progenitor cells from the periosteum were found to be distinct from that of bone marrow MSCs during fracture repair. Periosteal stem/progenitor cells were more migratory and contributed to the fracture callus more extensively compared to bone marrow mesenchymal cells[124]. The transcriptional profile between the periosteal and bone marrow stem/progenitor cells were also found to be distinct supporting the distinct nature of the MSC population separated by location[124]. Relatively recently, our laboratory has shown that Hoxa11eGFP expression is exclusive to a population of progenitor-enriched adult MSCs[86]. As mentioned above, *Hox*

expression is regionally restricted in the skeleton throughout life. Intriguingly, the *Hox* signature established during embryogenesis is retained strictly within MSCs (defined by *LepR*-lineage labeled cells) in bones isolated from various axial levels[86]. Consistent with these results, another group reported that *Hox* gene expression status in periosteal stem/progenitor cells from distinct anatomical sites were found to best define the differences found in their transcriptome[125]. Taken together, it is becoming evident that the skeleton is comprised of many different populations of MSCs that display distinct contributions to skeletal development, growth, maintenance, and injury repair. However, this raises an important question of whether there is a common origin to all of these sub-populations. Moreover, the question of whether a true stem cell exists within the skeleton is still unclear.

Summary of thesis work

The overarching goal of the work presented in this thesis is to understand the mechanism of *Hox* gene function in the adult mammalian skeleton. The forelimb zeugopod skeleton where *Hox11* is expressed was used as a model to gain insight into this question. Specifically, understanding the cellular nature of *Hox*-expressing cells within the skeleton, assessing the stem/progenitor capacity of *Hox*11-expressing cells *in vivo*, and to determine a continued function for *Hox* genes in the adult skeleton are presented in this thesis.

Previous work from our laboratory defined *Hox11*-expressing adult cells as mesenchymal stem cells (MSCs) characterized by co-expression of published MSC cell surface markers and *in vitro* multi-lineage potential[86]. However, whether the *Hox11*-expressing cells are capable of stem/progenitor activity *in vivo* was not clear. To address

this question, an inducible *Hoxa11-CreERT2* allele was generated (by Kyriel Pineault) in order to track the *Hox11*-expressing cells *in vivo* and examine their behavior throughout skeletal growth, development, and maintenance. Here, I show that *Hox11*-expressing cells give rise to all skeletal lineages including osteoblasts, chondrocytes, adipocytes, and most critically exhibit self-renewal throughout life. Additional insight into lineage relationships among other published sub-populations that exist within the skeleton was also revealed in this study. I performed all the flow cytometry experiments related to this work and my work demonstrates a life-long population of skeletal stem cells established during embryogenesis.

As mentioned previously, the requirement for *Hox* genes after the skeleton has been established has been largely unknown. As the stage-specific functions of *Hox* genes is difficult to separate in results from *Hox* compound mutants, a *Hoxd11* conditional allele was generated. This allows for the deletion of *Hox11* function at any stage while maintaining normal development and growth until deletion. In this work I show that the conditional loss of *Hox11* function at adult stages lead to a progressive replacement of normal lamellar bone with an abnormal woven bone-like matrix containing haphazardly organized collagen fibers. Lineage-analysis determined that while osteoblast differentiation is initiated, subsequent maturation does not occur, and downstream osteocytes are affected as well exhibiting differentiation and morphological defects. Critically, the function of *Hox11* remains regionally restricted as the humerus from the conditional mutants do not display defects. Collectively, this work demonstrates a continuing function for *Hox* genes beyond embryonic development by regulating the differentiation of regional *Hox*-expressing skeletal stem cells.

CHAPTER II

Hox11 Expressing Regional Skeletal Stem Cells Are Progenitors for Osteoblasts, Chondrocytes and Adipocytes Throughout Life

Summary

Multipotent mesenchymal stromal cells (MSCs) are required for skeletal formation, maintenance, and repair throughout life; however, current models posit that postnatally arising long-lived adult MSCs replace transient embryonic progenitor populations. We previously reported exclusive expression and function of the embryonic patterning transcription factor, Hoxa11, in adult skeletal progenitor-enriched MSCs. Here, using a newly generated *Hoxa11-CreER*^{T2} lineage-tracing system, we show *Hoxa11*-lineage marked cells give rise to all skeletal lineages throughout the life of the animal and persist as MSCs. *Hoxa11* lineage-positive cells give rise to previously described progenitor-enriched MSC populations marked by *LepR-Cre* and *Osx-CreER*, placing them upstream of these populations. Our studies establish that Hox-expressing cells are skeletal stem cells that arise from the earliest stages of skeletal development and self-renew throughout the life of the animal.

Introduction

Hox genes play well-established roles in patterning the embryonic skeleton. *Hox1* through *Hox13* paralogs are expressed and function regionally along the anterior-posterior axis of the axial skeleton, with the *Hox9-Hox13* paralogs co-opted to also pattern along the proximal to distal axis of the appendicular skeleton. The *Hox11* paralogs, *Hoxa11, Hoxc11* and *Hoxd11,* pattern the sacral region of the spine and the zeugopod region of the limb (radius/ulna and tibia/fibula)[20]. Loss of *Hoxa11* and *Hoxd11* function during development results in dramatic mis-patterning of the forelimb zeugopod skeleton[25]. In addition to complete loss-of-function phenotypes observed during development, compound mutants exhibit defects in skeletal growth during postnatal stages and in adult fracture repair[85–87].

Despite clear genetic evidence for *Hox* function in the skeleton, Hox expression is excluded from all mature skeletal cell types at all stages, including chondrocytes and osteoblasts[20,86,88]. Embryonically, Hox11 expression is observed in the developing zeugopod perichondrium immediately adjacent to Sox9-positive chondrocytes and, as the skeleton begins to ossify, expression continues in the periosteum, adjacent to Osterix-positive pre-osteoblasts[88]. At postnatal and adult stages, Hox11-expressing cells remain in the outer periosteal stroma adjacent to the osteoblast layer, and are additionally observed in the bone marrow and along the endosteal (inner) bone surface[20,86]. Adult Hox11-expressing stromal cells from the bone marrow and periosteum are exclusively identified by antibodies that mark progenitor-enriched mesenchymal stem/stromal cell (MSC) populations including PDGFRα/CD51 and Leptin-Receptor (LepR) as well as by *Leptin Receptor-Cre* (*LepR-Cre*)[86,108,112]. *In vitro, Hox11* mutant MSCs are unable to differentiate

into chondrogenic and osteogenic lineages, supporting a function for *Hox11* genes in this population[86].

Several previous lineage labeling models have reported labeling of progenitor-enriched, bone marrow MSC populations, however, with the exception of *Prx1-Cre*, which labels the entire limb lateral plate mesoderm[126], inducible lineage reporters only mark only a minor proportion of a multipotent, self-renewing population from postnatal stages, and only when induced at postnatal stages. These models include *Osterix-CreER (Osx-CreER), Sox9-CreER, Aggrecan-CreER, PthrP-CreER,* and *Gremlin1-CreER*[111,115,127,128]. The *LepR-Cre* lineage reporter, while not inducible, eventually marks the majority of the progenitor-enriched MSCs in the adult bone marrow[112,115]. Of note, this model does not give display robust contribution to osteoblasts until 5-6 months of age[112,115]. Recent evidence showed embryonic and postnatal *Gli1-CreER* lineage marked cells are multi-potent and give rise to LepR-positive bone marrow MSCs in the adult[129]. However, the pattern of contribution to the skeleton differs significantly based on the induction time points, indicating that this lineage-marked population is not equivalent at embryonic and postnatal stages.

Previous work has genetically established the importance of *Hox11* genes in embryonic skeletal development, postnatal growth, and adult fracture repair[85–87]. Considering the continuity in Hoxa11eGFP expression in the zeugopod skeleton throughout life and the recent identification of adult, Hox11-expressing cells as skeletal MSCs, we sought to test the progenitor capacity of the Hox11-expressing population throughout the life of the animal. To do this, we generated a *Hoxa11-CreER^{T2}* lineage-tracing allele and we find that *Hoxa11*-lineage marked cells continuously give rise to all

the skeletal mesenchymal lineages (cartilage, bone, and fat) during embryonic development, postnatal growth, at homeostasis and in response to injury. Even when lineage labeling is initiated at embryonic stages, *Hoxa11*-lineage marked stromal cells arising from this lineage co-express MSC markers PDGFRα/CD51 and LepR. In contrast to other reported embryonically-induced progenitor populations, the *Hoxa11*-lineage is maintained as progenitor-enriched MSCs in adult bone marrow and demonstrate strong lineage labeling of all skeletal lineages through at least one year of age. Further, *Hoxa11* lineage-marked MSCs also express Hoxa11eGFP at all stages examined. These results provide strong evidence for the *in vivo* self-renewal of this MSC population.

To understand the lineage relationships between Hox11-expressing cells and other genetically marked progenitor/MSC populations, we compared Hoxa11eGFP expression to cells genetically lineage labeled by *LepR-Cre* and *Osx-CreER*[112,115,127]. Herein, we show that Hox11-expressing cells serve as upstream progenitors that give rise to cells marked by these other genetic models. Taken together, these data support Hox-expressing skeletal, stromal cells as a *bona fide* skeletal stem cell population and demonstrates the presence of a specific, lineage-continuous skeletal stem cell population from embryonic stages throughout life.

Results

Hox11 expression defines a continuous progenitor population

Hox11 expression is regionally-restricted in the embryonic zeugopod limb (radius/ulna and tibia/fibula) and is observed in cells of the perichondrium surrounding the chondrocyte anlage [Figure 2.1a]. As osteoblast differentiation commences, *Hox11* continues to be expressed in the outer periosteum immediately adjacent to the differentiating osteoblast layer [Figure 2.1b and [88]]. Throughout embryonic, postnatal, and adult life, Hoxa11eGFP-expressing cells persist on the periosteal surface, but also become observed on the endosteal bone surfaces and as stromal cells within the bone marrow space beginning at postnatal stages [Figure 2.1c-f]. At later stages, Hoxa11eGFP expressing cells remain non-overlapping with osteoprogenitors on the bone surfaces [Figure 2.1g, arrowheads and [86]]. We previously demonstrated that adult Hoxa11eGFP-expressing cells are exclusively identified by co-expression of PDGFRα/CD51 and of LepR, cell surface markers for progenitor-enriched MSCs[86,108,112]. Consistent with the possibility that Hox11 expression defines skeletal mesenchymal progenitors throughout life, Hoxa11eGFP-expressing cells are observed in several regions that have been demonstrated to contain skeletal progenitors including the distal growth plate, the perichondrium/periosteum, and the trabecular bone. [Figure 2.1h and [47,52,128,130,131]]. Periostin expression was recently identified to mark MSCs with enriched bone-forming potential compared to bone marrow MSCs[124]. Intriguingly, Hoxa11eGFP-expressing cells in the outer periosteum are not positive for periostin at adolescent or adult stages, however, the more weakly-postive Hoxa11eGFP cells in the inner periosteal layer do overlap with periostin staining,

correlating the expression of both of these proteins with high progenitor activity in this region of the skeleton [Figure 2.1i-j].

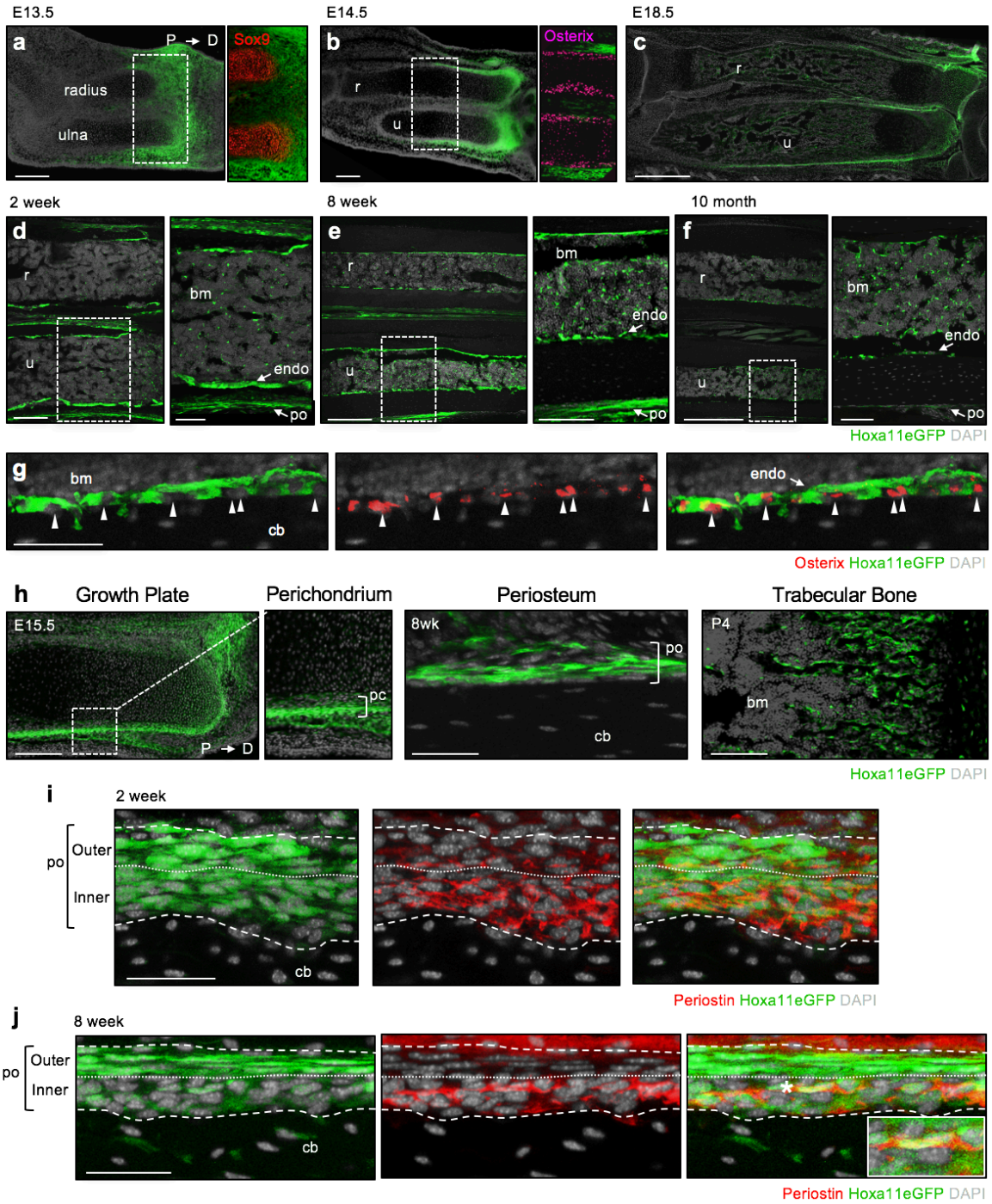

Figure 2.1. Hoxa11eGFP expression defines a continuous stromal population. (**a-f**) Hoxa11eGFP expression in the forelimb zeugopod (radius and ulna) shown from embryonic to adult stages with proximal on left and distal on right in all images.

Hoxa11eGFP expression in radius and ulna (**a-c**), higher magnification images show cartilage marker, Sox9 at E13.5 (**A**, red) and osteoblast marker, Osterix at E14.5 (**b**, magenta). (**d-f**) mid-diaphysis radius (r) and ulna (u) (higher magnification images of mid-diaphysis ulna, white dashed box, shown on right). (**g**) Hoxa11eGFP and Osterix (red) at 8 weeks, white arrowheads identify individual Osterix positive nuclei. (**h**) Hoxa11eGFP (green) in E15.5 distal growth plate and higher magnification of perichondrium (white boxed region, bracket), 8 week periosteum (bracket), and P4 trabeculae. (**i-j**) Periosteal Hoxa11eGFP and Periostin (red) at 2 week (**i**) and 8 weeks (**j**). Dashed white lines mark periosteal boundary dotted line separates inner and outer layers. (**j**) Cell marked by asterisk magnified in inset. In all images, green: Hoxa11eGFP, grey: DAPI. Bone marrow: bm, periosteum: po, endosteum: endo, cortical bone: cb, perichondrium: pc. Scale bars; (**a, b, d-f** left panels**, h** growth plate) 200μm, (**c**) 500μm, (**d-f** right panels, **h** trabecular bone) 100μm, (**g, h** periosteum, **i-j**) 50μm.

We analyzed Hoxa11eGFP-expressing cells from embryonic, postnatal, and adult stages for co-expression of PDGFRα/CD51 and LepR by flow cytometry. At embryonic stages, analyses were performed on the entire skeletal anlage, while at postnatal and adult stages, the bone marrow and bone adherent fractions were analyzed separately. Hoxa11eGFP-expressing cells from embryonic stages through one year of age co-label with PDGFRα and CD51 in both compartments [Figure 2.2a and Supplemental Figure 1b]. In agreement with previous reports, LepR expression does not initiate until approximately newborn stages[112,115]. Consistent with increasing expression in stromal progenitors during postnatal life, co-expression of LepR in the Hoxa11eGFP-expressing cells increases during this time; by adult stages, the majority of Hoxa11eGFP-expressing cells are also LepR-positive [Figure 2.2a and Supplemental Figure 2.1b]. Interestingly, LepR expression increases more slowly within the bone adherent compartment compared to the bone marrow compartment [compare Supplemental Figure 2.1b to Figure 2.2a]. While it has not been established whether adult MSC cell-surface markers label progenitors during embryogenesis, Hoxa11eGFP-expressing stromal cells maintain a constant cell surface signature from the stage when each marker is first expressed. Primitive postnatal

progenitors, coined mouse skeletal stem cells (mSSCs), are one of the earliest MSC populations defined by flow cytometry[121]. Overlap (50-60%) between Hoxa11eGFP-expressing cells and the mSSC population is observed demonstrating that a sub-population of postnatal Hox-expressing stromal cells are mSSCs [Figure 2b-c]. These collective data provide strong support for the hypothesis that Hoxa11eGFP-expression identifies a skeletal MSC population from early stages.

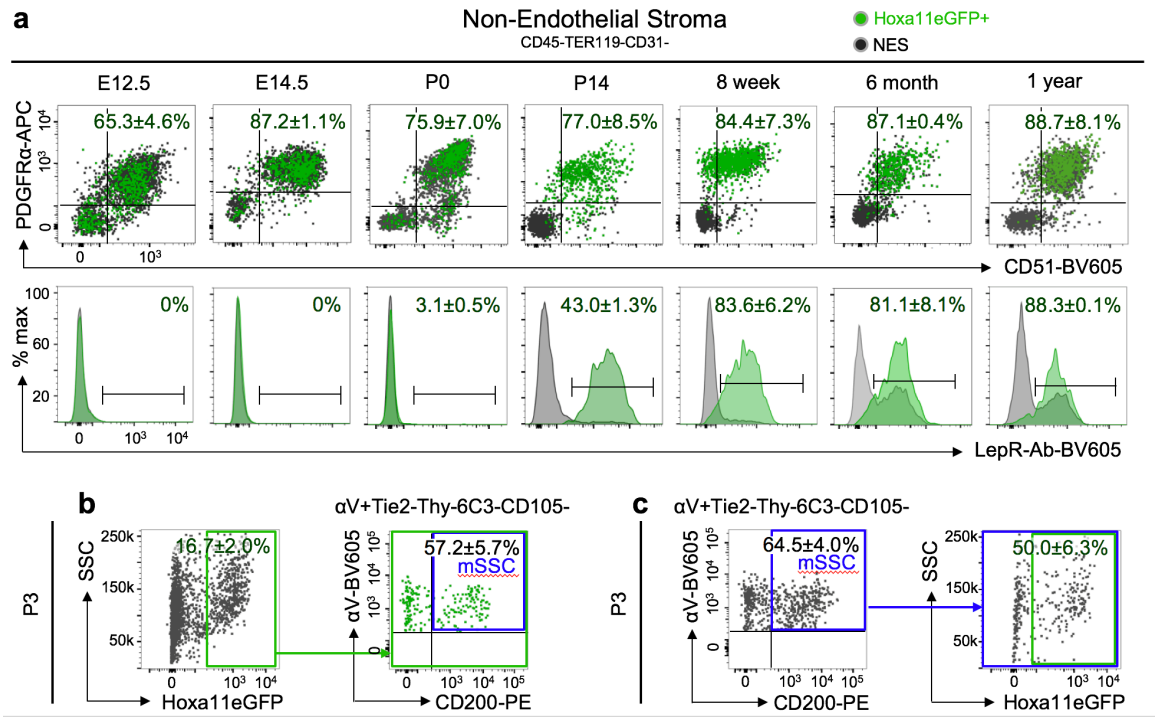

Figure 2.2. Hoxa11eGFP expressing cells co-express MSC markers throughout life. (**a**) Flow cytometry analyses of whole skeletal anlage (E12.5 [n=4], E14.5 [n=6], and P0 [n=6]) or flushed bone marrow (P14 [n=9], 8 week [n=10], 6 month [n=4], and 1 year [n=3]). Gating strategy and bone surface analyses Supplemental Figure 2.1a,b. Non-hematopoietic, non-endothelial stromal compartment (CD45-TER119-CD31-) was gated on PDGFRα/CD51 (top) or Leptin Receptor (LepR-Ab, bottom). Percentages reflect proportion of Hoxa11eGFP-positive population within double-positive gate (top) or bracketed region of histogram (bottom). Charcoal dots or grey histogram: total non-endothelial stroma (NES), green dots or green histogram: Hoxa11eGFP-expressing non-endothelial stroma (Hoxa11eGFP+). (**b-c**) Flow cytometry analyses of whole P3 bones. Gating strategy Supplemental Figure 2.1c. Non-hematopoietic, non-endothelial stromal compartment (CD45-TER119-CD31-) was gated for (**b**) Hoxa11eGFP-positive population

(green box) and subsequently for mouse skeletal stem cells(mSSC, αV+Tie2-Thy-6C3-CD105-CD200+, blue box) or (**c**) mSSC population (blue box) and subsequently for Hoxa11eGFP-expression (green box). Percentages reflect proportion of cells within indicated gate. 'n' values indicate biologically independent animals for each time point. All data presented as mean ± standard deviation.

Cas9/CRISPR generation of a Hoxa11-CreER^{T2} allele

To rigorously examine the lineage potential of Hox11-expressing cells *in vivo*, we generated a tamoxifen-inducible *Cre* knock-in at the *Hoxa11* locus using Cas9/CRISPR mediated gene editing [Supplemental Figure 2.2a]. Briefly, two guide RNA sequences were designed to cut near the boundaries of exon 1 and a recombination plasmid was generated containing a tamoxifen-inducible *Cre* cassette (*CreER^{T2}*) with the rabbit β-globin poly-adenylation sequence[132]. This recombinant template was flanked by 1.3kb of homology upstream and downstream of exon 1. The editing strategy resulted in replacement of exon 1 with *CreER^{T2}* followed by a strong stop sequence while maintaining the endogenous *Hoxa11* surrounding sequences. Founder animals were screened by PCR for insertion of *Cre* sequence [Supplemental Figure 2.2b]. Targeting to the *Hoxa11* locus was validated by Southern Blot analyses using 5' and 3' flanking probes as well as an internal probe for *Cre* [Supplemental Figure 2.2c]. *Hoxa11-CreER^{T2}* mice were crossed to *ROSA26-LSL-tdTomato* reporter mice and no tdTomato expression was observed in the absence of tamoxifen administration [Supplemental Figure 2.2d].

Hoxa11 lineage shows life-long contribution to skeleton

The *in vivo* lineage potential of Hox11-expressing cells was assessed by generating mice of the genotype *Hoxa11CreER^{T2}; ROSA26-LSL-tdTomato* to report lineage contribution to

the skeleton [Figure 2.3a]. A *Hoxa11eGFP* real-time reporter allele was also including in some animals to determine if *Hoxa11*-lineage marked cells persist as Hox11-expressing MSCs[133]. Lineage-tracing was initiated by administering tamoxifen to pregnant dams at E13.5, a time point at which embryonic Hoxa11eGFP expression has become restricted to the stromal population surrounding the condensed zeugopod cartilage, but several days prior to the formation of a bone marrow cavity [Figure 2.3b and [88]]. Embryonic *Hoxa11*-lineage marked cells (*Hoxa11*$^{E13.5}$) closely matched Hoxa11eGFP expression further confirming the integrity of the *Hoxa11-CreER*^{T2} allele [Figure 2.3b]. 24 hours following tamoxifen injection, the majority of lineage-marked cells are localized within the perichondrial/periosteal stroma surrounding the skeletal element with little to no overlap with Sox9-postive chondrocytes and Osx-positive osteoblasts [Figure 2.3c-d, brackets]. Two days after injection, at E15.5, the embryonic anlage has begun to mature, with cartilaginous growth plates on the distal ends and ossification initiating in the center of each skeletal element. *Hoxa11*$^{E13.5}$-lineage marked cells are observed throughout the perichondrium/periosteum surrounding the zeugopod elements and additionally within the growth plate and on the bone surface [Figure 2.3e]. Significant overlap of *Hoxa11*$^{E13.5}$-lineage marked cells and Hoxa11eGFP-expressing cells continues to be observed, while the *Hoxa11*-lineage marked population has expanded [Figure 2.3f and Supplemental Figure 2.3a]. By E18.5, *Hoxa11*$^{E13.5}$-lineage marked cells are observed throughout the zeugopod growth plate, within the primary spongiosa, and in the outer periosteal region [Supplemental Figure 2.3b-d]. *Hoxa11*$^{E13.5}$-lineage marked cells contribute to both growth plate chondrocytes and osteoblasts at E18.5, demonstrating that the Hox11-expressing population marks multipotent skeletal progenitors that function during embryogenesis

[Supplemental Figure 2.3b-d].

Following the *Hoxa11*$^{E13.5}$-lineage marked population after birth reveals continued lineage labeling throughout the periosteum, the endosteum, and within the established bone marrow space [Figure 2.3g and inset]. This pattern of distribution continues through adult stages where extensive lineage-labeling is observed [Figure 2.3h]. Consistent with the regional expression of Hoxa11eGFP, *Hoxa11*$^{E13.5}$-lineage marked cells only contribute to the zeugopod skeleton and no lineage labeling in the stylopod (humerus) is observed at any stage, demonstrating that this progenitor population remains regionally restricted [Figure 2.3h, inset]. *Hoxa11*$^{E13.5}$-lineage marked cells continue to show remarkably strong contribution to the skeleton as late as one year of age [Figure 2.3i-j].

Lineage-labeling was then initiated at postnatal stages, a time when other genetic models have demonstrated contribution to long-lived stromal MSC cells. Tamoxifen was administered at postnatal day 3 (P3) and the contribution of *Hoxa11* lineage-marked cells (*Hoxa11*^{P3}) was examined. During the first days following tamoxifen administration, *Hoxa11*^{P3}-lineage marked cells are observed within the perichondrium surrounding the distal growth plate and on the periosteal, the endosteal, and the trabecular bone surfaces [Figure 2.3k]. At 24 hours following tamoxifen administration, *Hoxa11*^{P3}-lineage labeled cells are largely restricted to the periochondrium/periosteum and again show little overlap with Sox9-positive chondrocytes and Osx-positive osteoblasts [Figure 2.3l-m, brackets]. The pattern of *Hoxa11*^{P3}-labeling shows clear overlap with Hoxa11eGFP expression [Figure 2.3n].

Following an 8-week chase, *Hoxa11*^{P3}-lineage marked cells contribute to the skeleton and are observed on periosteal and endosteal bone surfaces as well as throughout

the bone marrow space [Figure 2.3o]. Similar to E13.5 lineage-induction, *Hoxa11*^{P3}-lineage marked cells give rise to the skeletal lineages within the zeugopod and lineage contribution is not observed in the stylopod at this or any stage [Figure 2.3o, inset]. *Hoxa11*^{P3}-lineage marked cells persist and continue to contribute to the skeleton through one year of age [Figure 2.3p-q]. Of note, lineage induction at postnatal stages looks indistinguishable from embryonic induction, consistent with the Hox11-expressing population representing skeletal progenitors with equivalent capacity at both stages.

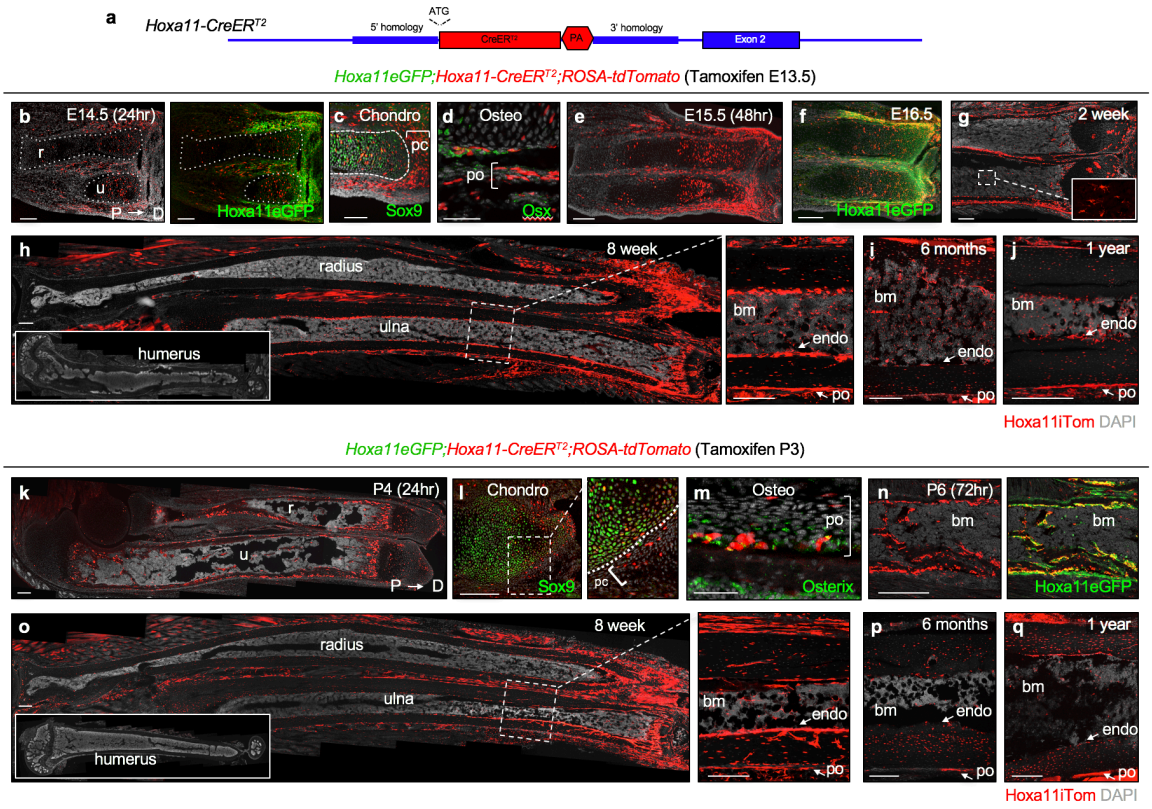

Figure 2.3. *Hoxa11*-lineage contributes to the zeugopod skeleton throughout life. (a) Schematic of *Hoxa11-CreER*^{T2} allele. Exon 1 of *Hoxa11* was replaced with *CreER*^{T2} followed by a rabbit β-globin poly-adenylation stop sequence (see materials and methods). Endogenous sequence in blue, edited sequence in red, start site marked by 'ATG'. (**b-j**) Pregnant females were given tamoxifen at E13.5 and resulting *Hoxa11eGFP;Hoxa11-CreER*^{T2}*;ROSA-tdTomato* animals were examined at indicated ages. Shown are complete limb (**b, e, h**), distal radius (r) and ulna (u) (**f-g**) or distal diaphysis region of tibia (**i-j**). (**c**) Expression of Hoxa11iTom and chondrocyte marker, Sox9 (green) at E14.5, dashed white lines demarcates anlage and bracket marks perichondrium (**d**) Expression of Hoxa11iTom and osteoblast marker, Osterix (green) at E14.5, bracket marks periosteum. (**f**) Co-

expression of Hoxa11eGFP and Hoxa11iTom. (**g**) Inset shows *Hoxa11*-lineage marked bone marrow stromal cells (white dashed box) (**k-q**) P3 pups received tamoxifen and *Hoxa11eGFP; Hoxa11-CreER^{T2}; ROSA-tdTomato* mice were examined at indicated ages. Shown are complete (**k**, **o**), mid-diaphysis ulna (**n**), or distal region of tibia (**p-q**). (**l**) Co-expression of Hoxa11iTom and chondrocyte marker, Sox9 (green) in the growth plate at P4 Boxed region enlarged to right, dashed white line demarcates perichondrial border. (**m**) Co-expression of Hoxa11iTom and osteoblast marker, Osterix (green) in the periosteum (bracket) at P4. (**b**, **n**) Right panel shows co-expression of Hoxa11iTom with Hoxa11eGFP (**h, o**) Inset shows complete humerus. Dashed white box shown magnified to right; view of mid-diaphysis ulna. All images shown with distal end of bone to right. In all images, red: *Hoxa11*-lineage marked cells (Hoxa11iTom), green: Hoxa11eGFP-expressing cells (unless otherwise noted), grey: DAPI. Bone marrow: bm, perichondrium: pc, periosteum: po, endosteum: endo. Scale bars: (**c, n**) 100μm, (**d**) 50μm. All other scale bars = 200μm.

Hoxa11 lineage becomes all skeletal/mesenchymal cell types

To assess the contribution of *Hoxa11-CreER^{T2}* lineage-marked cells to differentiated mesenchymal skeletal cell types at adult stages, we performed co-labeling with markers for cartilage, bone, and adipose tissues. *Hoxa11$^{E13.5}$*-lineage marked cells can be visually identified as differentiating into chondrocytes within the growth plate, co-staining with markers of differentiation identifies *Hoxa11$^{E13.5}$*-lineage cells as osteoblasts on the trabecular and endosteal bone surfaces, osteocytes embedded within the cortical bone, and as adipocytes in the bone marrow [Figure 2.4a]. Analysis out to one year of age shows that *Hoxa11$^{E13.5}$*-lineage marked cells continue to give rise to all skeletal lineages; chondrocytes, osteoblasts, osteocytes, as well as bone marrow adipocytes [Figure 2.4b]. At these stages, the growth plate has collapsed in mice, however *Hoxa11$^{E13.5}$*-lineage marked chondrocytes are observed throughout the articular cartilage [Figure 2.4b, yellow bracket]. It is important to note that, in adult mice, osteoblasts are reported to live for one month, therefore multiple rounds of osteoblast turnover have presumably occurred between E13.5 and 1 year of age[110,134–136].

The same analyses were performed on *Hoxa11*^{P3}-lineage marked stromal cells where essentially identical results are observed. *Hoxa11*^{P3}-lineage marked cells differentiate into all mesenchymal skeletal cell types, including chondrocytes, osteoblasts, osteocytes, and bone marrow adipocytes [Figure 2.4c]. *Hoxa11*^{P3}-lineage marked cells also continue to mark the same populations through one year of age [Supplemental Figure 2.4a].

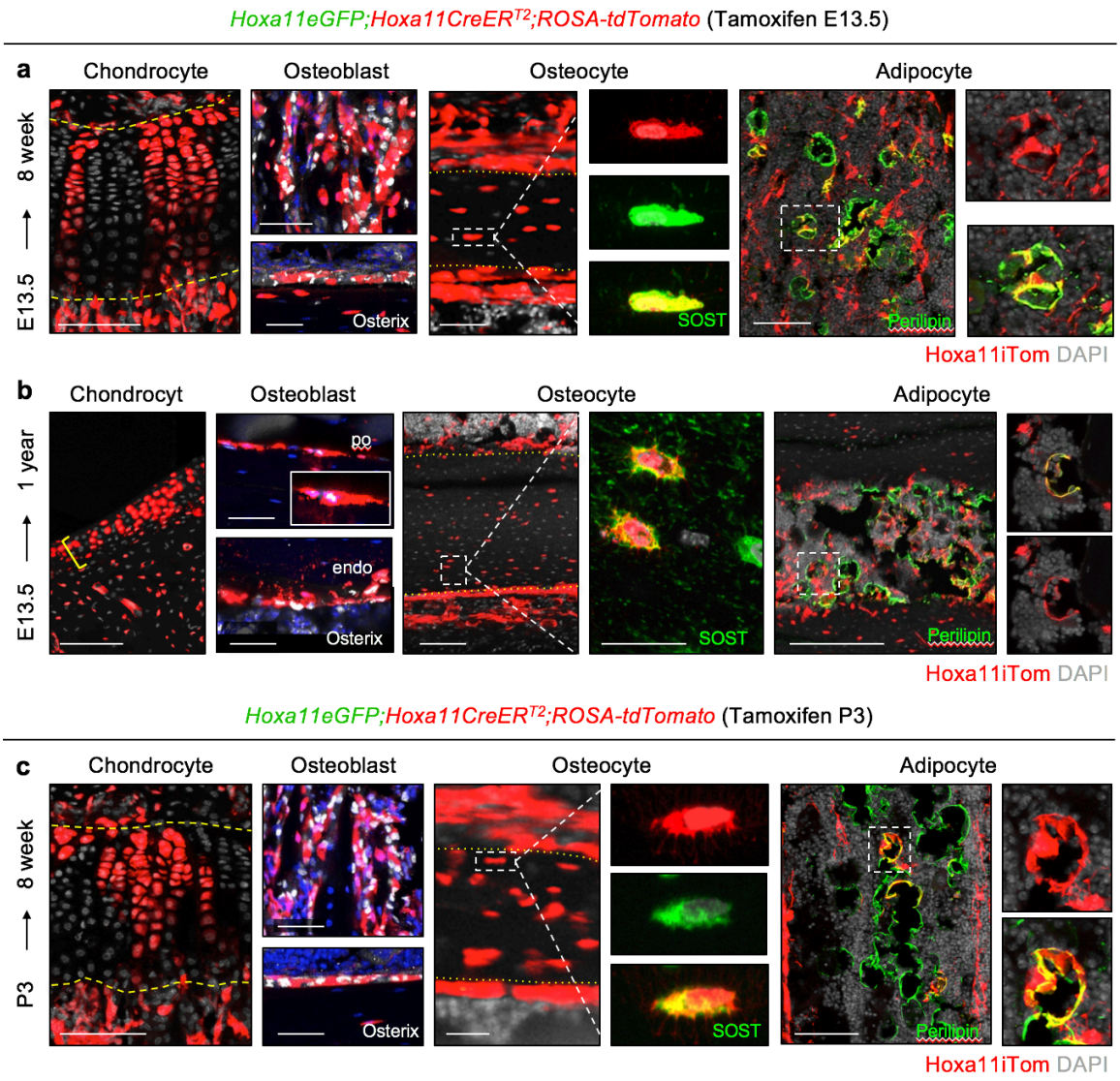

Figure 2.4. *Hoxa11*-lineage contributes to all skeletal/mesenchymal cell types. (**a-d**) Pregnant dams received E13.5 and resulting *Hoxa11eGFP;Hoxa11-CreER*^{T2}*;ROSA-tdTomato* mice were chased to (**a**) 8 weeks or (**b**) 1 year. (**c**) P3 pups received tamoxifen and *Hoxa11eGFP;Hoxa11-CreER*^{T2}*;ROSA-tdTomato* mice were chased to 8 weeks. All images, *Hoxa11* lineage-labeled cells (Hoxa11iTom, red). Shown are chondrocytes with

characteristic columnar morphology at distal end of growth plate, osteoblasts stained with Osterix (white) on trabecular (top) and endosteal bone (bottom), osteocytes within the cortical bone stained with SOST (green), and bone marrow adipocytes stained with Perilipin (green). Dashed yellow lines mark upper and lower boundaries of growth plate, dotted yellow lines mark periosteal and endosteal boundaries of cortical bone. White dashed boxed region of single (**a, c**) or multiple (**b**) osteocytes(s) magnified to right. White dotted box of single adipocyte magnified to right. In all images, grey or blue: DAPI. Scale bars: (chondrocyte and adipocytes images) 100μm, (osteoblast and osteocyte images) 50μm, (**b,** SOST) 25μm.

Hoxa11-marked progenitors are maintained throughout life

We next performed flow cytometry analyses on *Hoxa11*$^{E13.5}$-lineage marked stromal cells from the zeugopod bone marrow and bone surfaces to assess the cell surface identity of these cells. The majority of *Hoxa11*$^{E13.5}$-lineage marked stromal cells from both compartments were confined to the non-hematopoietic, non-endothelial stromal compartment (CD45-TER119-CD31-) [Supplemental Figure 2.3e]. Adult, *Hoxa11*$^{E13.5}$-lineage marked bone marrow stromal cells specifically express MSC markers PDGFRα/CD51 and LepR, demonstrating that the embryonically labeled Hoxa11-expressing cells give rise to adult, progenitor-enriched MSCs that are maintained throughout life [Figure 2.5a]. Similar flow cytometry profiles are observed for *Hoxa11*$^{E13.5}$-lineage marked cells that persist on the cortical bone surfaces, with the majority of labeled bone surface stromal cells co-expressing PDGFRα/CD51 and LepR as we have previously reported for real-time expression of Hoxa11eGFP [Figure 2.5a and [86]]. *Hoxa11*$^{E13.5}$-lineage marked cells continue to co-express these MSC markers through one year of age and beyond [Figure 2.5b]. Additionally, a majority of *Hoxa11*$^{E13.5}$-lineage marked cells co-express Hoxa11eGFP [Figure 5a and Supplemental Figure 2.3f, g]. Collectively these data provide evidence that the embryonic Hoxa11-expressing cell population gives rise to Hoxa11eGFP-expressing MSCs that persist throughout the life of the animal.

The same analyses were performed on *Hoxa11*^{P3}-lineage marked stromal cells and nearly identical results are observed. Flow cytometry analyses on adult, *Hoxa11*^{P3}-lineage marked bone marrow and bone surface stromal cells demonstrate that *Hoxa11*^{P3}-lineage marked cells are contained within the non-hematopoietic, non-endothelial stromal compartment and co-express progenitor-enriched MSC markers PDGFRα/CD51 and LepR in both the bone marrow and bone surface compartments and continue to co-express these MSC markers out to one year of age [Figure 2.5c-d and Supplemental Figure 2.4b]. *Hoxa11*^{P3}-lineage marked cells also express Hoxa11eGFP in both compartments [Supplemental Figure 2.4c].

Hoxa11-lineage regenerates bone and cartilage upon fracture

To examine whether *Hoxa11*-lineage marked cells serve as progenitors in regeneration and repair of the skeleton following injury, *Hoxa11CreER*^{T2}*;ROSA26-LSL-tdTomato* animals were administered tamoxifen at E13.5 or at P3 to initiate lineage-labeling and the ulna was fractured at adult stages (8-10 weeks of age). Contribution to regenerating cartilage and bone was analyzed 10 days post-injury (10 DPI). *Hox11*$^{E13.5}$- and *Hoxa11*^{P3}-lineage marked cells expand in response to fracture and are observed throughout the callus [Figure 2.6a, d]. Apparent expansion of both the periosteal stromal compartment and the bone marrow stromal compartment is observed. *Hoxa11* lineage-marked cells give rise to both Sox9-positive chondrocytes within the cartilaginous regions of the callus and to Osx-expressing osteoblasts within the woven bone regions of the callus [Figure 2.6b, c, e, f].

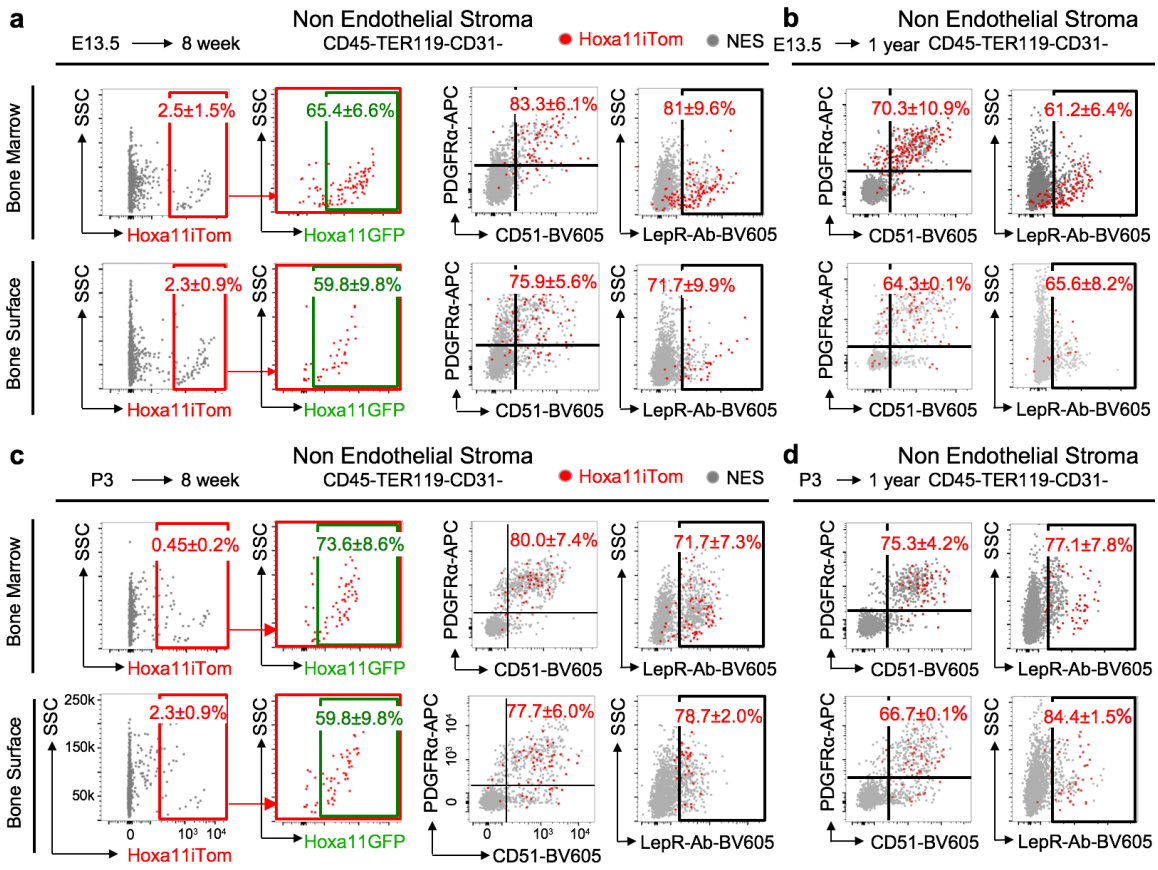

Figure 2.5. *Hoxa11*-lineage marked progenitors are maintained throughout life Pregnant dams received E13.5 and resulting *Hoxa11eGFP;Hoxa11-CreER^{T2};ROSA-tdTomato* mice were chased to (**a**) 8 weeks [n=3] or (**b**) 1 year [n=4]. P3 pups received tamoxifen and *Hoxa11eGFP;Hoxa11-CreER^{T2};ROSA-tdTomato* mice were chased to (**c**) 8 weeks [n=6] or (**d**) 1 year [n=3]. Flow cytometry analyses of non-hematopoietic, non-endothelial stromal compartment (CD45-TER119-CD31-, NES) in bone marrow (top panels) and bone surface (bottom panels). (**a, c**) First panel: *Hoxa11* lineage-marked cells (x-axis: Hoxa11iTom), second panel: analysis of Hoxa11iTom positive gate (red) for Hoxa11eGFP expression, third panel: co-expression analysis of PDGFRα/CD51, fourth panel: co-expression analysis of Leptin Receptor (LepR-Ab). (**b, d**) Left: co-expression analysis of PDGFRα/CD51, right: co-expression analysis of Leptin Receptor (LepR-Ab). Percentages reflect proportion of Hoxa11iTom population in identified gate. Grey dots: total non-endothelial stroma (NES), red dots: Hoxa11iTom. 'n' values indicate biologically independent animals for each time point. All data presented as mean ± standard deviation.

Contribution of *Hoxa11*-lineage marked cells to the regenerating skeletal tissues is qualitatively equivalent whether lineage-tracing is initiated at embryonic or postnatal

stages, demonstrating that Hoxa11-positive cells from both stages represent roughly equivalent, functional, adult skeletal MSCs.

To test the continued functionality of the *Hoxa11*-lineage marked progenitor population throughout life, we allowed lineage-marked animals to age to 10 months prior to ulnar fracture. At late adult stages, the *Hoxa11*^{P3}-lineage marked cell population expands robustly following injury and contributes to regenerating cartilage and bone 10DPI [Figure 2.6g-i]. Additionally, the expanded lineage-marked stromal cells are Hoxa11eGFP-positive, representing expanding progenitors as shown previously [Figure 2.6j and [86]]. Lineage-marked cells within the periosteal region of the fracture callus are also periostin-positive, consistent with expansion of Hox11-expressing periosteal stem cells following injury [Figure 2.6k].

Comparison of Hoxa11-lineage to other MSC populations

A critical knowledge gap in the field is an understanding of the relationships between various identified MSC progenitor populations. Significant differences exist in the lineage-dynamics of these populations, yet the reasons for these differences are not clearly understood. We sought to establish the relationship between Hox11-expressing cells and previously reported MSC populations genetically labeled by *LepR-Cre* and *Osx-CreER* using our *Hoxa11eGFP* real-time reporter crossed to *LepR-Cre;ROSA26-LSL-tdTomato* mice or *Osx-CreER;ROSA26-LSL-tdTomato* mice.

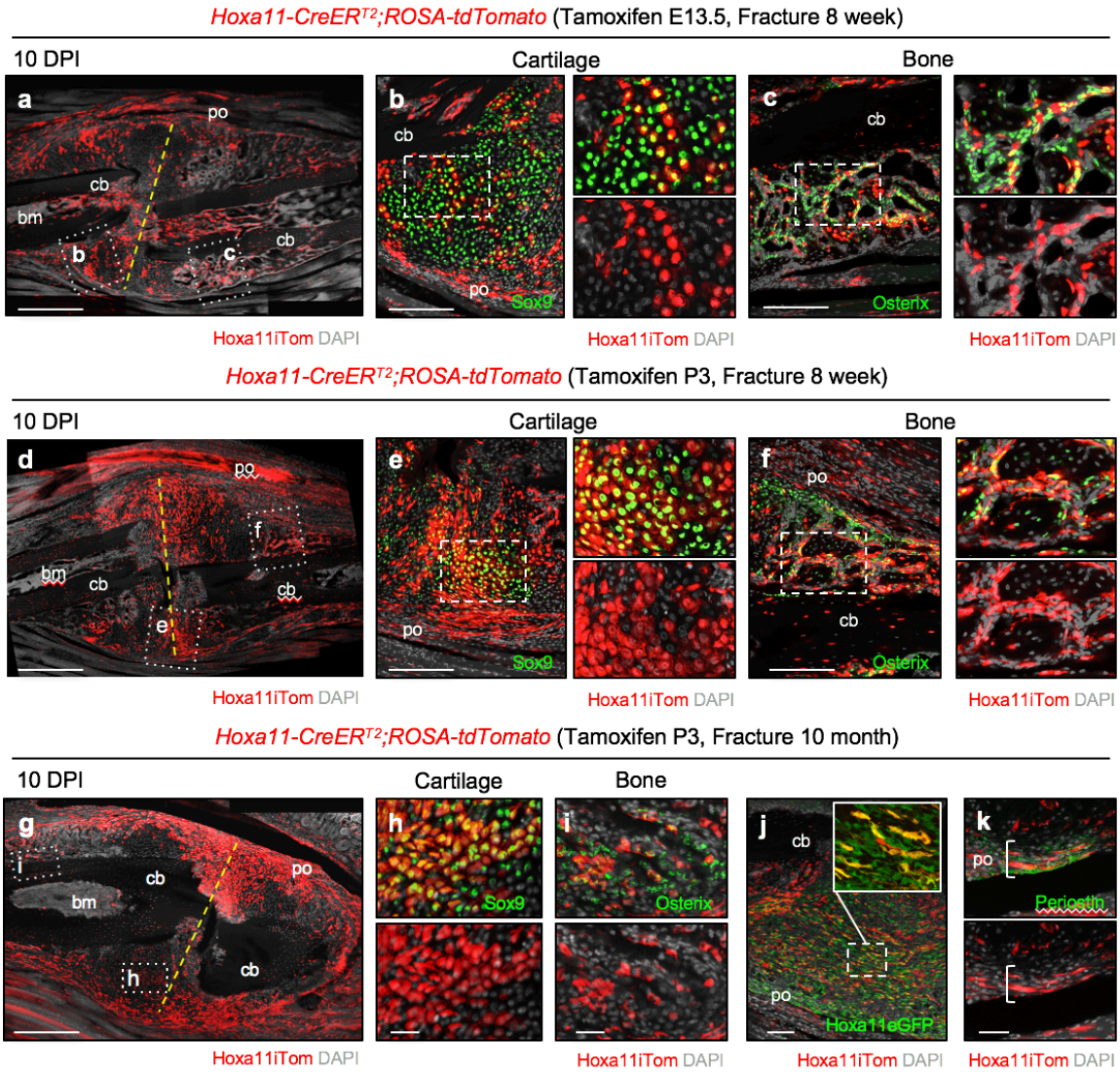

Figure 2.6. *Hoxa11*-lineage cells regenerate skeleton following fracture. Ulnar fracture was performed at 8 weeks of age (**a-f**) or 10 months (**g-k**) on *Hoxa11-CreER^{T2};ROSA-tdTomato* or *Hoxa11eGFP;Hoxa11-CreER^{T2};ROSA-tdTomato* mice following tamoxifen dosing at (**a-c**) E13.5 – to pregnant female, or (**d-k**) P3. (**a, d, g**) *Hoxa11* lineage-positive cells (Hoxa11iTom, red) within the fracture callus 10 days post-injury (DPI). Fracture line marked with dashed yellow line and cortical bone (cb), bone marrow (bm), and periosteum (po) are labeled. Dashed white lines indicate regions visualized with antibodies (green) for cartilage (Sox9, **b, e, h**) and bone (Osx, **c, f, i**). Higher magnification of regions marked by dashed white lines (**b, c, e, f**) with channels separated shown to right. (**j**) Expression of Hoxa11eGFP (green) and Hoxa11iTom within the expanded stromal population. White dashed box magnified in inset. (**k**) Expression of Periostin (green) and Hoxa11iTom within the expanded periosteal compartment (bracket). In all images, grey: DAPI. Scale bars: (**a, d, g**) 500μm, (**b-c, e-f**) 200μm, (**j**) 100μm, (**h-i, k**) 50μm.

LepR-Cre lineage-marked cells first appear during late embryonic stages within the primary spongiosa [Figure 2.7a and [112,115,126]]. At this stage, Hoxa11eGFP-expressing cells are more extensively observed throughout the periosteum and along the bone surfaces of the primary spongiosa. There is only very rare overlap between *LepR-Cre* lineage-marked cells and Hoxa11eGFP at early stages [Figure 2.7a, arrowheads]. The number of *LepR-Cre* lineage-marked cells increases markedly during postnatal development. In the bone marrow, the overlap between Hoxa11eGFP and *LepR* lineage-marked cells also progressively increases with age with more of the Hoxa11eGFP-positive cells also becoming LepR-positive [Figure 2.7b-e and Supplemental Figure 2.5]. By 15 weeks, the majority of Hoxa11eGFP-expressing bone marrow stromal cells are also *LepR*-lineage positive [Figure 2.7e and Supplemental Figure 2.5 and [86]]. The number of *LepR-Cre* lineage-marked cells on the periosteal and endosteal bone surfaces also increases with age, however even as late as 15 weeks of age, only half of Hoxa11eGFP, bone-adherent cells are *LepR*-lineage positive [Figure 2.7b'-e' and Supplemental Figure 2.5]. Interestingly, there is a population of Hoxa11eGFP-expressing cells on the outer perichondrial surface that remains *LepR-Cre* lineage-negative at all stages examined [Figure 2.7d'-e', arrowheads]. These results are consistent with *LepR*-lineage labeling continuing to initiate in Hoxa11-positive cells [Figure 2.7f]. Differences in the overlap between the bone marrow and bone adherent populations reveal a unique Hoxa11-expressing population in the periosteum, perhaps explaining, at least in part, the earlier and more extensive *Hoxa11*-lineage contribution to differentiated skeletal cells.

Previous reports demonstrate O*sx*-lineage contribution to MSCs when induction is initiated at postnatal stages but the absence of long-term lineage contribution when induced

at embryonic stages[115,127]. We induced *Osx*-lineage labeling in *Hoxa11eGFP;Osx-CreER;ROSA26-LSL-tdTomato* animals at E13.5 or at P3 to compare these populations to Hoxa11eGFP-expressing cells. One day following tamoxifen administration at E13.5, embryonic *Osx*-lineage ($Osx^{E13.5}$) marked cells are restricted to the inner periosteal, pre-osteoblast layer, while Hox11-expressing cells are restricted to

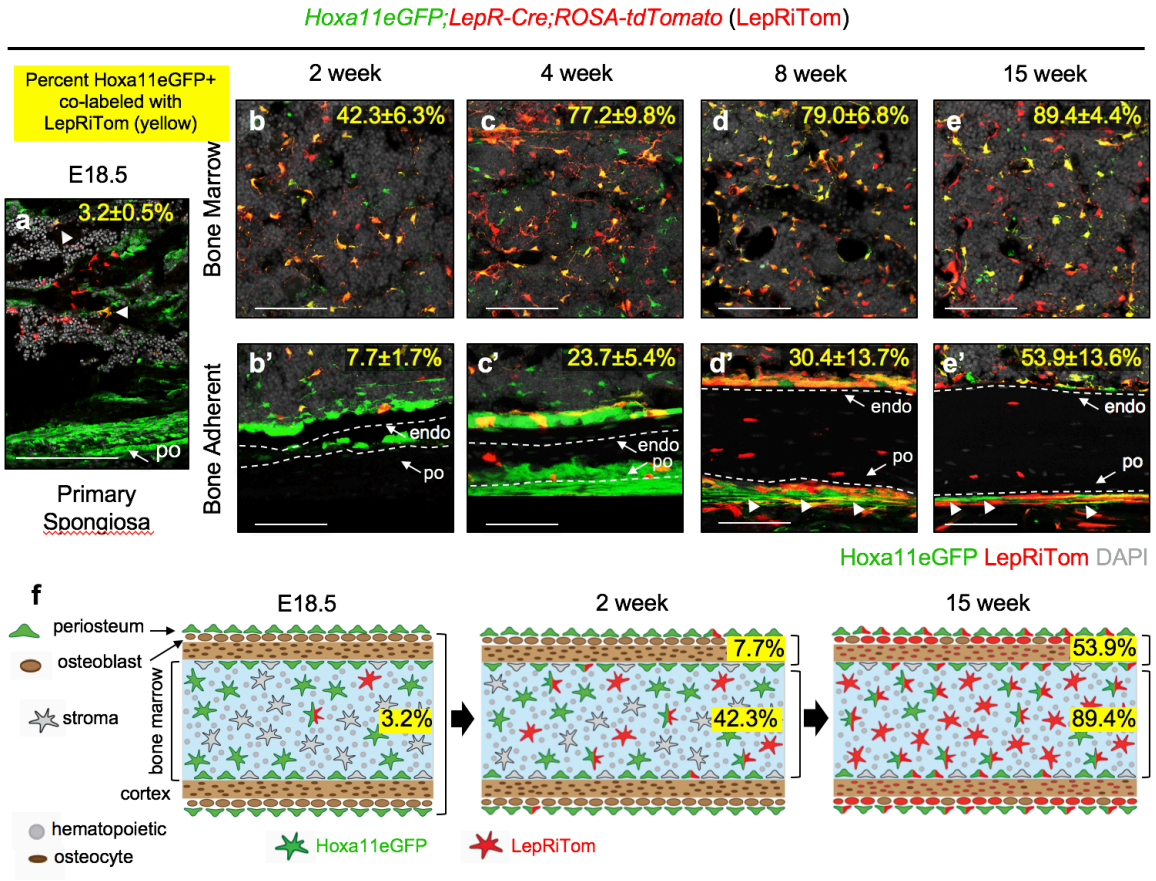

Figure 2.7. *LepR-Cre* progressively marks existing Hoxa11eGFP-positive cells. Analysis of the co-expression of Hoxa11eGFP (green) and LepR-Cre lineage-marked cells (LepRiTom, red) in *Hoxa11eGFP;LepR-Cre;ROSA-tdTomato* mice. Percentages (yellow) reflect proportion of Hoxa11eGFP-positive cells that also express LepRiTom. Flow cytometry analyses shown in Supplemental Figure 5. (**a**) magnified view of primary spongiosa and developing cortical bone surface at E18.5 [n=3]. (**b-e'**) High magnification view of mid-diaphysis of ulna (**b-e**) bone marrow, or (**b'-e'**) cortical bone. (**d',e'**) at 2 [n=4], 4 [n=3], 8 [n=3], and 15 weeks [n=3]. Arrowheads identify non-overlapping Hoxa11eGFP-positive periosteal cells. In all images; grey: DAPI. Data presented as mean ± standard deviation. 'n' values indicate biologically independent animals for each time point. (**f**) Diagram of data at E18.5, 2 weeks, and 15 weeks. All scale bars: 100μm.

the outer periosteal layer with little to no overlap observed [Figure 2.8a-b]. *Osx-CreER* lineage induction at E13.5 also labels hypertrophic chondrocytes in the developing bone. The pattern of $Osx^{E13.5}$-lineage marked cells is consistent with Osterix protein expression using an anti-Osterix antibody [compare Figure 2.8b and Figure 2.1b]. By E18.5, $Osx^{E13.5}$-lineage marked cells are observed throughout the primary spongiosa and minimal co-expression with Hoxa11eGFP is observed [Figure 2.8c-e, arrows]. Hoxa11eGFP-expressing cells and $Osx^{E13.5}$-lineage marked cells continue to exhibit an almost mutually exclusive stratified pattern in the periosteum, with $Osx^{E13.5}$-lineage marked cells in the inner pre-osteoblast layer and Hoxa11eGFP the adjacent outer periosteal layer [Figure 2.8e]. OsxE13.5-lineage marked cells and Hoxa11eGFP-expressing cells show a small degree of overlap in the adult bone marrow and on the endosteal bone surface [Figure 2.8f-i]. However, $Osx^{E13.5}$-lineage marked cells are rare at adult time points and represent only 2.7±0.3% of the total Hoxa11eGFP-positive population [Figure 2.8i]. Flow cytometry analyses of the small population of bone marrow $Osx^{E13.5}$-lineage marked cells shows 74.0±3.4% co-express PDGFRα/CD51 and 69.3±8.3% co-expresses Hoxa11eGFP [Figure 2.8i]. Virtually no $Osx^{E13.5}$-lineage marked cells remain on the bone surfaces by adult stages, having presumably differentiated into osteoblasts and osteocytes by 8 weeks [Figure 2.8g, i]. As these two populations do not progressively overlap with age, these data reveal that the Hoxa11eGFP-positive perichondrial/periosteal population is distinct from the embryonic $Osx^{E13.5}$-lineage marked cells [Figure 2.8j].

At the earliest stages of limb development, Hox11 expression is not confined to the zeugopod but is broadly expressed in the lateral plate mesoderm[88]. Tamoxifen was administered to *Hoxa11-CreER*^{T2}*;ROSA-tdTomato* animals at E11.5 ($Hox11^{E11.5}$), two days

prior to initiation of Osterix expression in the developing skeleton, and the contribution of *Hoxa11*$^{E11.5}$-lineage marked cells to the skeleton was assessed. At E14.5, *Hoxa11*$^{E11.5}$-lineage marked cells have contributed significantly to the developing skeleton including Osx-positive osteoprogenitors within the developing periosteum [Figure 2.8k, inset]. There is additionally contribution to Sox9-positive chondro-progenitors throughout the distal growth plate consistent with Hox11-expressing cells serving as upstream progenitors for this population as well, as expected for a broad marker of lateral plate mesoderm [Figure 2.8l]. *Hoxa11*$^{E11.5}$-lineage marked cells continue to contribute extensively to the developing skeleton, including significant contribution to osteoblasts on the trabecular and cortical bone surfaces [Figure 2.8m-p]. These data show that the *Hoxa11*-lineage arises prior to the *Osx*-lineage, and that Hox11-expressing cells serve as primitive progenitors that give rise to early osteoprogenitor and the osteoblast lineage.

Consistent with the reported progenitor capacity of the postnatal *Osx*-lineage marked population (*Osx*^{P3}), some overlap is observed between Hoxa11eGFP-expressing cells and *Osx*^{P3}-lineage marked cells at this stage. Three days following tamoxifen administration, *Osx*^{P3}-lineage marked cells are localized to the bone surfaces (periosteal, endosteal, and trabecular) [Figure 2.9a-b]. The Hoxa11eGFP-expressing cells that are observed in the periosteum overlap with *Osx*^{P3}-lineage marked cells at the innermost periosteal layer, but additional non-overlapping Hoxa11eGFP-positive cells are observed in the outer periosteum [Figure 2.9b]. Hoxa11eGFP-positive cells are also already present at this stage throughout the bone marrow space and no co-expression with rare *Osx*^{P3}-lineage marked bone marrow cells is observed [Figure 2.9c, arrow]. Following an 8-week chase, *Osx*^{P3}-lineage marked cells contribute to bone, fat, and bone marrow stromal cells,

consistent with previous reports [Figure 2.9d-f and [115]]. Most *Osx*^{P3}-lineage marked cells in the bone marrow co-express Hoxa11eGFP and markers for progenitor-enriched MSCs, PDGFRα/CD51 [Figure 2.9f-g]. On the bone surfaces, only about half of *Osx*^{P3}-lineage marked cells co-express PDGFRα/CD51 and Hoxa11eGFP [Figure 2.9e, g]. The remaining population likely reflects lineage-marked pre-osteoblasts. Interestingly, the majority of overlap between Hoxa11eGFP-expressing cells and *Osx*^{P3}-lineage marked cells is observed on the endosteal surface, while a stratified, non-overlapping expression pattern continues to be observed on the periosteal surface [Figure 2.9d-e]. Of note, *Osx*^{P3}-lineage marked cells at adult stages represent only a small fraction of the total Hoxa11eGFP-positive population, ~11% [Figure 2.9g]. These data show that *Osx-CreER* marks a sub-population of Hox11-expressing MSCs at postnatal stages that persist to adult stages [Figure 2.9h]. These data additionally highlight the unique Hox11-expressing population in the outer periosteum, adjacent to the Osx-positive inner pre-osteoblast periosteal layer that does not overlap with *Osx*-lineage marked cells at any stage examined.

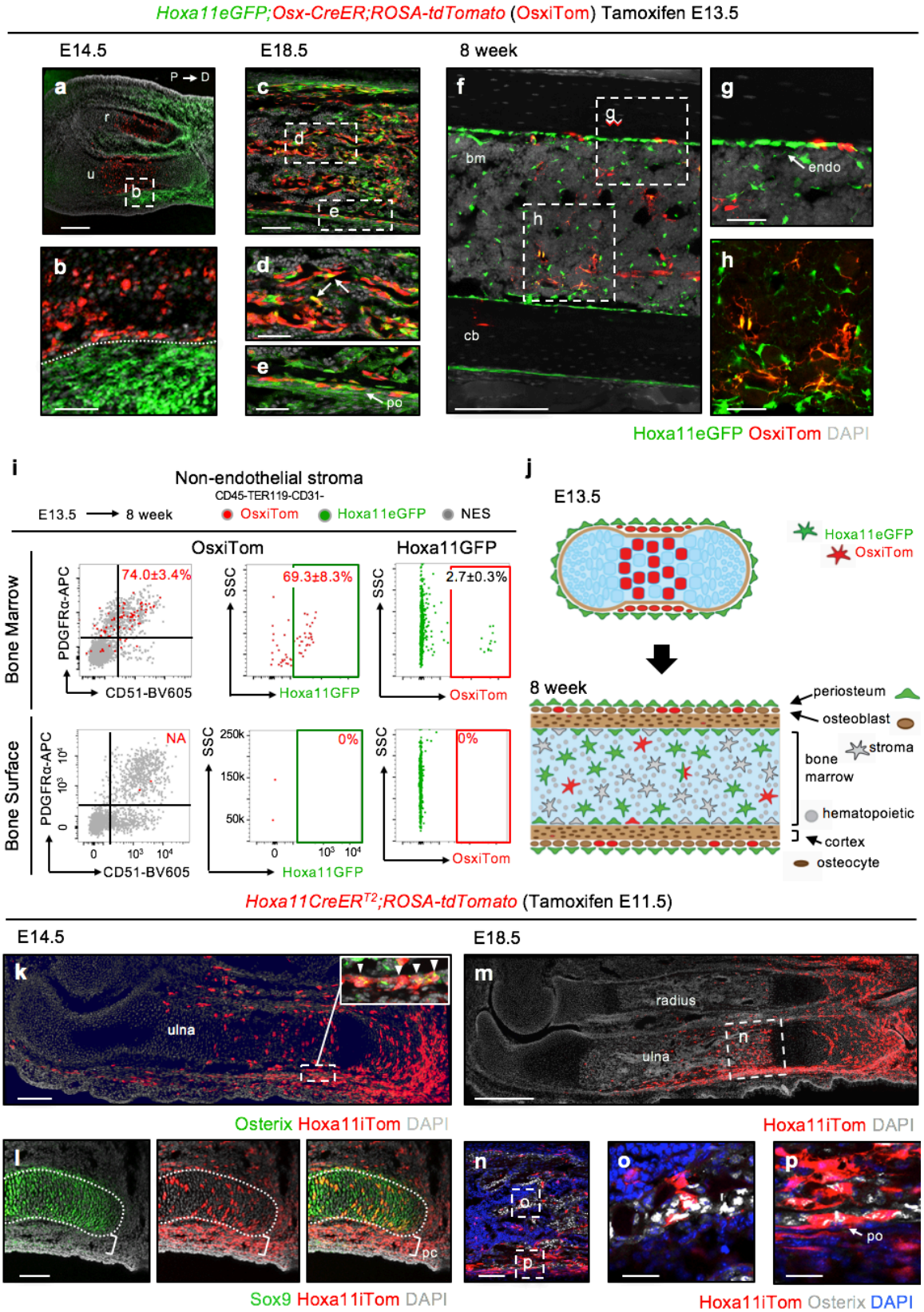
Hoxa11eGFP;Osx-CreER;ROSA-tdTomato (OsxiTom) Tamoxifen E13.5
E14.5
E18.5
8 week
Hoxa11eGFP OsxiTom DAPI
Non-endothelial stroma
CD45-TER119-CD31-
E13.5 → 8 week
OsxiTom
Hoxa11eGFP
NES
Bone Marrow
Bone Surface
74.0±3.4%
69.3±8.3%
2.7±0.3%
NA
0%
PDGFRα-APC
CD51-BV605
SSC
Hoxa11GFP
periosteum
osteoblast
stroma
bone marrow
hematopoietic
cortex
osteocyte
Hoxa11CreER^T2;ROSA-tdTomato (Tamoxifen E11.5)
ulna
radius
Osterix Hoxa11iTom DAPI
Hoxa11iTom DAPI
Sox9 Hoxa11iTom DAPI
Hoxa11iTom Osterix DAPI

Figure 2.8. Hoxa11eGFP-positive MSCs are distinct from embryonic *Osx*-lineage. Comparison of Hoxa11eGFP (green) and *Osx-CreER* lineage-marked cells (OsxiTom, red) was performed in *Hoxa11eGFP;Osx-CreER;ROSA-tdTomato* mice. (**a-g**) Pregnant females received tamoxifen at E13.5 and co-expression of Hoxa11eGFP and embryonic *Osx*-lineage was examined at (**a-b**) E14.5, (**c-d**) E18.5 and (**f-i**) 8 weeks. (**a**) Complete radius (r) and ulna (u) 24 hours after tamoxifen with proximal to the left and distal to the right. White box region magnified in (**b**) anlagen boundary indicated by dotted white line. (**c**) Mid-diaphysis ulna; white dashed boxes indicate magnified region of (**d**) primary spongiosa and (**e**) periosteum. (**f**) Mid-diaphysis tibia; white dashed boxes indicate magnified region of adult (**g**) endosteal surface and (**h**) bone marrow. (**i**) Flow cytometry analysis of non-hematopoietic, non-endothelial stroma (CD45-TER119-CD31-, NES) in bone marrow (top panels) and bone adherent (bottom panels) compartments. First panel: analysis of OsxiTom population for PDGFRα/CD51, second panel: analysis of OsxiTom for Hoxa11eGFP, third panel: analysis of Hoxa11eGFP-positive cells (green) for OsxiTom expression. OsxiTom cells are very rare (0.018±0.03 of total NES) on bone surface (lower left panel). n=3 biologically independent animals. Flow cytometry dot plots, grey dots: total non-endothelial stroma (NES). Data presented as mean ± standard deviation. (**j**) Diagrammatic representations of data. **(**k**)** Pregnant females received tamoxifen at E11.5 and *Hoxa11-CreER^{T2};ROSA-tdTomato* embryos were analyzed at (**k-l**) E14.5 and (**m-p**) E18.5. (**k**) White boxed region shown in inset, co-expression of Hoxa11iTom (red) and Osterix (green). (**m**) white boxed region of primary spongiosa magnified in **n**. (**n**) white dashed boxes indicate magnified regions of (**o**) trabeculae and (**p**) periosteum. Periosteum: po, bone marrow: bm, cortical bone: cb, endosteum: endo All fluorescent images, grey: DAPI. Scale bars: (**a, f, k**) 200μm, (**b, d-e, g-h**) 50μm, (**c, i, n**) 100μm, (**o-p**) 25μm.

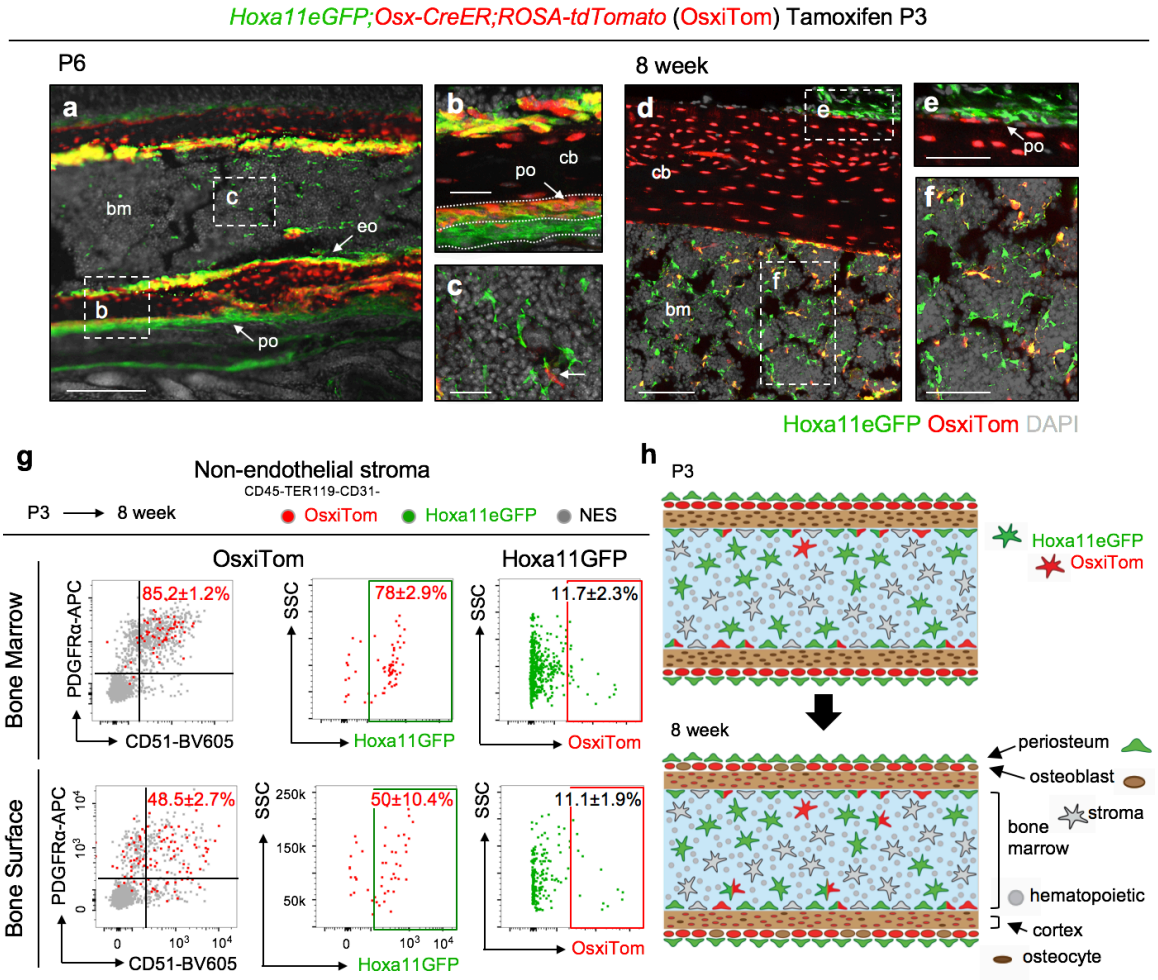

Figure 2.9. Postnatal *Osx*-lineage marginally overlaps with Hoxa11eGFP-positive cells. Comparison of Hoxa11eGFP (green) and *Osx-CreER* lineage-marked cells (OsxiTom, red) was performed in *Hoxa11eGFP;Osx-CreER;ROSA-tdTomato* mice. P3 pups received tamoxifen and co-expression of Hoxa11eGFP and postnatal *Osx*-lineage was examined at (**a-c**) P6 and (**d-f**) 8 weeks. (**a**) Mid-diaphysis ulna; dashed white boxes indicate magnified (**b**) cortical bone and (**c**) bone marrow, rare OsxiTom stromal cell (arrow). (**d**) Mid-diaphysis tibia, white dashed boxes indicate magnified (**e**) periosteum and (**f**) bone marrow. (**g**) Flow cytometry analysis of non-hematopoietic, non-endothelial stroma (CD45-TER119-CD31-) in bone marrow (top panels) and bone surface (bottom panels) compartments. First panel: analysis of OsxiTom population for PDGFRα/CD51, second panel: analysis of OsxiTom for Hoxa11eGFP, third panel: analysis of Hoxa11eGFP-positive cells (green) for OsxiTom expression. n=4 biologically independent animals. Flow cytometry dot plots, grey dots: total non-endothelial stroma (NES). Data presented as mean ± standard deviation. (**h**) Diagrammatic representations of data. Periosteum: po, bone marrow: bm, cortical bone: cb, endosteum: endo All fluorescent images, grey: DAPI. Scale bars: (**a**) 200μm, (**b-c, e-f**) 50μm, (**d**) 100μm.

Discussion

Previous lineage analyses support a model whereby transient, embryonic, skeletal progenitors are replaced with *bona fide* adult skeletal stem cells that are established during early postnatal life[107,137]. A substantial caveat to many of these genetic tools is that tamoxifen-inducible *Cre* expression is driven by promoters for genes that function in early lineage commitment to skeletal cell types (for instance chondrocyte – *Sox9-CreER*, *PthrP-CreER*, and *Aggrecan-CreER*, or osteoblast – *Osx-CreER*)[115,127] (reviewed by [138]). Therefore, the bulk of these lineage-marked cells will be committed to the chondrocyte or osteoblast fate while only a small population of progenitors will be marked by these alleles. Labeling of long-term skeletal progenitors by these models is incomplete and the temporal differences in MSC capacity observed likely reflects depletion of early committed progenitors over time. Other genetic models, driven by promoters of genes involved in key signaling pathways such as Hedgehog (*Gli1-CreER*), BMP (*Gremlin1-CreER*) or Parathyroid hormone-related protein (*PthrP-CreER*), also demonstrate temporal differences in progenitor capacity over time[111,128,129]. These signaling pathways are important for chondrogenic and osteogenic differentiation and differences in the progenitor capacity of these lineage-marked populations with time may reflect changes in the signaling environment of the skeleton and reporter/lineage expression, in these cases, would not be expected to specifically label the skeletal progenitor pool[139–142].

Prior reports establish that *Hox* expression is excluded from differentiated skeletal cell types at all stages and loss-of-function analyses at embryonic, postnatal, and adult stages provide evidence for *Hox* gene function in the skeleton throughout life[85–87]. Herein, we present evidence that Hox11-expressing stromal cells, marked by *Hoxa11-CreER*^{T2}

from both embryonic and postnatal stages, specifically enrich for a population of skeletal progenitors throughout the life of the animal and are likely to encompass a *bona fide* skeletal stem cell population. In contrast to models asserting that developmental progenitors are later replaced by postnatally arising adult MSCs, these data reveal a lineage-continuous population that is maintained from embryonic through adult stages. *Hoxa11* lineage-marked cells contribute extensively to the skeleton, giving rise to all skeletal cell types including chondrocytes, osteoblasts, osteocytes, and bone marrow adipocytes at all stages examined. *Hoxa11* lineage-marked cells additionally persist within the bone marrow space and on the cortical bone surfaces throughout life and maintain co-expression of MSC markers. Further, Hoxa11eGFP/*Hoxa11* lineage-marked cells expand following fracture injury and contribute to regenerating cartilage and bone, even when injury is induced at late adult stages, demonstrating that Hox11-expressing MSCs functionally give rise to new skeletal cells throughout life. The collective evidence demonstrates a continuous lineage relationship between the embryonic and the adult Hox11-expressing skeletal progenitor, MSC population. The data provides *in vivo* evidence that the Hox11-expressing stromal population enriches for life-long, self-renewing skeletal MSCs.

Assessing the relationship between different genetically-defined populations of skeletal progenitors is critical for understanding how these populations behave and can provide information on the spatiotemporal dynamics of skeletal stem cells. *Hoxa11* lineage-marked progenitors arise days prior to the differentiation of pre-osteoblasts (as defined by *Osx* expression that begins ~E13.5) or *LepR-Cre* (initiates ~E17.5). Given *LepR-Cre* is not a temporally controlled Cre, the progressive overlap of Hoxa11eGFP and

LepR-lineage marked cells suggest that *LepR-Cre* transgenic expression, and thus, the *LepR*-lineage, is increasingly initiated within the Hoxa11eGFP-positive population. Also, considering the adjacent but non-overlapping organization of Hoxa11eGFP-expressing cells and *Osx*-lineage marked cells in the periosteum, these data lead to the conclusion that Hox-expressing progenitors in the outer periosteum give rise to the population marked by *Osx-CreER*, and subsequently the complete osteo-lineage. These comparative experiments demonstrate that the *Hoxa11eGFP*-expressing stromal population serves as the upstream population that gives rise to populations labeled by *Osx-CreER* and *LepR-Cre*.

Examination of the spatial overlap between Hoxa11eGFP-expressing cells and the populations marked by *Osx-CreER* or *LepR-Cre* revealed a Hoxa11eGFP-expressing population that is uniquely present in the outer periosteum. This population is non-overlapping with either the *LepR* lineage-marked population or the *Osx-CreER*-marked population after short- or long-term lineage-labeling. The periosteal compartment has recently been shown to contain skeletal stem cells, identified by expression of periostin, with greater capacity to regenerate bone compared to bone marrow MSCs[124]. Hox11-expressing cells in the inner periosteal layer overlap with the pattern of periostin expression, at homeostasis and following fracture, providing evidence to corroborate that this spatially defined sub-population of periosteal cells may be, at least in part, the *bona fide* skeleton stem cell population. Through a series of sophisticated transplantation studies, Duchamp de Lageneste *et al*. demonstrated that adult periosteal and adult bone marrow MSCs both derive from the local embryonic perichondrial/periosteal mesenchyme[124]. Our *Hoxa11*-lineage tracing data provides direct *in vivo* evidence that is in complete concordance with this conclusion.

We previously reported that adult bone marrow MSCs from different anatomical regions display a differential Hox expression profile. Specifically, each skeletal compartment maintains the *Hox* expression that is established during embryonic development[86]. Importantly, *Hox* expression in the adult bone marrow is confined to only progenitor-enriched MSCs. *Hoxa11-CreER^{T2}* allows for the unique, *in vivo* labeling of the zeugopod-restricted MSC population and shows that skeletal contributions of MSCs remain regional throughout life. Skeletal MSCs are not mobile; they remain at or near their site of origin. Our data support a model whereby regional, Hox-expressing stem cell populations in the skeleton are established during embryonic development and give rise to regionally-restricted, skeletal mesenchymal stem cells that self-renew and function throughout the life of the animal.

Supplemental Information

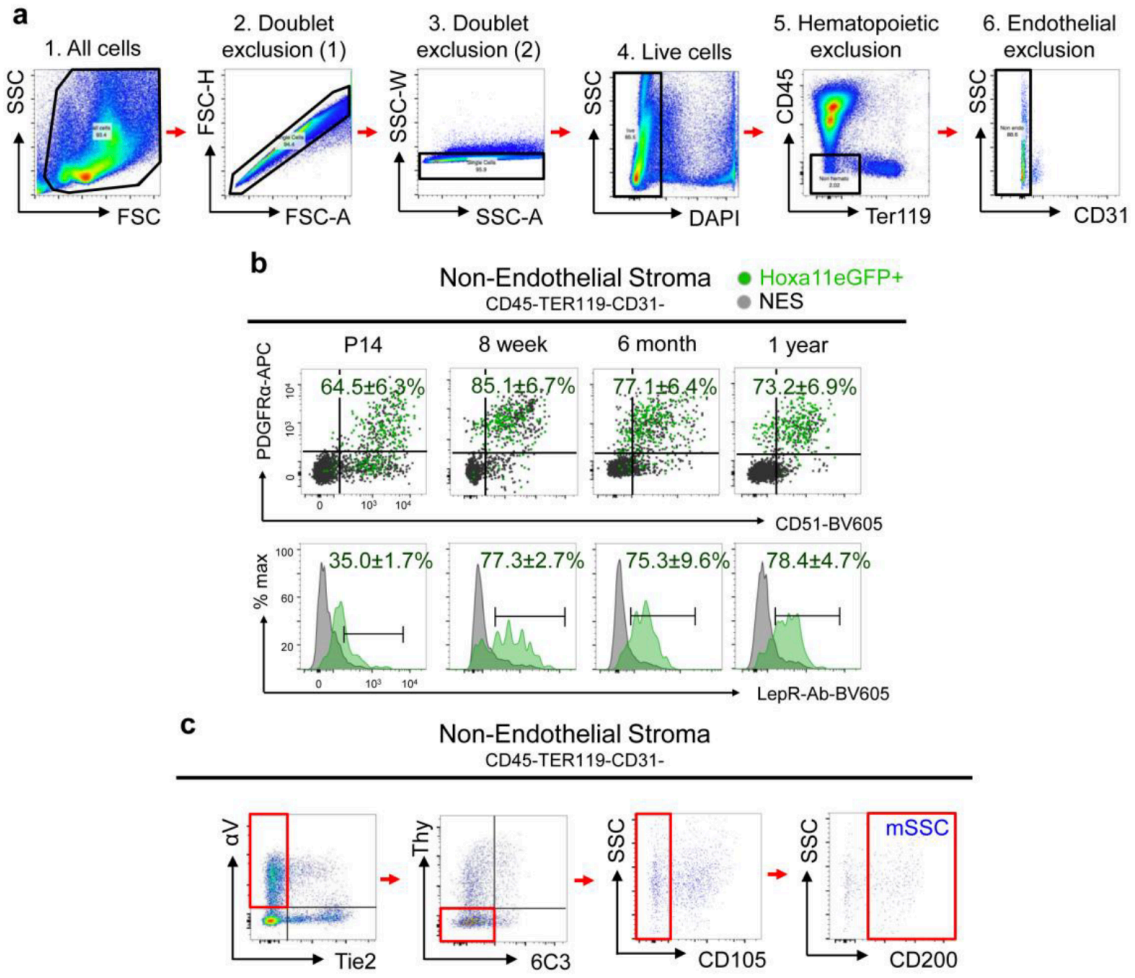

Supplemental Figure 2.1. Bone adherent Hoxa11eGFP-positive cells express MSC markers PDGFRα/CD51 and Leptin Receptor. (**a**) Gating strategy to obtain non-hematopoietic, non-endothelial stromal compartment. Example from adult (8-10wk) bone marrow. Strategy applies to data generated in Figures 2.2, 2.5, 2.7, 2.8i, and 2.9g and Supplemental Figures 1b, 3e, 4b, and 5. (**b**) Compliment to Figure 2a, flow cytometry analyses of bone adherent compartment (P14, 8 week, 6 month, and 1 year). Non-hematopoietic, non-endothelial stromal compartment (CD45-TER119-CD31-) was gated on PDGFRα/CD51 (top) or Leptin Receptor (LepR-Ab, bottom). Percentages reflect proportion of Hoxa11eGFP-positive population within double positive gate (top) or bracketed region of histogram (bottom). Charcoal dots or grey histogram: total non-endothelial stroma (NES), green dots or green histogram: Hoxa11eGFP-expressing non-endothelial stroma (Hoxa11eGFP+). All data presented as mean ± standard deviation. (**c**) Gating strategy to obtain mouse skeletal stem cell (mSSC) population (CD45-TER119-CD31-αV+Thy-6C3-CD105-CD200+) from non-endothelial stroma population. Strategy applies to Figure 2.2b-c.

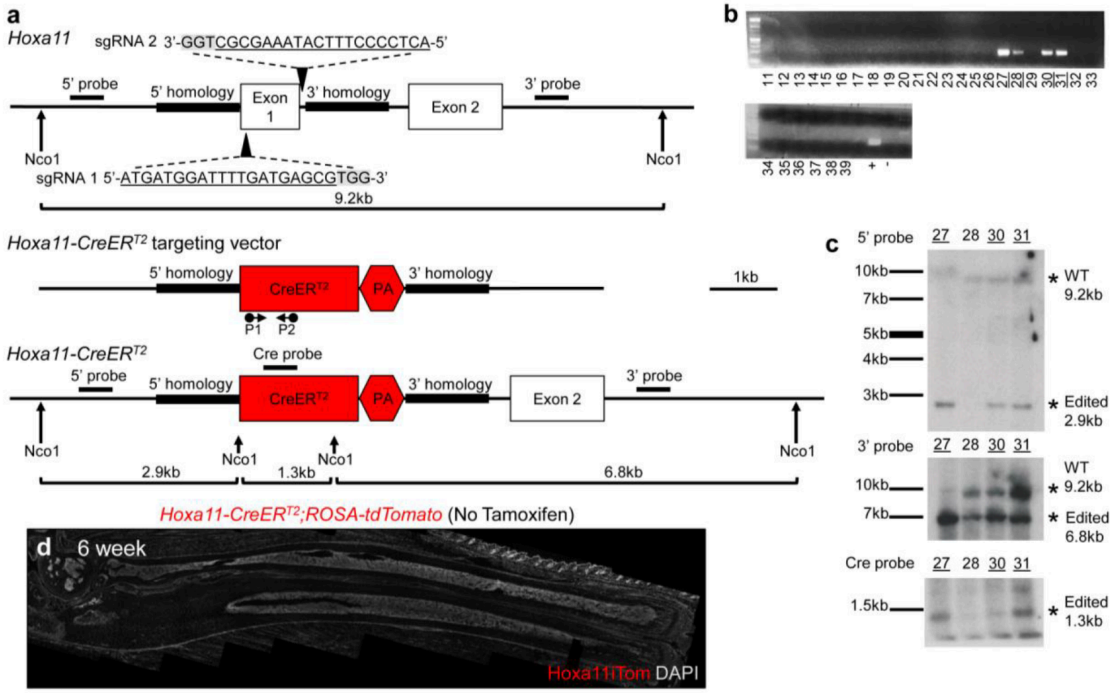

Supplemental Figure 2.2. Cas9/CRISPR generation of a *Hoxa11-CreERT2* allele: (**a**) Schematic of Cas9/CRISPR targeting of *Hoxa11* locus for generation of *Hoxa11-CreERT2* allele. Top: *Hoxa11* locus, positions and sequence of sgRNAs (grey box: PAM), Nco1 restriction sites, positions for 5' and 3' Southern Blot probes and size of wild-type (WT) fragment generated. Middle: *Hoxa11-CreERT2* targeting vector, 5' and 3' homology regions (thick black line), CreERT2 and rabbit globin poly-adenylation (PA) insertion (red), and location of Cre PCR primers. Bottom: *Hoxa11-CreERT2* allele, Nco1 restriction sites, positions for 5', 3' and Cre Southern Blot probes and size of edited fragments generated. (**b**) PCR analysis for Cre sequence on 29 live births. (**c**) Southern Blot on four Cre-positive animals using 5' probe (top), 3' probe (middle) and Cre probe (bottom). Wild-type and edited bands and sizes as marked. (**d**) *CreERT2* recombination in the absence of tamoxifen in *Hoxa11-CreERT2;ROSA-tdTomato* mice at 6 weeks of age. Fluorescent image - red: *Hoxa11* lineage-marked cells (Hoxa11iTom), grey: DAPI.

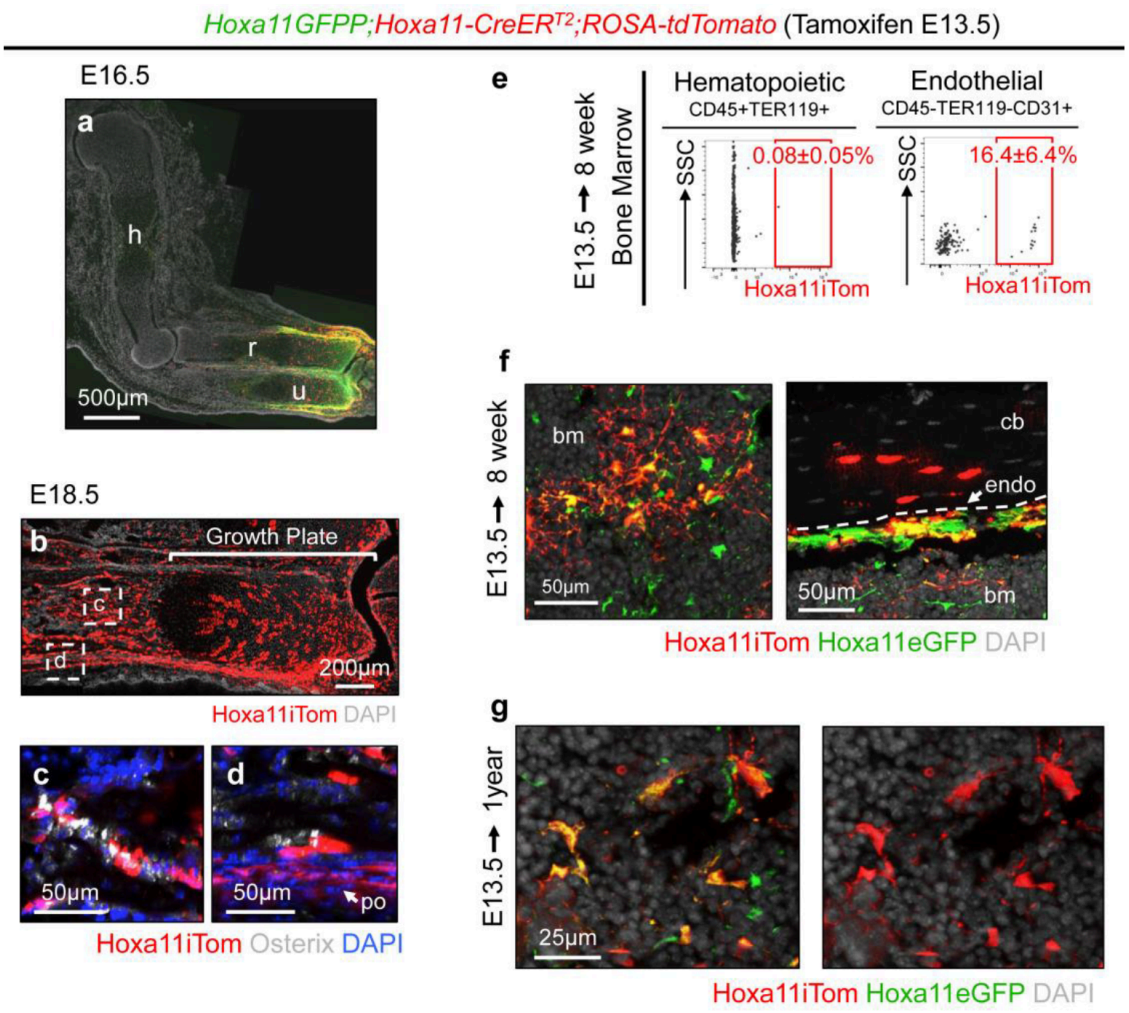

Supplemental Figure 2.3. Embryonic *Hoxa11*-lineage contributes to the skeleton during development and marked stromal cells co-express Hoxa11eGFP and persist throughout life. Pregnant dams received tamoxifen at E13.5 and resulting *Hoxa11eGFP;Hoxa11-CreERT2;ROSA-tdTomato* mice were chased to (**a**) E16.5, (**b-d**) E18.5 (**e-f**) 8 weeks or (**g**) 1 year. (**a**) Hoxa11eGFP (green) expression and lineage contribution of *Hoxa11* lineage-marked cells (Hoxa11iTom, red) in forelimb (humerus (h), radius (r), and ulna (u)). Compliment to Figure 3f. (**b**) High magnification view of ulna growth plate. Dashed white boxes show approximate location of high magnification images (**c-d**). Co-expression of Hoxa11iTom and Osterix (white) in (**c**) primary spongiosa (**d**) periosteum (po). (**e**) Flow cytometry analyses of Hoxa11iTom cells in the hematopoietic (left, CD45+TER119+) and endothelial (right, CD45-TER119-CD31+) compartments in the bone marrow. Flow cytometry data presented as mean ± standard deviation. Percentages reflect proportion of Hoxa11iTom population within identified gate. Grey dots: total non-endothelial stroma (NES), red dots: Hoxa11iTom. (**f**) Co-expression of Hoxa11iTom and Hoxa11eGFP in the bone marrow (left) and on the bone surface (right). Cortical bone: cb, bone marrow: bm, dashed white line marks endosteal (endo) bone surface. (**g**) Hoxa11eGFP in Hoxa11iTom bone marrow stromal cells after one-year chase. All images, grey or blue: DAPI.

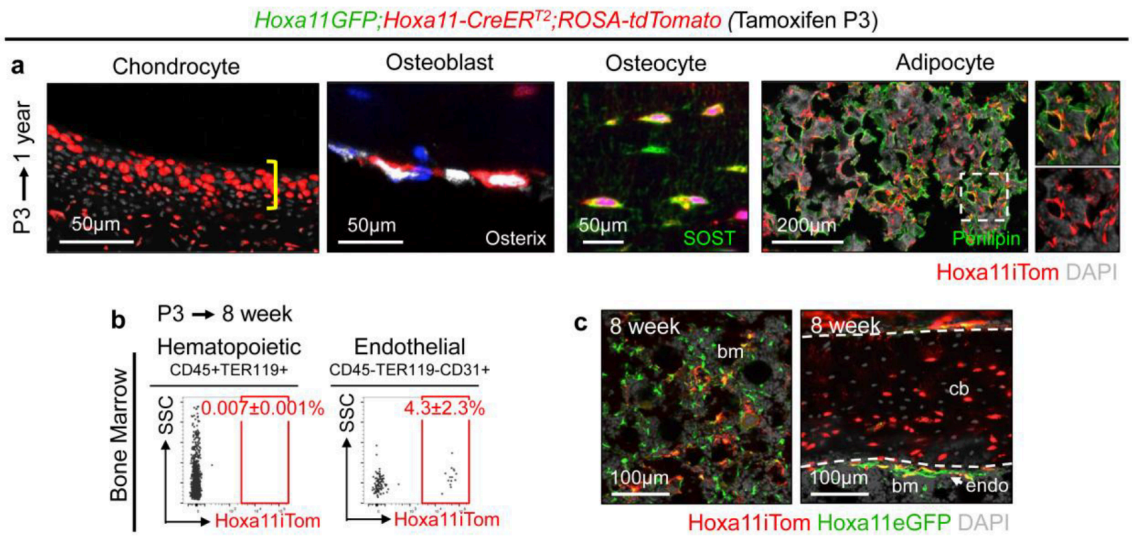

Supplemental Figure 2.4. Postnatal *Hoxa11*-lineage contributes to all skeletal/mesenchymal lineages at 1 year. P3 pups received tamoxifen and *Hoxa11eGFP;Hoxa11-CreERT2;ROSA-tdTomato* mice were chased to (**a**) 1 year or (**b-c**) 8 weeks. (**a**) *Hoxa11* lineage-marked cells (Hoxa11iTom, red) within articular cartilage, and immunolabeling for osteoblasts (Osterix, white) on endosteal bone surface, osteocytes (SOST, green) in cortical bone, and adipocytes (Perilipin, green) in bone marrow. Articular chondrocytes marked by yellow bracket. (**b**) Flow cytometry analyses of Hoxa11iTom cells in the hematopoietic (left, CD45+TER119+) and endothelial (right, CD45-TER119-CD31+) compartments in the bone marrow. Flow cytometry data presented as mean ± standard deviation. Percentages reflect proportion of Hoxa11iTom population within identified gate. Grey dots: total non-endothelial stroma (NES), red dots: Hoxa11iTom. (**c**) Hoxa11iTom and Hoxa11eGFP (green) in bone marrow (left) and on bone surface (right). Bone marrow: bm, cortical bone: cb, white dashed lines mark periosteal and endosteal (endo) surfaces. All images, blue or grey: DAPI.

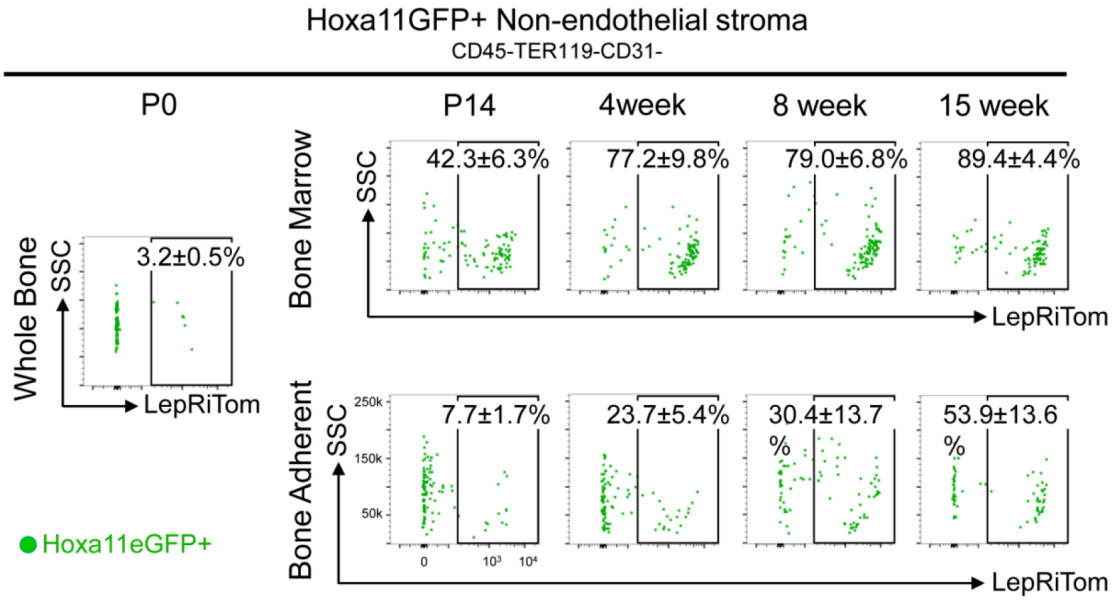

Supplemental Figure 2.5. *LepR-Cre* lineage progressively overlaps with Hoxa11eGFP-positive population. Flow cytometry analyses of Hoxa11eGFP-expressing stromal cells (green) and *LepR*-Cre lineage (LepRiTom) in whole bone at P0, or bone marrow (top) and bone adherent (bottom) compartments from P14 to 15 weeks. Analysis in non-hematopoietic, non-endothelial (CD45-Ter119-CD31-) compartment. Percentages reflect proportion of Hoxa11eGFP-positive population within indicated gate. All data presented as mean ± standard deviation.

Materials and Methods

Mouse models

All mice were maintained in a C57BL/6 background. *Hoxa11eGFP*[133], *Leptin Receptor-Cre*[143], *Osterix-CreER^{T2}* [52], mice have been described elsewhere. Rosa26-CAG-loxp-stop-loxp-tdTomato ([144], JAX stock #007909) were obtained from Jackson Laboratory. Both male and female mice were used for experiments. Animals were sacrificed for experiments through CO_2 exposure followed by removal of a vital organ. All procedures described here were conducted in compliance with the University of Michigan's Committee on Use and Care of Animals, protocol PRO00006651 (Wellik) and protocol PRO00006763 (Goldstein).

Generation of *Hoxa11-CreER^{T2}* mice

Two guide sequences targeting exon 1 of *Hoxa11* were designed and cloned into the pT7-Guide Vector (Blue Heron Biotech, LLC). The guide sequence and approximate locations of both sgRNA's, including the corresponding PAM sequence, are illustrated in Supplemental Figure 2a. MEGAshortscript T7 kit (Life Technologies) was used to generate *in vitro* transcribed sgRNA's from the pT7-Guide Vector and products were subsequently purified using the MEGAclear kit (Life Technologies). Using the pT7-Cas9-Nuclease vector (gift from Dr. Moises Mallo), Cas9 mRNA was *in vitro* transcribed using the mMESSAGE mMACHINE T7 ULTRA kit (Life Technologies) and purified using the MEGAclear kit (Life Technologies).

Homologous sequences flanking exon 1 of *Hoxa11* were synthesized by Blue Heron Biotech, LLC into the pUCminusMCS vector as a continuous insert separated by sequence containing restriction sites for EcoRI, NotI, and HindIII to allow for sub-cloning

of *CreER*^{T2} and rabbit β-globin poly-adenylation signal. The 5' homology arm contained 1.3kb immediately upstream of the endogenous *Hoxa11* start site and 3' homology arm contained 1.3kb of sequence immediately downstream of sgRNA 2 as illustrated in Supplemental Figure 2a. Sequence for CreERT2 and rabbit β-globin poly(A) signal was sub-cloned from pCAG-CreERT2 vector (gift from Connie Cepko, Addgene plasmid #14797, [132]). Targeting of CreERT2 to *Hoxa11* locus preserved endogenous upstream and downstream sequence and creates a null allele; expressing CreERT2 in place of Hoxa11.

Zygote injections were performed as previously described with minor modifications[145]. C57BL/6 female mice were superovulated and mated with C57Bl/6 male mice and one-cell stage embryos were collected for microinjection. CRISPR reagents were microinjected at the following concentrations: Cas9 mRNA (100ng/μL), each sgRNA (50ng/μL), and targeting plasmid (20ng/μL). Freshly injected eggs were transferred into pseudopregnant females and resulting progeny were initially screened for potential *CreER*^{T2} insertion via PCR. The following internal primers for CreER sequence were used: Cre Fwd: 5' GGACATGTTCAGGGATCGCCAGGC 3', Cre Rev: 5' CGACGATGAAGCATGTTTAGCTG 3'. Approximate location of primers indicated in Supplemental Figure 2a. Cre-positive animals by PCR were analyzed by Southern Blotting to confirm targeting using 5' and 3' flanking probes and a Cre internal probe with Nco1 digested DNA. Approximate locations of probes are illustrated in Supplemental Figure 2a. The 453 bp 5' probe was generated using primers: 5' probe Fwd: 5' TTTCGGTTCTCCTAGACGCC 3' and 5' probe Rv: 5' CACGGCGTTTGCATGAGATT 3', the 533 bp 3' probe was generated using primers: 3' probe Fwd: 5' TCTGTAGTGAGCGCCTTTGG 3' and 3' probe Rv: 5'

GAGGTTCCCGAGAGACTCCT 3', and the 408 bp Cre probe was generated using primers: Cre probe Fwd: 5' GCATTACCGGTCGATGCAACGAGTGATGAG 3' and Cre probe Rv: 5' GAGTGAACGAACCTGGTCGAAATCAGTGCG 3', that were randomly labeled with ^{32}P-dCTP. Four animals were CreER positive via PCR and three animals showed correct targeting via Southern Blot [Supplemental Figure 2b-c]. Animal #27 displayed germline transmission of the allele. Animals from this founder were used in all subsequent experiments.

Tamoxifen treatment

For embryonic induction, *Hoxa11-CreER^{T2}* or *Osx-CreERT2* male mice were mated to *Rosa$^{tdTomato/tdTomato}$* or *Hoxa11eGFP;ROSA$^{tdTomato/tdTomato}$* female mice and the vaginal plug was checked every morning. Pregnant mice received 2mg of tamoxifen (Sigma T5648) and 1mg/mL progesterone (Sigma P0130) dissolved in corn oil intraperitoneally at indicated embryonic day. For postnatal induction, pups of the genotype indicated in figures received 0.25mg of tamoxifen intragastrically at P3. At least three embryos, pups, or adult animals of the indicated genotypes were examined at time points shown in figures.

Ulnar fracture

Following procedure previously described in detail[86]. Tamoxifen was administered as described above, and animals were aged to adult stages (8-10 weeks or 10 months). Briefly, animals were anesthetized with isoflurane during procedure and provided buprenorphine pre- and postoperatively and carprofen during recovery period. A small incision was made along the posterior ulnar surface and the bone was exposed via blunt dissection. Using fine wire cutters, the ulna was cut at the mid-shaft. Skin was closed using

sutures. Animals were sacrificed for analysis at 10 days post injury. At least three animals from each tamoxifen induction time point were examined.

Immunohistochemistry

Limb skeletal tissues were collected at the indicated ages or time point following fracture injury. All specimens were dissected in PBS on ice and skin was removed prior to fixation for postnatal and adult tissues. Samples were fixed in 4% paraformaldehyde in PBS (embryo: 1-3 hours, postnatal (P3-P7): 4-6 hours, adult (2wk+): 1-2 days) rocking at 4°C. Postnatal and adult tissues were decalcified in 14% EDTA for 1-7 days depending on age. Samples were equilibrated in 30% sucrose overnight prior to embedding into optimal cutting temperature medium. Cryosections were collected at 12-30 μm through indicated segments of the limb or fracture callus using the Kawamoto tape method[146]. Immunohistochemical staining was performed using standard methods. Sections were blocked with donkey serum and incubated with primary antibodies overnight at 4°C against Sox9 (Millipore, AB5535, 1:500), Osterix (Abcam, ab22552, 1:300), and Perilipin (Sigma, P1873, 1:100). Secondary antibodies were incubated at room temperature for 2 hr: donkey-anti-rabbit-Alexa Fluor 647 (Thermo Fisher, A31573, 1:1000) and donkey-anti-rabbit-Alexa Fluor 488 (Thermo Fisher, A21206, 1:1000). A modified signal amplification protocol was used to visualize SOST. Following blocking, primary antibody against SOST (R&D Systems, AF1589, 1:100) was incubated overnight at 4°C followed by donkey-anti-goat-biotin secondary (Jackson ImmunoResearch, 705-067-003, 1:400). The biotinylated secondary was detected using Vectastain Elite ABC kit (Vector Laboratories, PK-6100) and signal was amplified by Alexa Fluor 488 Tyramide reagent (Thermo Fisher, B40853). To minimize imaging complications from autofluorescence in postnatal and adult tissues,

Hoxa11eGFP was visualized using chicken-anti-GFP (Abcam, ab13970, 1:2000) and donkey-anti-chicken-Alexa Fluor 488 (Invitrogen, A11039, 1:1000) in combination with aforementioned antibodies. tdTomato expression was dim at 24-72hr post-tamoxifen induction and was visualized using rabbit-anti-RFP (Rockland, 600401379, 1:1000) and donkey-anti-rabbit-Alexa Fluor 555 (Invitrogen, A31572, 1:1000). Following longer chases, tdTomato was imaged directly without the use of an antibody.

Fluorescent images were captured on an Olympus BX-51 microscope with an Olympus DP-70 camera or Leica Upright Sp5x 2-photon confocal microscope. Confocal z-stacks were obtained through entire sections at a thickness of 2 μm and images were stacked using ImageJ software. When applicable, 10x images were stitched together using Photoshop software to obtained images of entire limbs and fracture calluses.

Flow cytometry analysis

Bone marrow cells were harvested by flushing the marrow cavity with digestion buffer (2 mg/mL collagenase IV and 3 mg/mL dispase in 1X PBS) using a 30G needle for both the radius and ulna. To obtain bone adherent cells, the remaining bone following bone marrow flushing was minced in digestion buffer and subjected to subsequent digestion. The digestion of all samples was carried out at 37°C with three rounds of agitation to achieve a single cell suspension. After each cycle of digestion/agitation, cells in suspension were collected into media (DMEM, 10% calf serum) and kept at 37°C until the entire digestion protocol was finished. Red blood cells were lysed on ice using lysis buffer at a final concentration of 1X. For staining, cells were resuspended in staining buffer (1X PBS, 0.5% BSA, 2mM EDTA) at a concentration of 1 x 10^6 cells/30μl in a solution containing the following antibodies. For hematopoietic exclusion: CD45-AF700 (eBioscience, clone

30-F11, 1:100) and TER119-APC-Cy7 (Becton Dickinson, clone TER119, 1:100). For endothelial cell exclusion: CD31-PerCPCy5.5 (Becton Dickinson, clone MEC13.3, 1:100). For MSC identification: PDGFRα/CD140a-APC (eBioscence, clone APA5, 1:100) and biotinylated rat-anti-CD51 (Biolegend, clone RMV-7, 1:100) or biotinylated goat-anti-leptin receptor (R&D, BAF497, 1:50) and streptavidin-Brilliant Violet 605 (Biolegend, 405229, 1:500). For mSSC identification: CD90.1-Brilliant Violet 510 (Biolegend, clone OX-7, 1:100), CD90.2-Brilliant Violet 510 (Biolegend, clone 53-2.1, 1:100), Ly51-PerCPCy5.5 (Biolegend, clone 6C3, 1:100), CD200-PE (Biolegend, clone OX-90, 1:100), CD202b-APC (Biolegend, clone TEK4, 1:100). Following staining on ice, all samples were washed twice with staining buffer and resuspended in staining buffer containing DAPI (1:10,000) for analysis. All analyses were carried out on an LSRII Fortessa flow cytometer (BD) and results were analyzed with FlowJo (v10.2) software. Gating strategy outlined in Supplemental Figure 1a, c. Results are presented as mean values ±standard error of the mean (SEM). No statistical method was used to predetermine sample size. Sample size was determined on the basis of previous literature and our previous experiments to give sufficient standard error of the mean, and feasible generation of experimental animals. N-values represent number of animals in each analyses. The experiments were not randomized and investigators were not blinded during experiments and assessment of results.

Data Availability

The data that support the findings of this study are available from the corresponding author upon reasonable request

CHAPTER III

Hox Genes Function in the Adult Mammalian Skeleton

Summary

Hox genes are indispensable for the proper patterning of the skeletal morphology of the axial and appendicular skeleton during embryonic development. Recently, it has been demonstrated that *Hox* expression continues from embryonic stages through postnatal and adult stages exclusively in a skeletal stem cell population. However, whether *Hox* genes continue to function after development has not been rigorously investigated. Using a newly generated *Hoxd11* conditional allele and conditional loss-of-function analyses, we show that *Hox11* genes play critical roles in the skeletal homeostasis of the forelimb zeugopod (radius and ulna). Conditional loss of *Hox11* function at adult stages leads to replacement of normal lamellar bone with an abnormal woven bone-like matrix of highly disorganized collagen fibers. Examining the lineage from the *Hox*-expressing mutant cells demonstrates no loss of stem cell population. Differentiation in the osteoblast lineage initiates with Runx2 expression, which is observed similarly in mutants and controls. With loss of Hox11 function, however, osteoblasts fail to mature with no progression to osteopontin or osteocalcin expression. Osteocyte-like cells become embedded within the abnormal bony matrix, but they completely lack dendrites as well as the characteristic lacuno-canalicular network and do not express SOST. Together, our

studies show that *Hox11* genes continuously function in the adult skeleton in a region-specific manner by regulating differentiation of *Hox*-expressing skeletal stem cells into the osteolineage.

Introduction

Hox genes are important transcription factors responsible for establishing vertebral axial morphology along the anteroposterior (AP) axis during embryogenesis[16]. Additionally, the *Hox9-Hox13* paralogs are indispensable for development of the proximodistal (PD) axis of the limb[20,25–27]. The *Hox11* paralogous group, *Hoxa11*, *Hoxd11* and *Hoxc11*, regulate the patterning of the sacral region of the vertebral column and the zeugopod skeleton of the forelimb and hindlimb (radius/ulna, tibia/fibula)[20,25]. *Hox* paralogous genes functionally compensate for one another in skeletal patterning and all paralogs expressed in a region need to be removed for defects to fully manifest. In the forelimb, the *Hoxa11* and *Hoxd11* paralogs are expressed, thus the removal of these two genes lead to a severe malformation of the zeugopod skeletal elements[20,25].

Using a Hoxa11eGFP reporter knock-in allele, we have shown that Hox expression initiates broadly at ~E9.5 within the developing limb bud mesenchyme, but very quickly becomes restricted to the zeugopod region[88,133]. While previous work has focused largely on the embryonic role of *Hox* genes, we observed that expression is continuous in the skeleton and extends beyond development into postnatal and adult stages[85–88,147]. Importantly, *Hox* expression remains regionally restricted and maintains the expression pattern that has been established during development[68,86,148]. Conditional adult loss-of-function has not been examined, but *Hox11* compound mutants (animals in which three of the four paralogs are mutated) display normal embryonic development. However, compound mutants begin to exhibit skeletal growth phenotypes at postnatal stages and adults are not able to enact proper fracture repair, consistent with potential continuing functions[85–87]. The interpretation of this phenotype is complicated by the fact

that three alleles are absent throughout embryonic development, making it is impossible to separate embryonic defects that manifest later in life from continued function at adult stages.

We previously demonstrated that *Hox11* expression in the skeleton is exclusively restricted to a population of regional, progenitor-enriched mesenchymal stem/stromal cells (MSCs)[86,147]. Using a *Hoxa11-CreER^{T2}* lineage-tracing system, we recently established that the *Hox11* lineage contributes to the development, growth and homeostasis of the zeugopod skeleton by giving rise to all of the mesenchymal lineages in the bone—osteoblasts, osteocytes, chondrocytes, and bone marrow adipocytes. Notably, this *Hox11*-expressing cell population is also maintained as self-renewing adult stem cells throughout life, demonstrating that *Hox*-expressing cells are *bona fide* skeletal stem cells (SSCs), continuously supplying the progenitors for bone maintenance and repair throughout the life of the animal[147].

While these previous studies have provided rigorous information on the *Hox*-lineage, they have not addressed whether *Hox* function is required at later stages. This study sought to examine whether *Hox* genes continue to function in the adult skeleton within the skeletal stem cell population. In order to interrogate this potential, we generated a conditional *Hoxd11* allele that, when combined with a *Hoxa11* null allele, allows us to delete *Hox11* function at any stage. We find that deleting *Hox11* function at adult stages results in a progressive and dramatic remodeling of the zeugopod skeleton. Using our *Hoxa11-CreER^{T2}* allele to simultaneously delete *Hox11* function and lineage-label *Hox11* mutant cells, we establish that the phenotype spatiotemporally correlates with the initiation of *Hox11* deletion. Adult conditional mutants accumulate woven bone-

like matrix with disorganized collagen that progressively replaces normal lamellar bone. Further, we find that the *Hox11* conditional mutant animals generate pre-osteoblasts, but osteoblasts and osteocytes do not fully mature. For the first time, we establish that *Hox* genes do not functionally solely as embryonic patterning factors in the skeleton but continue to play an important role throughout life.

Results

Regional adult Hoxa11-expressing skeletal stem cells continuously contribute to the adult zeugopod skeleton

During development, Hox11 expression is restricted to the zeugopod region where it is observed in the perichodrium region surrounding the developing cartilage anlage[88]. *Hox11* expression continues in cells present in the perichondrium/periosteum as the skeleton develops, also becoming visible on the endosteal bone surface, trabecular bone surface as well as in bone marrow stromal cells as the bone marrow space is created during late embryogenesis[86,147]. This expression pattern is then maintained throughout life[86] (**Figure 3.1A, inset**). Our previous work demonstrated that embryonic and postnatal *Hox11*-expressing cells are regionally-restricted skeletal stem cells and that this lineage provides progenitors for all skeletal mesenchymal lineages as well as exhibits continuous self-renewal as stem cells throughout life[147]. As expected, this lineage and behavior is recapitulated when lineage labeling is initiated at adult stages. By inducing lineage labeling at adult stages in *Hoxa11-CreER^{T2}*;*ROSA-LSL-tdTomato* animals, we show downstream lineage cells become osteoblasts on the trabecular as well as endosteal bone surfaces, and sclerostin-expressing osteocytes embedded within the cortical bone (**Figure 1B, C; Supplemental Figure 3.1A, B**).

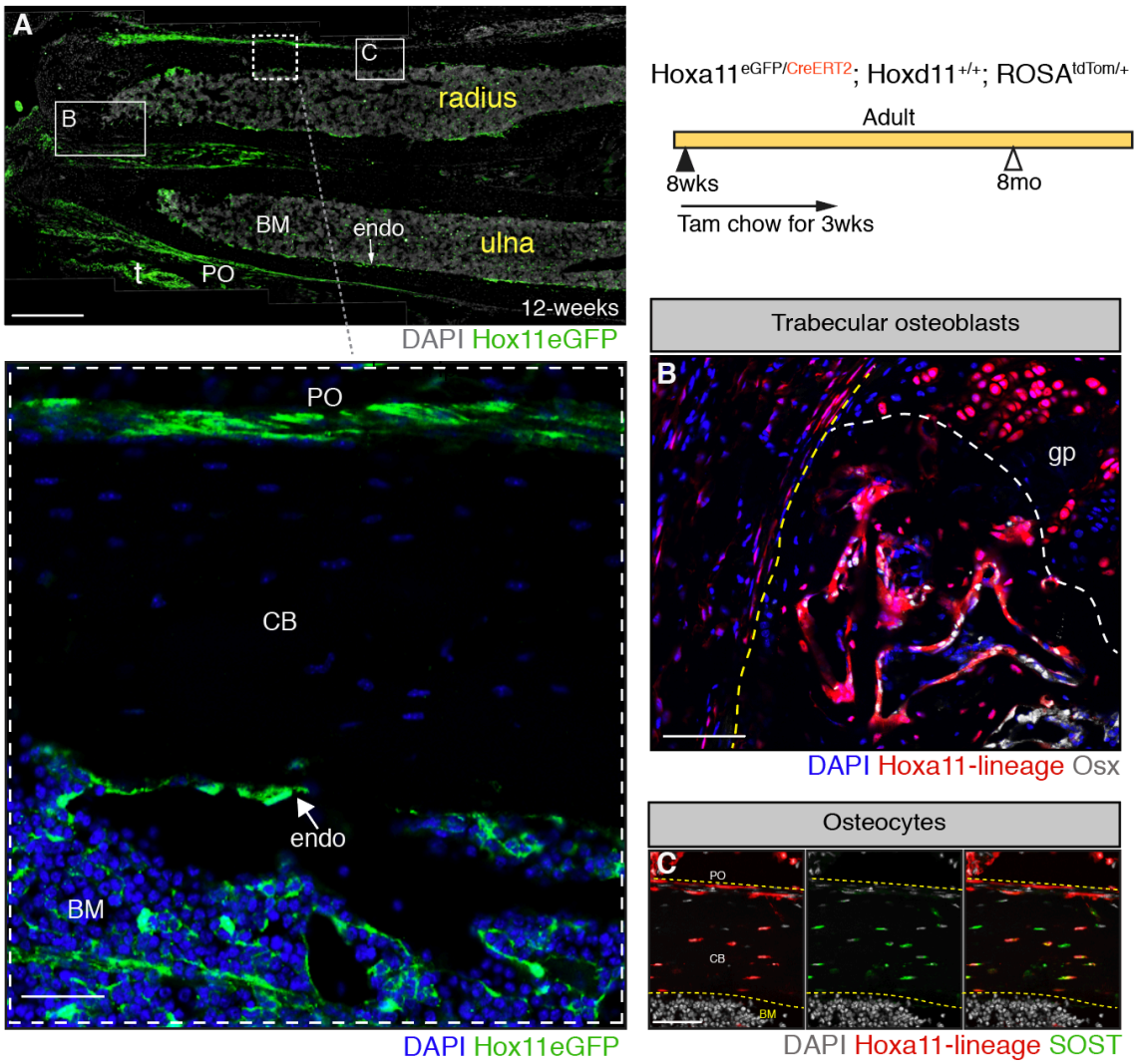

Figure 3.1. Adult Hox11-expressing skeletal stem cells continuously give rise to osteoblasts and osteocytes. (A) Hoxa11-eGFP real-time reporter allele demonstrates continuous expression of Hoxa11 (green) at 12-weeks of age. t = tendon, D = distal, P = proximal. DAPI: gray. Scale bar: 200µm. A higher magnification image of the boxed area in (A) showing localization of Hoxa11 expression (green) in the periosteum, endosteum, and bone marrow compartment. PO = periosteum, CB = cortical bone, endo = endosteum, BM = bone marrow. DAPI: blue. Scale bar: 75µm. Animals of the indicated genotype were fed on tamoxifen chow at 8-10 weeks of age for a duration of 3 weeks to induce deletion and collected after a 6-month chase at 8-months of age. **(B)** Approximate location marked with a white box with corresponding letter in (A). Hoxa11-lineage marked cells (red) are found in the trabecular bone co-expressing osterix (white, green arrows). Yellow dashed line outlines the cortical bone and white dashed line demarcates the growth plate border. gp= growth plate. DAPI: blue. Scale bar: 75µm. **(C)** Approximate location marked with a white box with corresponding letter in (A). Hoxa11-lineage marked cells (red) are also found as osteocytes embedded within the cortical bone co-expressing SOST (green). Hoxa11-lineage marked cells and DAPI (gray) in the far-

left panel, SOST (green) and DAPI (gray) in the middle panel, and the merged image is shown in the far-right panel. Scale bar: 60μm. All images, PO = periosteum, CB = cortical bone, endo = endosteum, BM = bone marrow.

Cas9/CRISPR generation and functional validation of a conditional Hoxd11 allele

To induce loss of *Hox11* function at adult stages after the normal development and growth of the zeugopod skeleton, we generated a *Hoxd11* conditional allele. As all *Hox* genes contain two exons with the DNA-binding homeodomain present in exon 2, we flanked exon 2 with loxP sites using CRISPR/Cas9-mediated gene editing[145]. *Cre*-mediated removal of exon 2 is expected to lead to loss-of-function of *Hoxd11* (**Figure 3.2A**). In brief, two guide RNAs were targeted to regions of low conservation 5' and 3' of *Hoxd11* Exon 2 and single stranded oligo donors were designed containing loxP sequence and 60bp of flanking homology sequence on each side for targeted insertion of LoxP sites flanking *Hoxd11* Exon 2. The loxP sites were targeted sequentially to the locus to generate a *Hoxd11* conditional allele through two rounds of zygote microinjection. Targeted insertion of each loxP site was confirmed by PCR and subsequent sequencing (**Supplemental Figure 3.2A, B**).

The *Hoxd11* conditional allele was first assessed for deletion of the region flanked by the loxP sites. Females with the genotype $Hoxa11^{eGFP/+};Hoxd11^{loxP/loxP}$ were mated to males with the genotype $ROSA^{CreERT2/+};Hoxa11^{+/-};Hoxd11^{loxP/loxP}$ to generate embryos with the genotype $ROSA^{CreERT2/+};Hoxa11^{eGFP/-};Hoxd11^{loxP/loxP}$. PCR analyses on embryonic tissue were performed and the *Hox11* conditional mutant embryos produced a robust recombined band and an absence of a detectable control band indicating efficient deletion (**Figure 3.2B**).

To functionally validate this new allele, we deleted *Hoxd11* at embryonic stages in the background of *Hoxa11* null mutants. It is important to note that the *Hoxa11-eGFP* allele is a knock-in that renders it non-functional. Therefore, animals that carry the genotype *Hoxa11*$^{eGFP/-}$ are functionally null for *Hoxa11* but their forelimbs are indistinguishable from that of wildtype littermates from embryonic through adult stages serving as a good control for the conditional mutants (compare **Figure 3.2C, D**)[25]. We induced deletion by feeding pregnant dams tamoxifen chow for 1 week beginning at E9.5. This stage is approximately when *Hox11* expression begins within the limb bud, therefore should recapitulate the *Hox11* null phenotype when loss-of-function of *Hox11* is induced at this stage. Resulting embryos were collected at E17.5 and skeletal preparations demonstrated that Hox11 conditional mutants phenocopy *Hoxa11*$^{-/-}$*; Hoxd11*$^{-/-}$ mutants, confirming that the *Hoxd11* conditional allele results in deletion of *Hoxd11* function (**Figure 3.2E, F**).

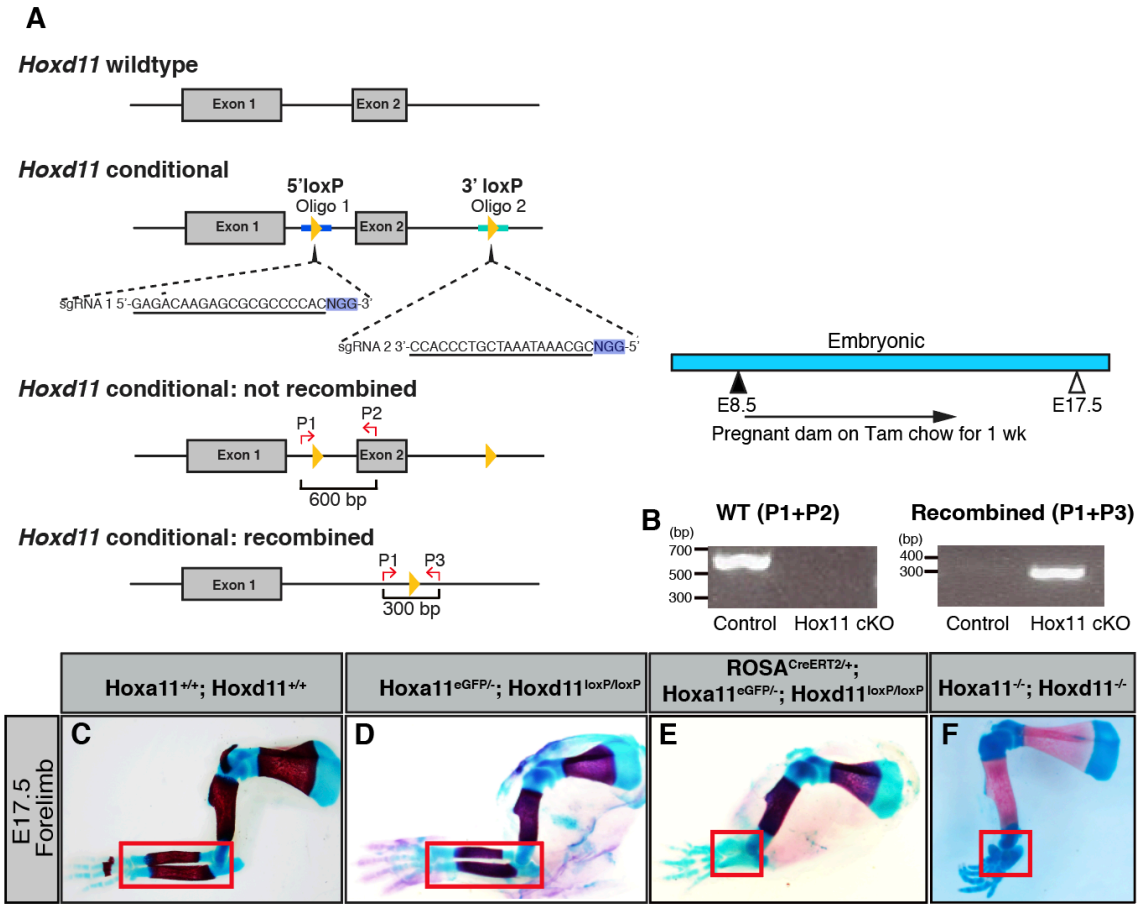

Figure 3.2. Conditional deletion of Hox11 function recapitulates the germline null mutation. (A) Cartoon schematic illustrating the *Hoxd11* locus. Two guide RNAs with the indicated sequences (underlined) along with their corresponding PAM (highlighted blue) were used to flank exon 2 of *Hoxd11* in order to insert loxP sites. Homology sequence used in the donor sequences are highlighted with thick dark blue line (5' loxP) and thick light blue line (3' loxP). Red arrows mark the location of the PCR primers used to confirm recombination. Corresponding PCR product sizes are indicated as well. The PCR elongation time was adjusted so that a 300bp PCR product would appear only if recombination had occurred between the loxP sites. Pregnant dams were fed on tamoxifen chow for 1 week to induce recombination and the resulting embryos were collected at E17.5. **(B)** PCR analysis using the PCR primers produce a robust 600bp control band only present in the controls and a 300bp recombined band only present in the conditional mutants. Skeletal preparations of limbs from **(C)** wildtype, **(D) littermate** control for Hox11 conditional mutant, **(E)** Hox11^{ROSACreERT2} conditional mutant, and **(F)** Hox11 germline null mutant. Red box highlights the zeugopod skeleton.

Adult deletion of Hox11 function results in a progressive replacement of lamellar bone with abnormal bony matrix

To assess the role of *Hox11* during adult skeletal homeostasis, animals with the genotype $ROSA^{CreERT2/+};Hoxa11^{eGFP/-};Hoxd11^{loxP/loxP}$ (referred to as $Hox11^{ROSACreERT2}$ conditional mutants) and corresponding controls (including animals of identical genotype minus the *ROSA26-*$CreER^{T2}$ with tamoxifen administration, and animals with the *ROSA26-*$CreER^{T2}$ in the absence of tamoxifen administration) were examined. Of note, there was minimal recombination in the absence of tamoxifen administration in animals with *ROSA26-*$CreER^{T2}$ allele; these animals did not produce a phenotype nor show any evidence of recombination at the *Hoxd11* locus as assessed by PCR (**Supplemental Figure 3.2C, D**).

Both control and conditional mutant adult animals were fed tamoxifen chow for 3 weeks beginning at 8-10 weeks of age and chased for 2, 4, or 10 months after the initiation of deletion. Tail samples were processed to use for PCR analysis and confirmed high levels of recombination out to the 1-year time points (**Figure 3.3A**). Notably, recombination was measured at the same degree in tail samples as in the zeugopod skeleton (**Supplemental Figure 3.2E**). A few of the $Hox11^{ROSACreERT2}$ conditional mutants displayed a residual WT band, indicating incomplete recombination however, qRT-PCR analyses revealed robust loss of *Hoxd11* in all cases (**Figure 3.3B**). Despite robust loss-of-function, it is critical to note that the *Hox11*-expressing skeletal stem cells are maintained in the conditional mutant bones out to the 1-year old time points as supported by continued *Hoxa11eGFP* expression (**Supplemental Figure 3.3A, B**).

MicroCT measurements did not reveal significant distinctions between the control and *Hox11*^{ROSACreERT2} conditional mutants at 6 months of age (four months after deletion, **Supplemental Figure 3.4A, B**). However, histological inspection revealed progressive changes in the appearance of the cortical bone in *Hox11*^{ROSACreERT2} conditional mutants compared to controls. Conditional mutant bones become notably hypercellular, and quantification revealed significantly higher cell numbers in the abnormal bony matrix (**Figure 3.3C-I**). Presumed osteocytes embedded within the hypercellular matrix displayed a round morphology compared to the ellipsoid morphology in controls (**Figure 3.E, inset**). This phenotype resembles the histology of woven bone, which has a higher density of osteocytes within its matrix along with the round shape of the lacunae[149]. It is important to note that these abnormalities remain regionally restricted as the humerus of *Hox11*^{ROSACreERT2} conditional mutants was not affected even as late as the 1-year time point (**Figure 3.3J, K**).

Abnormal bony matrix in adult Hox11 conditional mutants display disorganized collagen

The shape of osteocyte lacunae is strongly influenced by the orientation of the collagen fibers within the bone. Normal adult bone is comprised of lamellar bone with collagen fibers arranged in organized parallel sheets or layers and this contributes to the ellipsoid shape of the lacunae[55,150]. Woven bone, in contrast, is characterized by a haphazard organization of collagen fibers and contain osteocyte lacunae with a spherical shape, similar to what is observed in the *Hox11* conditional mutants. The collagen network within cortical bone can be visualized by picrosirus red stain. Picrosirius red increases the birefringence of the collagen fibers and subsequent observation under

polarized light reveals the organization of the collagen network[151,152]. The picrosirirus red staining in control bone demonstrates a well-organized, parallel structure of collagen fibers characteristic of normal, mature lamellar bone, while the *Hox11*^{ROSACreERT2} conditional mutant bones displayed a striking disorganization of the collagen matrix that correlates exactly with the hypercellular region (**Figure 3.4A-F**). Notably, both the region of disorganized collagen matrix and the hypercellular region increase with longer chases after deletion. (**Figure 3.3 and Supplemental Figure 3.5A-L**).

In efforts to further examine collagen organization, a $(flpHypGly)_7$ collagen mimetic peptide (CMP) conjugated to a cyanine 5 (Cy5) dye was used to stain sections of control and *Hox11*^{ROSACreERT2} conditional mutant bone. The ^{Cy5}CMP mimics the proline-hydroxyproline-glycine amino acid triplet motif that is prevalent in collagen (constituting ~10.5% of the protein sequence) and selectively anneals to disrupted sites in collagen[153]. Control bone sections were virtually devoid of any staining, as expected for a highly organized collagen matrix while conditional mutant bones displayed strong binding of throughout the regions of abnormal matrix (**Figure 3.4G-J**). Use of a compositional isomer (^{Cy5}CI) that differs in sequence from ^{Cy5}CMP did not stain either control or mutant bone sections as expected (**Supplemental Figure 3.5M, N**)[153].

As osteoclasts have a strong influence on bone integrity, we examined osteoclast number and localization in the controls and conditional mutants. Tartarate resistant acid phosphatase (TRAP) is a metalophosphoesterase that participates in osteoclast-mediated bone resorption and is used to visualize osteoclasts[154]. In control bones, TRAP staining is concentrated along the endosteal bone surface. In the *Hox11*^{ROSACreERT2} conditional mutant bones, TRAP staining is also observed on the endosteal bone surface, however there are

also trails of TRAP stain present within the abnormal cortex of the conditional mutant bones (**Figure 3.4K, L**). A higher magnification of the osteoclasts on the control bone surface demonstrate that the osteoclasts and TRAP stain localized at the surface of the bone as expected. High magnification of the conditional mutant bone shows TRAP enzyme within the abnormal bone matrix in addition to the bone surface. However, there were no cells associated with the TRAP stain, leading to the conclusion that the abnormal matrix is allowing diffusion of the enzyme into the matrix (**Supplemental Figure 3.6A-D).** While TRAP staining is broader in the conditional mutant bones, quantification of the bone surface osteoclasts showed no significant difference in the number of osteoclasts in the control and conditional mutants (**Figure 3.4M)**. The disorganized collagen matrix in conjunction with the diffusion of TRAP staining in the cortical matrices indicates the presence of a defective matrix in the *Hox11*^{ROSACreERT2} conditional mutant bone.

Abnormal bony matrix arises from Hox11-lineage cells

We next used the *Hoxa11-CreER*^{T2} allele to simultaneously conditionally delete the function of *Hox11* and lineage-trace the *Hox*-expressing cells by including a *ROSA26-LSL-tdTomato* allele. Females with the genotype *Hoxa11*$^{eGFP/+}$*;Hoxd11*$^{loxP/loxP}$ were mated to males with the genotype *Hoxa11*$^{CreERT2/+}$*;Hoxd11*$^{loxP/loxP}$*;ROSA*$^{LSL\text{-}tdTom/LSL\text{-}tdTom}$ to generate embryos with the genotype *Hoxa11*$^{CreERT2/eGFP}$*;Hoxd11*$^{loxP/loxP}$*;ROSA*$^{LSL\text{-}tdTom/+}$ (referred to as Hox11^{Hoxa11CreERT2} conditional mutants). Conditional mutant animals, along with their corresponding controls, were given tamoxifen chow for 3 weeks and chased for 2 months following the initiation of deletion and the contribution of the Hox11-expressing cells to bone was observed. The extent of lineage contribution

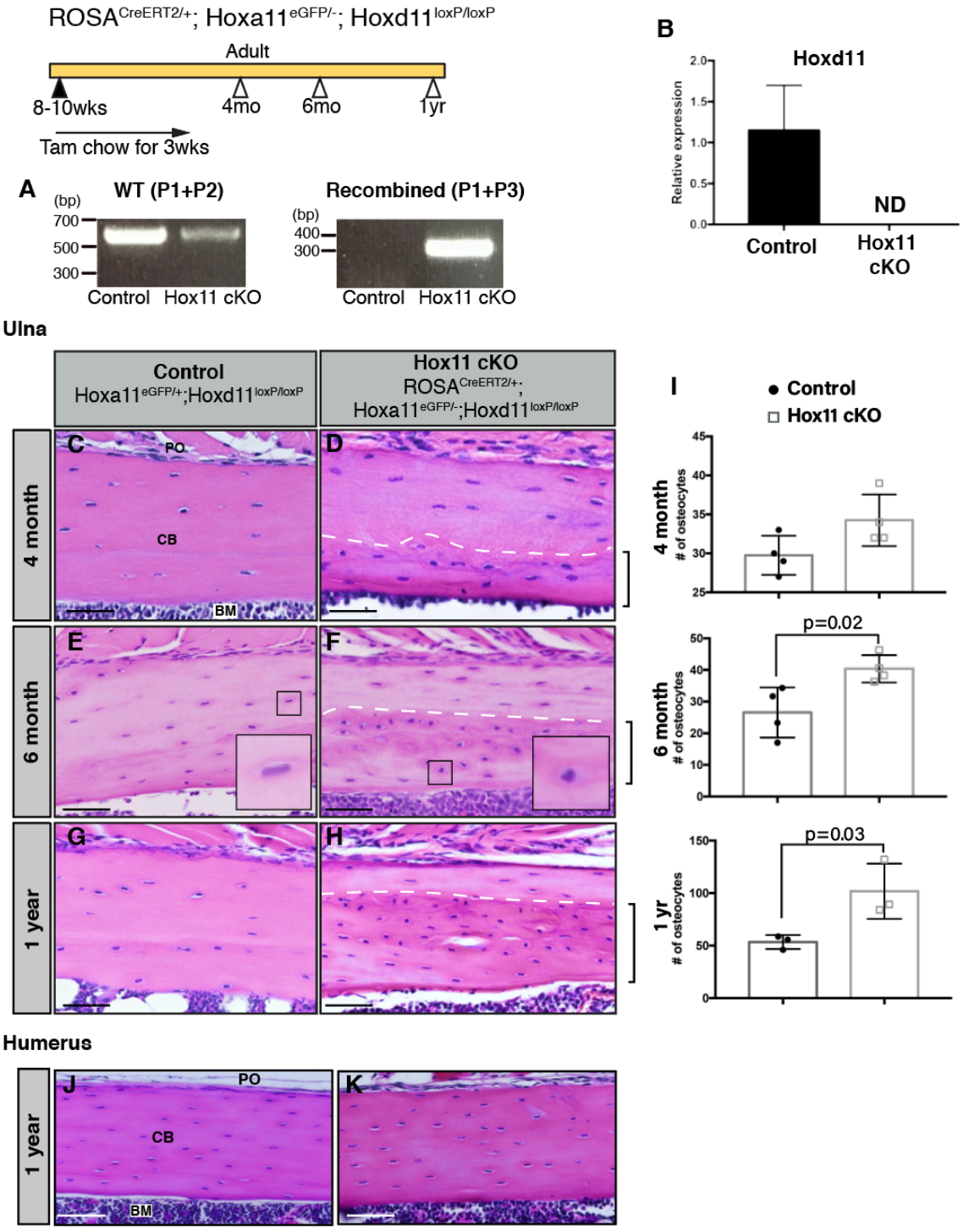

Figure 3.3. Deletion of Hox11 function at adult stages result in the regional disruption in cortical bone homeostasis. Hox11 conditional mutants with the *ROSA-CreER^{T2}* (genotype indicated) allele along with control animals were fed on tamoxifen chow at 8-10 weeks of age for 3 weeks to induce deletion of *Hox11* function and chased for 2 months (4-months of age), 4 months (6-months of age), and 10 months (1 year of age). **(A)** Tail samples from all animals collected were analyzed *via* PCR to assess

recombination. A robust 300bp band in the conditional mutants demonstrate strong recombination. **(B)** qRT-PCR of Hoxa11eGFP-expressing zeugopod skeletal cells of the conditional mutants show robust deletion of *Hoxd11* in the conditional mutants. Data is presented relative to mouse GAPDH using the ΔΔCt method. ND, none detected. Error is represented as mean ± SEM. **(C-H)** H&E stains of paraffin bone sections (ulna) of control and Hox11^{ROSACreERT2}conditional mutant animals. Dashed line demarcates the border between lamellar (above) and abnormal (below) bone. Inset in (E) and (F) show close-up of osteocyte to highlight distinct morphology. Brackets demarcate the abnormal matrix. **(J, K)** H&E stains of bones from the humerus of control (J) and Hox11 conditional mutant (K) show no differences in morphology at 1-year of age. **(I)** Quantification of cells embedded within the abnormal matrix at 4-months, 6-months, and 1-year of age show a significant increase in cell number in Hox11^{ROSACreERT2} conditional mutant bone. Error is represented as mean ± SEM. Statistics by Student's t test; *p < 0.05. All images, PO = periosteum, CB = cortical bone, BM = bone marrow. Scale bar in all images: 100μm.

observed between the control and *Hox11*^{Hoxa11CreERT2} conditional mutant bones is similar with no obvious differences in the cortical thickness of lineage-marked cells embedded in the bone matrix (**Figure 5A, B**). Control bones displayed a well-organized bone structure with lineage-labeled osteocytes embedded in the lamellar bone (**Figure 5A**). In contrast, the region with *Hox11*-lineage mutant cells precisely correlate with the abnormal matrix region clearly distinguishable in brightfield images (**Figure 5B, bracket**). These results strongly support that the abnormal matrix formed in the conditional mutant bones arise from the descendants of the cells that have lost *Hox11* function.

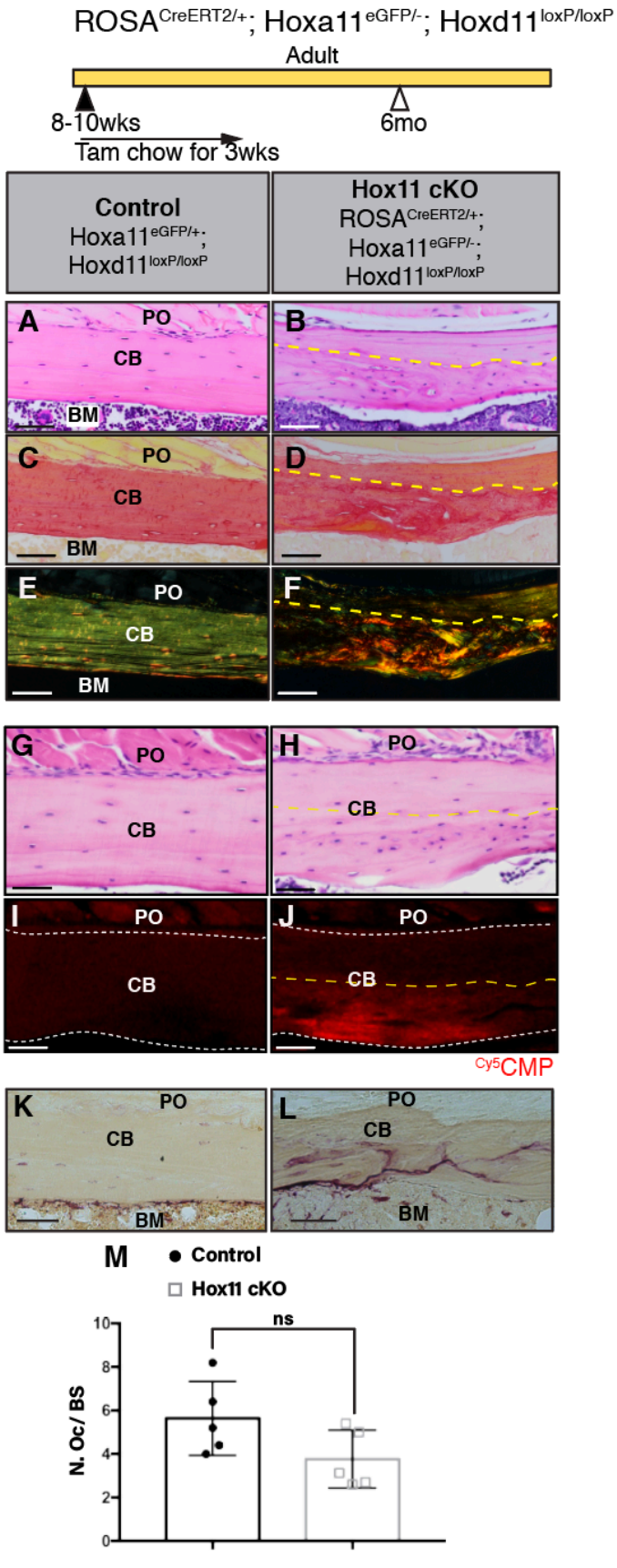
ROSA CreERT2/+; Hoxa11 eGFP/-; Hoxd11 loxP/loxP
Adult
8-10wks
6mo
Tam chow for 3wks
Control
Hoxa11 eGFP/+;
Hoxd11 loxP/loxP
Hox11 cKO
ROSA CreERT2/+;
Hoxa11 eGFP/-;
Hoxd11 loxP/loxP
A
B
C
D
E
F
G
H
I
J
K
L
PO
CB
BM
Cy5CMP
M
Control
Hox11 cKO
ns
N. Oc/ BS
10
8
6
4
2
0

Figure 3.4. Woven bone region in the Hox11 conditional mutant bones have a disorganized collagen matrix. Hox11 conditional mutants with the *ROSA-CreER^{T2}* (genotype indicated) allele along with control animals were fed on tamoxifen chow at 8-10 weeks of age for 3 weeks to induce deletion and chased for 4 months (6-months of age). **(A, B)** H&E stains of paraffin processed bone sections of control and Hox11^{ROSACreERT2} conditional mutant animals. **(C, D)** Brightfield images of picrosirius red stain of consecutive bone sections from B and C. (**E, F)** Polarized light images of picrosirius red stain of bone sections from D and E. **(G, H)** H&E stains of paraffin processed bone sections of control and Hox11^{ROSACreERT2} conditional mutant animals. **(I, J)** Consecutive bone sections from H and I stained with the collagen mimetic protein probe (red). White dashed line marks border of cortical bone. **(K, L)** Control (K) and Hox11^{ROSACreERT2} conditional mutant (L) bone sections stained with TRAP. Note the distinct distribution of TRAP stain in conditional mutant. Scale bar: 200μm. **(M)** Quantification of osteoclast number on bone surface using the Bioquant Osteo software. Statistics by Student's t test; *$p < 0.05$. Error is represented as mean ± SEM. All images are from the ulna, PO = periosteum, CB = cortical bone, BM = bone marrow. Yellow dashed line demarcates border between lamellar (above) and abnormal (below) bone. Scale bar in all images: 100μm.

Hox11 conditional mutant osteoblasts exhibit deficient differentiation

In vivo, mature osteoblasts are primarily defined by their morphology as definitive cellular markers are currently lacking. They appear on the bone surface as large cuboidal cells with a round nucleus located in the cell away from the bone surface[155]. As *Hox11* is not expressed in fully mature cells, we identified bone surface osteoblasts as *Hoxa11eGFP*-negative, *Hoxa11*-lineage-positive (red) cells. In control bones, we observed mature osteoblasts that present the classical, cuboidal morphology and nuclear localization (**Figure 3.5C-C'', arrowhead**). Noticeably, bone surface cells that retained *Hoxa11eGFP*-expression displayed a rounder morphology but were not cuboidal in shape, nor was the localization of the nucleus polarized away from the bone surface, indicating that these cells may be in the process of beginning to differentiate. All bone surface cells in the conditional mutant bones, in contrast, appeared flatter compared to those in controls with no nuclear migration away from bone surface (**Figure 3.5C-D'',**

arrowhead).

During normal osteoblast differentiation, Runx2 marks cells that have committed to the osteoblast lineage (pre-osteoblasts). Maturation of osteoblasts leads to the expression of osteopontin (Opn) at relatively early stages of osteoblastic differentiation, and osteocalcin (Ocn) is expressed in fully mature osteoblasts coincident with their assuming the characteristic cuboidal shape[156]. To determine whether *Hox* mutant cells initiate differentiation, Runx2 expression was examined. Runx2 expression was observed in both control and mutant bones on the cell surface of the endosteal bone (**Figure 3.5E, F**). However, Hox11^{Hoxa11CreERT2} conditional mutant bones were almost completely devoid of both Opn and Ocn staining whereas, in contrast, expression of both markers lined the endosteal surface of the control bones (**Figure 3.5G-J**). These data provide strong evidence that differentiation towards the osteoblast lineages is able to initiate in *Hox11* mutant skeletal stem cells, but terminal differentiation of osteoblasts is disrupted.

Osteocyte differentiation and morphology is disrupted with loss of Hox11 function in bone

Osteocytes are terminally differentiated osteoblasts that become embedded within the bone matrix and are the primary mechanosensory cells of the bone with important roles in bone homeostasis[65,157]. Long dendritic processes are characteristic of osteocytes; these are used to connect neighboring osteocytes to each other as well as to bone surface cells, including the cell surface osteoblasts and osteoclasts[63,64]. To examine whether maturation of osteocytes was also affected by the loss of *Hox11* function, we used a silver nitrate stain to visualize the dendritic processes. We observed a complete absence of the

formation of dendrites and a complete absence of the normal canalicular network in *Hox11* conditional mutant osteocytes present within abnormal bone matrix regions (**Figure 3.6B-E**).

Mature osteocytes produce and secrete the protein sclerostin, encoded by the *SOST* gene. Following a 2-month chase using our *Hoxa11-CreER*^{T2} allele, *Hox11*-lineage marked, osteoycyte-like cells are found embedded in both the control and *Hox11*^{Hoxa11CreERT2} conditional mutant bones (**Figure 3.6G, H**). While virtually all of the lineage-marked osteocytes in the control bone express SOST, most *Hox11*^{Hoxa11CreERT2} conditional mutant lineage-marked osteocytes failed to express SOST (**Figure 3.6I-M**), demonstrating a requirement for *Hox* function in proper osteocyte differentiation.

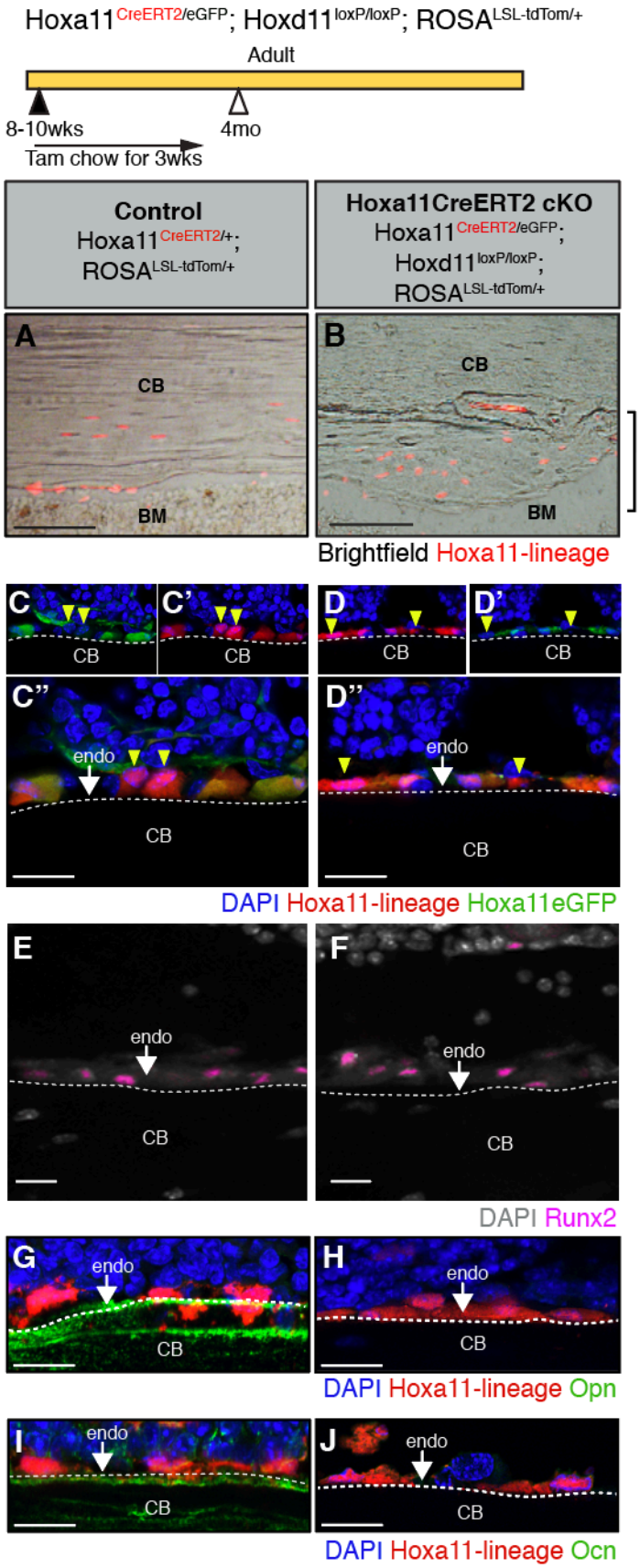
Hoxa11CreERT2/eGFP; Hoxd11loxP/loxP; ROSALSL-tdTom/+
Adult
8-10wks
4mo
Tam chow for 3wks
Control
Hoxa11CreERT2/+;
ROSALSL-tdTom/+
Hoxa11CreERT2 cKO
Hoxa11CreERT2/eGFP;
Hoxd11loxP/loxP;
ROSALSL-tdTom/+
A
B
CB
BM
Brightfield Hoxa11-lineage
C
C'
D
D'
C"
D"
endo
DAPI Hoxa11-lineage Hoxa11eGFP
E
F
DAPI Runx2
G
H
DAPI Hoxa11-lineage Opn
I
J
DAPI Hoxa11-lineage Ocn

Figure 3.5. Hox11 conditional mutant cells directly give rise to the woven bone. Hox11 conditional mutants with the *Hoxa11-CreER^{T2}* allele (genotype indicated) along with control animals were fed on tamoxifen chow for 3 weeks starting at 8-10 weeks of age and collected following a 2-month chase (4-months of age). **(A)** Brightfield image of a bone section from a control animal overlaid with Hox11-lineage marked cells (red) shows contribution to osteocytes. **(B)** Brightfield image of bone section from a Hox11^{Hoxa11CreERT2} conditional mutant overlaid with Hox11-lineage positive cells (red) shows contribution to abnormal bone matrix. **(C-D'')** Hoxa11eGFP (green) and DAPI (blue) in C and D, Hoxa11-lineage marked cells (red) and DAPI (blue) in C' and D', and merged images in C'' and D''. Control (C-C'') and Hox11^{Hoxa11CreERT2} conditional mutant (D-D'') bone sections show Hoxa11-lineage marked (red), non-Hoxa11eGFP (green) endosteal surface osteoblasts (yellow arrowhead). Notice stark difference in morphology. **(E, F)** Control (E) and Hox11^{Hoxa11CreERT2} conditional mutant (F) bone stained with RUNX2 (magenta). DAPI: gray. **(G, H)** Control (G) and Hox11^{Hoxa11CreERT2} conditional mutant (H) bone stained with osteopontin (OPN, green). **(I, J)** Control (I) and Hox11^{Hoxa11CreERT2} conditional mutant (J) bone sections stained with osteocalcin (OCN, green). All images are from the ulna, DAPI: blue (unless noted otherwise), Hox11-lineage marked cells: red, endo = endosteum, CB = cortical bone, and white dashed line demarcates the endosteal surface. Scale bars in all images: 50μm.

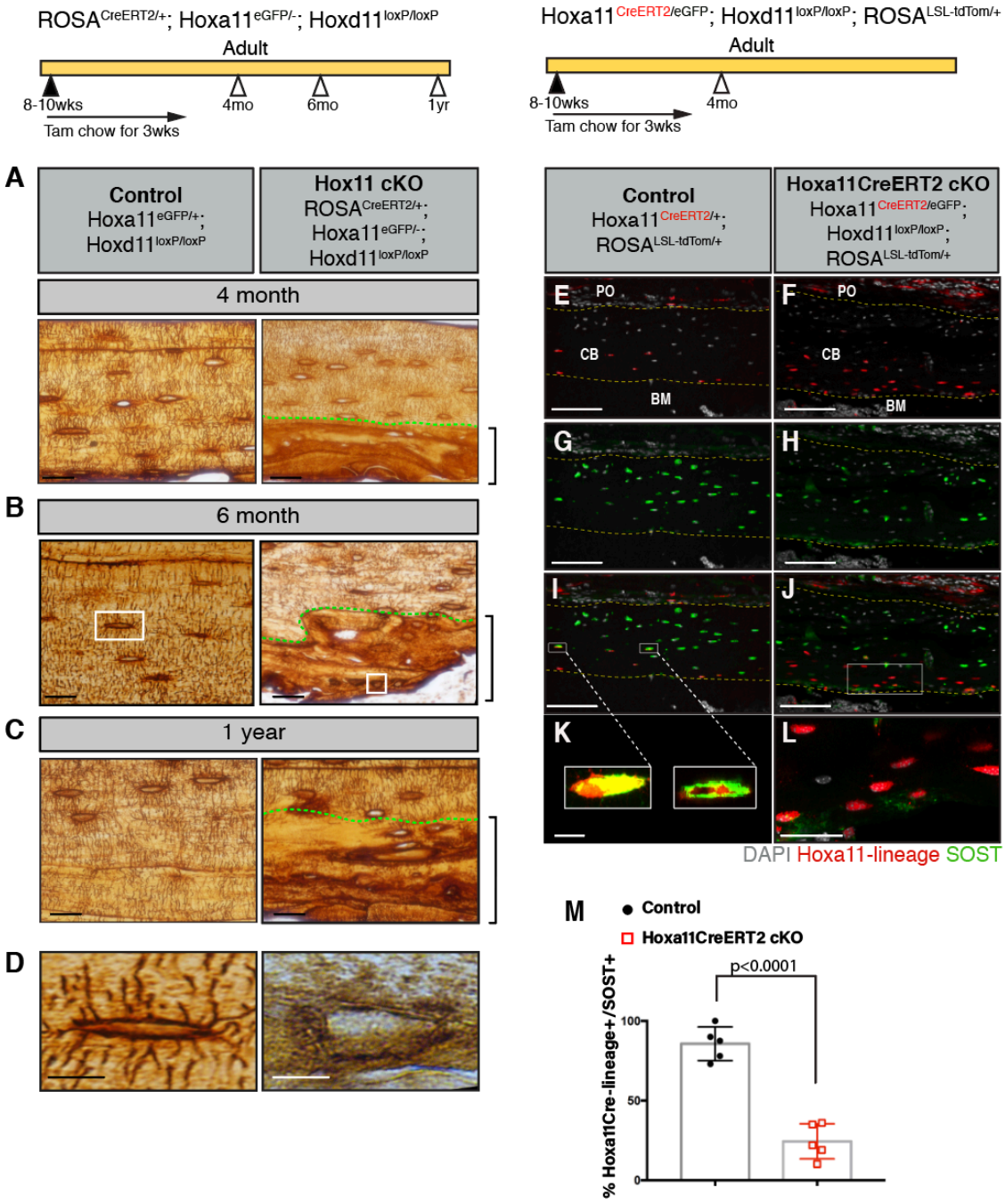

Figure 3.6. Hox11 conditional mutant osteocytes fail to form dendrites or express SOST. Hox11 conditional mutants with the *ROSA-CreER*^{T2} (genotype indicated) allele along with control animals were fed on tamoxifen chow at 8-10 weeks of age for 3 weeks to induce deletion of *Hox11* function and chased for 2 months (4-months of age), 4 months (6-months of age), and 10 months (1 year of age) for panels C-E. **(A-C)** Control (left panels) and Hox11^{ROSACreERT2} conditional mutants (right panels) were treated with silver nitrate. Green dashed lines demarcate the lamellar (above) and abnormal (below) bone. Brackets outline mark abnormal bone matrix. **(D)** High magnification of osteocytes

from the white-boxed area. Hox11 conditional mutants with the *Hoxa11-CreER^{T2}* allele (genotype indicated) alone with control animals were fed on tamoxifen chow for 3 weeks starting at 8-10 weeks of age and collected following a 2-month chase (4-months of age) for panels G-O. **(E, F)** Control (E) and Hox11^{Hoxa11CreERT2} conditional mutant (F) bone sections showing Hox11-lineage marked cells (red) that contributed to osteocytes. **(G, H)** Control (G) and Hox11^{Hoxa11CreERT2} conditional mutant (H) bone sections stained with SOST (green). **(I, J)** Merged images of E, G in (I) or F, H in (J) showing overlap or the lack thereof of Hox11-lineage marked cells (red) and SOST (green). (**K, L)** Close up of osteocytes in white-boxed region in K and L. (**M)** Quantification of Hox11-lineage marked cells (red) that also express SOST (green). Error is represented as mean ± SEM. Statistics by Student's t test; *$p < 0.05$. All images are from the ulna, DAPI: gray, PO = periosteum, CB = cortical bone, BM = bone marrow. Scale bar: 25μm (B-D), 10μm (E), 100μm (G-L), 10μm (M-N).

Discussion

Woven bone is made primarily during the rapid bone growth of embryogenesis or following bone injury (e.g. fracture)[158,159]. In both cases, the initial woven bone matrix is remodeled and replaced by lamellar bone through a process that is not fully understood. The accumulation of woven bone with no signs of lamellar remodeling in our *Hox11* conditional mutants demonstrate that proper skeletal matrix formation during homeostasis is dependent on *Hox* function. All of the evidence presented in this study supports defective differentiation of osteolineage cells with the loss of *Hox11* function. Osteoblasts originate from skeletal stem cells and previous work from our lab as well as results presented here unequivocally demonstrate that *Hox11*-expressing skeletal stem cells give rise to osteoblasts. As *Hox11* expression is restricted to the stem cell population and is not observed in differentiated skeletal cells, we conclude that Hox proteins function in the stem cells at early stages of differentiation.

The results from our conditional Hox11 loss-of-function model correlates with earlier investigations into embryonic null mutants. When *Hoxa11/Hoxd11* mutants were examined at E14.5, the stage at which when overt osteoblasts are beginning to differentiate in the zeugopod skeletal anlage, Runx2 expression was observed in the perichondrial region[160]. Consistent with our observation in the *Hox11* conditional mutants, subsequent maturation of osteoblasts are clearly perturbed in the *Hoxa11/Hoxd11* mutants as their zeugopod skeletal elements do not develop further resulting in two grossly stunted elements (**Figure 3.2F and** [20]**).** Intriguingly, these results are consistent with a similar function for Hox in the skeleton throughout life, however, this would require further investigation to conclude.

The abnormal collagen matrix secreted by the abnormally-differentiated osteoblasts in the adult conditional mutants may have a compounding role in the skeletal phenotype. Mice that harbor a mutation in *Col1a1* that produces type 1 collagen molecules resistant to cleavage by collagenase manifest a haphazard endosteal bone growth reminiscent of the *Hox11* conditional mutant bones[161]. The binding of CMP to collagen strands in our *Hox* conditional mutant bone supports abnormal processing of collagen. The similarity in bone phenotypes suggest that the abnormal collagen matrix is a critical manifestation of the *Hox* conditional loss-of-function phenotype. It is possible that collagen helices produced by *Hox* mutant osteoblasts do not undergo the proper processing required for the normal organization to lamellar bone or there may be an absence of enzymes or other molecules necessary for remodeling the collagen matrix. Further interrogation is required to understand the molecular mechanisms that lead to this defect.

Our results test a hypothesis put forward by Bradaschia-Correa, *et al*. that states *Hox* expression in periosteal stem/progenitor cells determines the cell fate of those stem/progenitor cells in adult animals[125]. In this report, the authors associated *Hox*-expressing periosteal stem/progenitor cells with more primitive, stem cell-like gene ontology terms and exhibited more accessible chromatin at transcriptional start sites[125]. Recent work from our laboratory demonstrating that *Hox* expression is associated with skeletal stem cells are consistent with their findings[86,147]. Results presented here genetically support their hypothesis that *Hox* genes confer differentiation cues to these stem cells throughout life. Bradaschia-Correa, *et al.* also hypothesize that *Hox* function may be required for maintenance of the stem cell population[125]. However, previously we

have shown that *Hox11*-expressing skeletal stem cells are maintained in *Hox11* compound mutants at relatively comparable numbers compared to controls[86]. We more directly test complete loss-of-function in this study and we find Hoxa11eGFP-positive conditional mutant cells are still present 10 months after deletion of *Hox* function. Furthermore, the progressive nature of the phenotype observed in our *Hox11* conditional mutants support maintenance of the *Hox11*-expressing skeletal stem population for continued (abnormal) contribution to the osteolineage. Cumulatively, these data provide compelling evidence that maintenance of the skeletal stem cell pool is independent of *Hox* function.

Herein, we show that *Hox* gene function in the skeleton is not restricted to development and that *Hox* genes play a crucial, functional role in adult bone homeostasis. Adult *Hox11* loss-of-function leads to a replacement of the lamellar cortical bone with an abnormal woven bone-like matrix. We have demonstrated strong evidence that this woven bone matrix is directly produced by the *Hox11* conditional mutant cells and the woven bone matrix is associated with the deficient differentiation and maturation of osteoblasts resulting from the loss-of-function of *Hox11* in the zeugopod skeletal stem cells.

Whether other *Hox* paralogous genes function to maintain the adult skeleton remains an intriguing question for future studies. Previous studies from our laboratory showing the preservation of region-specific *Hox* expression specifically within progenitor-enriched stem cell populations at adult stages support this likelihood[86]. While embryonic loss-of-function has clearly established that *Hox* genes impart region-specific function that differentially controls skeletal patterning and morphology, results from this

study raise the question of whether differential *Hox* gene function continues to be conveyed in a region-specific manner or whether all *Hox* function is similar once the skeleton has been established.

Supplemental Information

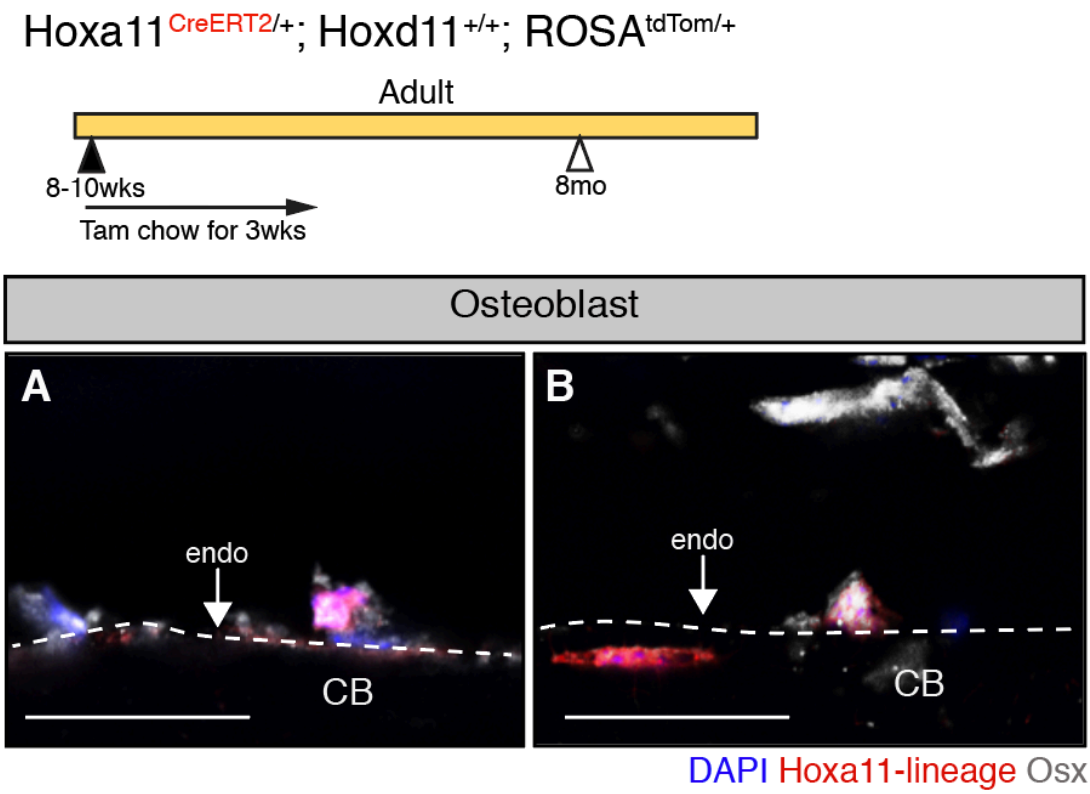

Supplemental Figure 3.1. Adult Hox11-expressing skeletal stem cells continuously contribute to endosteal osteoblasts. Animals harboring the *Hoxa11-CreER*^{T2} allele (genotype indicated) were fed on tamoxifen chow for 3 weeks starting at 8-10 weeks of age and collected after a 6-month chase at 8-months of age. **(A, B)** High magnification images of Hoxa11-lineage marked osteoblasts (red) co-expressing Osx (white) on the endosteal surface. White dashed line demarcates the endosteal surface. DAPI: blue. All images are from the ulna, endo = endosteum, CB = cortical bone. Scale bar, 25μm**.**

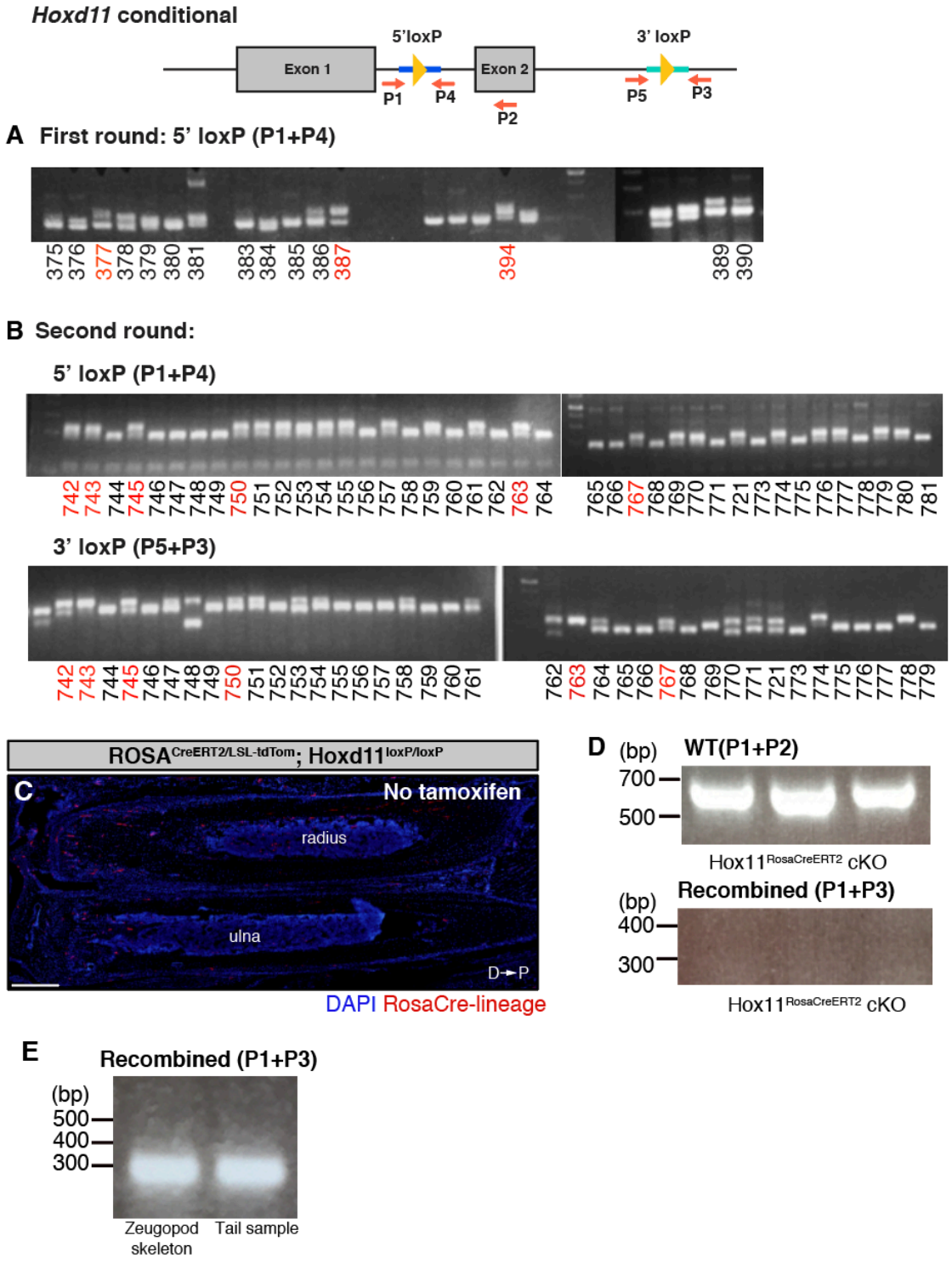

Supplemental Figure 3.2. CRISPR/Cas9 generation of the *Hoxd11* conditional allele. **(A)** PCR genotyping of founder (F0) animals for insertion of the 5' loxP site. Animals #377, 387, and 394 were sequence verified and male F1 animals were used as stud males for second round of targeting. **(B)** PCR genotyping of F0 animals for insertion at the 5'

loxP (top panel) and 3' loxP (bottom panel). Animals # 742, 743, 745, 750, 763 and 767 were heterozygous for 5' loxP and sequence verified to harbor correctly targeted 3' loxP. Animals #742 and 745 were found to be chimeric. Animal #763 contained the loxP sites in *trans*. Animals # 743, 750 and 767 contained the loxP sites in *cis* and #743 was selected to be the final founder. **(C)** 8-week old adult with the genotype $ROSA^{CreERT2/LSL\text{-}tdTomato}$; $Hoxd11^{loxP/loxP}$ without tamoxifen administration shows minimal recombination visualized by ROSA-lineage marked cells (red). DAPI: blue. Scale bar: 200µm. **(D)** PCR analysis shows that the minimal recombination seen in the zeugopod bones do not result in detectable recombined bands (right panel) and robust control band (left panel). All three samples are from $Hox11^{ROSACreERT2}$. **(E)** Equally strong detection of the recombined PCR band between zeugopod skeleton and tail sample taken from $Hox11^{ROSACreERT2}$ conditional mutant.

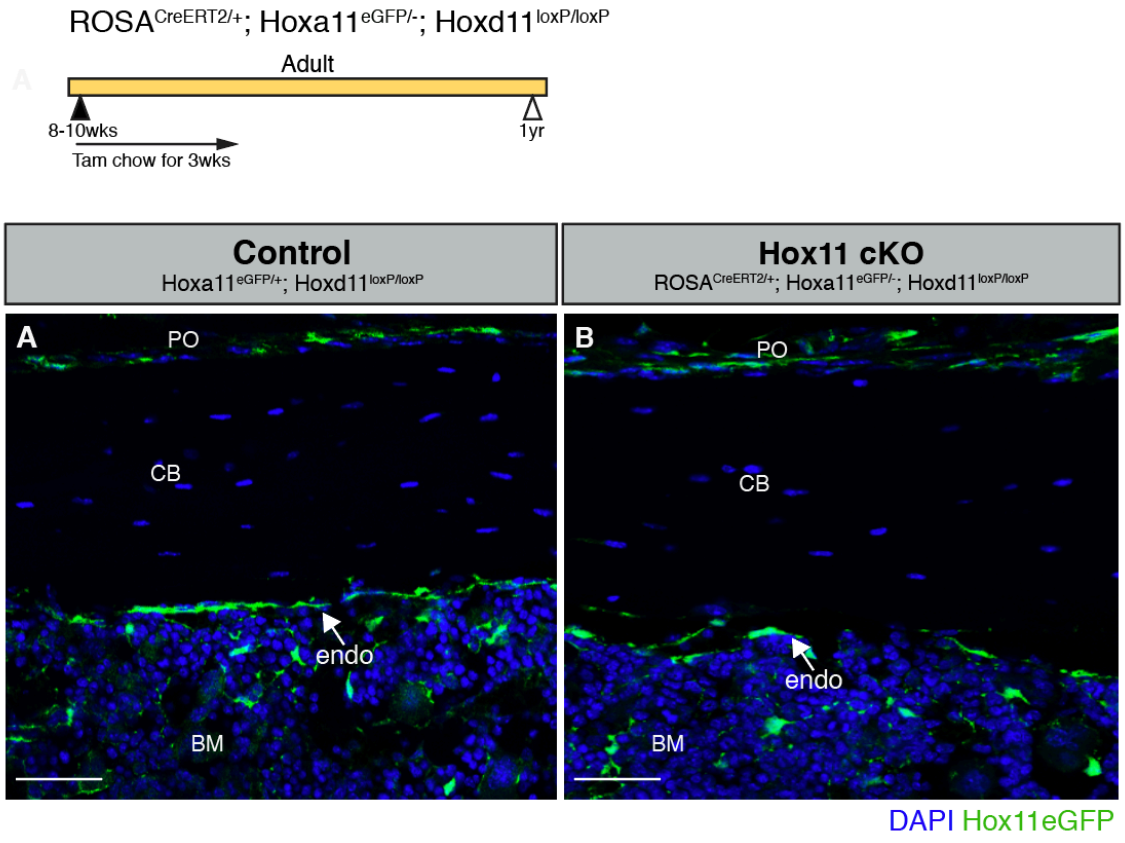

Supplemental Figure 3.3. Hox11-expressing skeletal stem cells are maintained in the Hox11 conditional mutants. Animals harboring the *Hoxa11-CreER^{T2}* allele (genotype indicated) were fed on tamoxifen chow for 3 weeks starting at 8-10 weeks of age and collected after a 10-month chase at 1-year of age. **(A, B)** Hox11eGFP-expressing skeletal stem cells (green) are present in the expected locations at 1-year of age in both the control (A) and Hox11 conditional mutants (B). All images are from the ulna, PO = periosteum,

CB = cortical bone, endo = endosteum, BM = bone marrow. DAPI: blue. Scale bar, 75μm.

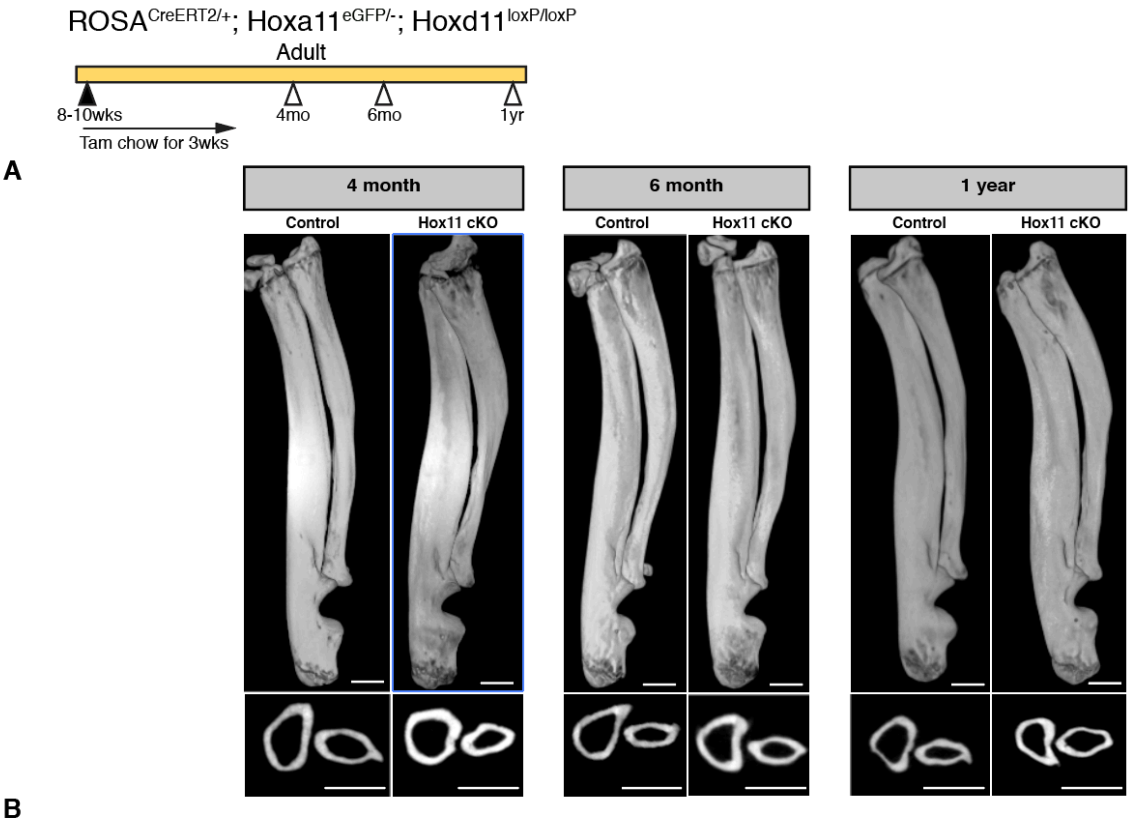

B

Parameter measured		4 month *Control n=6*	4 month *Hox11 cKO n=6*	6 month *Control n=5*	6 month *Hox11 cKO n=6*	1 year *Control n=6*	1 year *Hox11 cKO n=6*
Periosteal perimeter (mm)	radius	2.39±0.2	2.47±0.3	2.42±0.07	2.49±0.1	2.46±0.1	2.50±0.09
	ulna	2.9±0.1	2.88±0.1	3.0±0.04	2.87±0.4	3.02±0.1	2.89±0.2
Endosteal perimeter (mm)	radius	1.13±0.1	1.13±0.13	1.15±0.1	1.15±0.2	1.2±0.2	1.12±0.4
	ulna	1.3±0.2	1.27±0.3	1.32±0.1	1.25±0.3	1.30±0.5	1.21±0.07
Marrow area (mm^2)	radius	0.17±0.06	0.18±0.07	0.19±0.02	0.18±0.01	0.21±0.06	0.19±0.08
	ulna	0.15±0.01	0.17±0.01	0.16±0.03	0.15±0.01	0.20±0.05	0.15±0.02
Cortical thickness (mm)	radius	0.29±0.03	0.29±0.1	0.28±0.02	0.29±0.02	0.27±0.02	0.30±0.3
	ulna	0.32±0.05	0.31±0.03	0.30±0.04	0.31±0.06	0.29±0.02	0.32±0.1

Supplemental Figure 3.4. Long-term deletion of Hox11 function at adult stages do not lead to noticeable gross morphological differences. Hox11 conditional mutants with the *ROSA-CreER^{T2}* (genotype indicated) allele along with control animals were fed

on tamoxifen chow at 8-10 weeks of age for 3 weeks to induce deletion of *Hox11* function and chased for 2 months (4-months of age), 4 months (6-months of age), and 10 months (1 year of age). **(A)** Top panel: 3D rendering from microCT scans of the zeugopod skeleton (radius/ulna) from control and $Hox11^{ROSACreERT2}$ conditional mutants. Bottom panel: Cross section of the zeugopod skeleton through the distal end at 10% of the entire length of the ulna. **(B)** Table outlining the morphological measurements generated from microCT scans. Statistics by Student's t test; $*p < 0.05$.

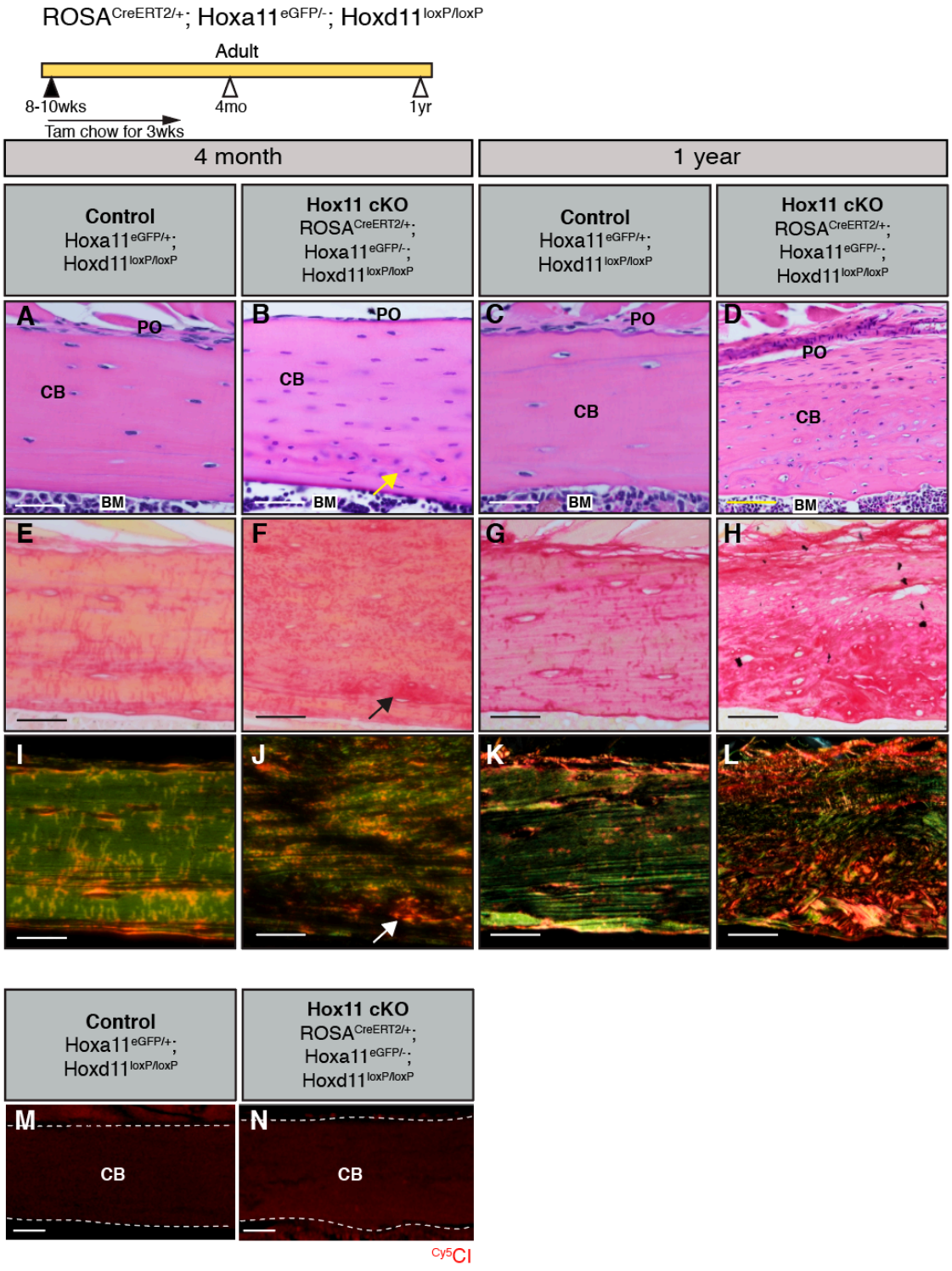

Supplemental Figure 3.5. Adult conditional deletion of Hox11 function lead abnormal matrix. Hox11 conditional mutants with the *ROSA-CreER*^{T2} (genotype indicated) allele along with control animals were fed on tamoxifen chow at 8-10 weeks of age for 3 weeks to induce deletion of *Hox11* function and chased for 2 months (4-months of age) and 10 months (1 year of age). **(A-D)** H&E stains of control (A, C) and

Hox11^{ROSACreERT2} conditional mutant (B, D) at 4-months and 1-year of age. **(E-H)** Brightfield images of picrosirius red stain of consecutive bone sections from A-C. (**I-L)** Polarized light images of picrosirius red stain of bone sections from E-H. Arrows (yellow (B), black (F) white (J)) highlight the abnormal matrix in 4-month old conditional mutant bone.**(M, N)** Bone sections from control (M) and Hox11^{ROSACreERT2} conditional mutant (4-month chase) were stained with ^{Cy5}CI. Both bone sections do not show staining. White dashed line marks border of cortical bone. All images are from the ulna, PO = periosteum, CB = cortical bone, BM = bone marrow. Scale bar in all images: 100µm.

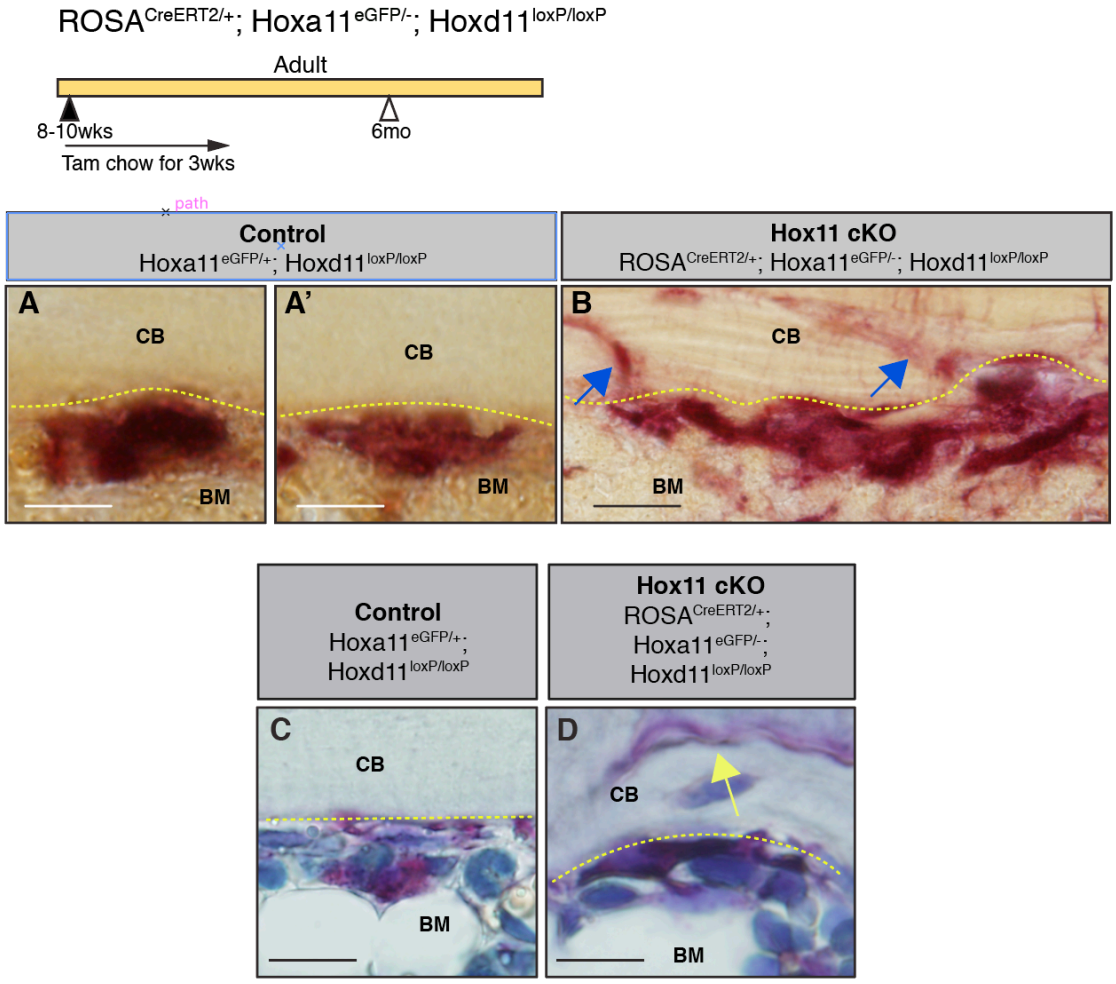

Supplemental Figure 3.6. Distribution of TRAP staining, but not number of osteoclasts is distinct in Hox11 conditional mutant bones. Hox11 conditional mutants with the *ROSA-CreER^{T2}* (genotype indicated) allele along with control animals were fed on tamoxifen chow at 8-10 weeks of age for 3 weeks to induce deletion of *Hox11* function and chased for 4 months (6-months of age). **(A-B)** Higher magnification of osteoclasts to show apparent TRAP stain leakage into cortical bone matrix. Yellow dashed line demarcates the endosteal bone surface. TRAP enzyme leaked into the bone

matrix in mutants (blue arrow). Scale bar: 25μm **(C, D)** TRAP stain with hematoxylin for visualization of nuclei. No cells were associated with TRAP stain in cortical bone (yellow arrow). Yellow dashed line demarcates the endosteal bone surface. Scale bar: 25μm. All images are from the ulna, PO = periosteum, CB = cortical bone, BM = bone marrow.

Materials and methods

Mice

All mice were maintained in a C57BL/6 background. Both male and female mice were used for all experiments. The mouse models *Hoxa11-eGFP*[133] and *Hoxa11-CreERT2*[85] have been previously described. The ROSA26-CAG-loxP-stop-loxP-tdTomato (JAX stock #007909) and ROSA26-CreERT2 (JAX stock #008463) were purchased from Jackson Laboratory. The *Hoxd11*-floxed animals were obtained by breeding founder *Hoxd11*-floxed animals to wildtype C57BL/6 animals for 5 generations followed by breeding *Hoxd11*-loxP heterozygotes to each other to produce *Hoxd11*-floxed animals. These animals were periodically bred to wildtype C57BL/6 animals to avoid genetic drift. The *Col2.3-GFP* mice were kindly provided by Dr. Noriaki Ono then bred with our *Hoxa11* and *Hoxd11* mice to generate animals of appropriate genotype. All animal experiments described in this article were reviewed and approved by the University of Michigan's Committee on Use and Care of Animals, protocol PRO0000-8674 (Wellik).

Generation of *Hoxd11* conditional allele

The *Hoxd11* conditional allele was generated in two injection rounds, targeting each loxP site sequentially. Two guide sequences were targeted to regions of low conservation within the *Hoxd11* intron (5', upstream) and downstream of the 3' untranslated region (UTR) (3', downstream) flanking exon 2 of the *Hoxd11* locus were cloned into the pT7-Guide Vector (Blue Heron Biotech, LLC). The guide sequence, approximate locations, and corresponding PAM sequences are indicated in **Figure 2A**.

Donor oligos contained 60bp of flanking homology sequence, the loxP sequence (bold letters), and a unique restriction site (EcoRI [5' loxP] or NheI [3' loxP], capital letters) for optional use in confirming accurate targeting. Single stranded DNA oligos were purchased from Integrated DNA Technologies.

5' loxP donor oligo sequence (from 5' to 3'):

gttgatgagtgggaacacgagagcctcctgcctttcagggagagggtaagtgatctgcc GAATTC **ataacttcgtataatgtatgctatacgaagttat** gcactggacttaaccccaacctctggctg gcgctcagctcggagttgagcagatgctcctg

3' loxP donor oligo sequence (from 5' to 3'):

tctgattagacttacatcatctctagcatttgaaagcaatttgccaccctgctaaataa GCTAGC **ataacttcgtataatgtatgctatacgaagttat** acgctggcactttataaaatatagaa caaagtaaaatatagttatattgtttcgtaaac

The guide RNAs were *in vitro* transcribed from the pT7-Guide Vector using the MEGAshortscript T7 kit (Life Technologies, AM1354) and products were subsequently purified using the MEGAclear kit (Life Technologies, AM1908). Using the pT7-Cas9-Nuclease vector (gift from Dr. Moises Mallo), the Cas9 mRNA was *in vitro* transcribed using the mMESSAGE mMACHINE T7 ULTRA kit (Life Technologies, AMB13455) and purified using the MEGAclear kit (Life Technologies, AM1908).

Zygote injections were performed as previously described with minor modifications[145]. C57BL/6 and SJL mixed background female mice were superovulated and mated with C57Bl/6 and SJL mixed background male mice and one-cell stage embryos were collected for microinjection. CRISPR reagents were microinjected at the following concentrations: Cas9 mRNA (100ng/μL), sgRNA (50ng/μL), and DNA oligo

(50ng/μL). Injected zygotes were transferred into pseudopregnant females and resulting progeny were initially screened for potential recombination events via PCR.

The intronic loxP site was targeted first. PCR primers, 5'-ATGAGTGGGAACACGAGAGC-3' and 5'- AGGCTGGCACTGAGATAGGA-3' were used to screen for loxP insertion. PCR products were cloned for sequencing using the TOPO TA cloning kit (Thermo Fisher, 450071). Male mice validated to contain correctly targeted loxP sequence from the first round of injection were used as stud males for targeting of the 3' region of *Hoxd11* exon2. PCR primers 5'-AAAGCAATTTGCCACCCTGC-3' and 5'- ACAGGTAAACCAATGCCCAGA-3' were used to screen for loxP insertion at the 3' region of the *Hoxd11* exon2. Targeting was verified by PCR and sequencing as above. Animals (male or female) confirmed to contain two correctly targeted loxP sites were mated to wild-type Bl6 animals and genotyping analyses of the resulting progeny using the PCR primers indicated above were used to screen for germline transmission and the presence of both loxP sites in *cis* along the chromosome.

Tamoxifen treatment

Mice were fed on tamoxifen chow (Envigo, TD. 130860) at 8-10 weeks of age for a duration of 3 weeks. Based on approximate daily food intake of 4g/mouse[162] and body weight of 20-25g, mice consumed a concentration of 40mg/kg of tamoxifen per day. The chow was replaced weekly. Both control and conditional mutants were fed on tamoxifen chow.

Bone tissue preparations

Mice were euthanized and both forelimb zeugopod skeletons were collected by dissecting off the soft tissue, taking care not to disturb the periosteum. All bones were then fixed shaking in 4% paraformaldehyde (PFA) for 2 days at 4°C then scanned for microCT if required. Specimens for frozen sections were decalcified in 14% EDTA for 7 days and equilibrated in 30% sucrose overnight prior to embedding in OCT media. Cryosections were collected at 10-12µm using the Kawamoto tape method[146]. Specimens for paraffin sections were decalcified in 14% EDTA for 7 days and dehydrated in 70% ethanol prior to overnight paraffin processing. Paraffin sections were collected at 5µm.

Histology, immunohistochemimstry, histomorphometry, microCT, and quantification

As *Hox11* expression within the zeugopod skeleton is higher in the ulna compared to the radius, all detailed analyses were carried out in the ulnar bone. Histological stains were performed using standard methods[163]. Paraffin sections were de-paraffinized and rehydrated by incubating in xylene followed by a series of washes in decreasing ethanol content (100%, 95%, 70%, ddH_2O). H&E stains were processed as previously reported[163]. Tartrate-resistant acidic phosphatase (TRAP) staining (Sigma-Aldrich, 387A-1KT) and picrosirius red stain (Abcam, ab150681) were performed according to manufacturer's protocol. For the visualization of the osteocyte lacuna-canilicular network, the bone sections were processed as previously reported with minor modifications[164]. All histological images were acquired on an Eclipse E800 microscope (Nikon).

For immunostaining, cryosections were blocked with 5% donkey serum and incubated with primary antibodies overnight at 4°C against Osterix (Abcam, ab22552, 1: 300), Osteopontin (R&D Systems, AF808, 1:200), and Osteocalcin (antibody no longer commercially available, RayBiotech, DS-PB-01521, 1:200). Secondary antibodies were incubated at room temperature for 1h: donkey-anti-rabbit-Alexa Fluor 647 (Thermo Fisher, A31573, 1:500), donkey-anti-goat-Alexa Fluor 488 (Thermo Fisher, A11055, 1:500). SOST was visualized using a modified signal amplification protocol. Sections were incubated in SOST (R&D Systems, AF1589, 1:100) overnight at 4°C followed by donkey-anti-goat-biotin secondary (Jackson ImmunoResearch, 705-067-003, 1:400). The biotinylated secondary was detected using the Vectastain Elite ABC kit (Vector Laboratories, PK-6100) and signal was amplified by Alexa Fluor 488 Tyramide reagent (Thermo Fisher, B40853). Endogenous Hoxa11eGFP fluorescence was quenched after the decalcification process and was visualized using chicken-anti-GFP (Abcam, ab13970, 1:1000) and donkey-anti- chicken-Alexa Fluor 488 (Invitrogen, A11039, 1:500). All fluorescent images were acquired on a Leica Upright SP5x 2-photon confocal microscope. Confocal z-stacks were captured through entire sections at a thickness of 1-2μm and images were stacked using Photoshop. Large images were stitched (when necessary) using Photoshop.

Fluorophore-labeled CMP and CI were synthesized as described previously[153]. Briefly, ^{Cy5}CMP has the sequence: Cy5-Gly-(SerGly)2-(flpHypGly)7-OH, where flp refers to (2S,4S)-4-fluoroproline and Hyp refers to (2S,4R)-4-hydroxyproline. ^{Cy5}CI has the sequence: Cy5-Gly-(SerGly)2-(HypflypGly)7-OH. Paraffin bone sections were stained in the dark for 1 hour at room temperature, then washed with 1X PBS.

Quantification of osteocytes and tdTomato+/SOST+ cells were obtained by taking three 40X images at the distal, medial, and proximal region along the ulna and the cells were manually quantified using ImageJ. An average among the three regions was calculated for each animal. At least 5 animals from each indicated genotype were examined. Quantification of osteoclasts was performed using the Bioquant Osteo software V17.2.6 (Bioquant Image Analysis Corp., Nashville, TN) according to standard procedures[165].

MicroCT analyses were performed using a lab microCT (Skyscan 1176; Bruker, Billerica, MA, USA) at 9 μm isotropic resolution utilizing a 0.3° rotation step, 0.5 mm aluminum filter, and 2 frame averaging. Data from the microCT scans were processed and analyzed using MicroView (v2.1.2 Advanced Bone Application; GE Healthcare Preclinical Imaging).

Skeletal Preparations

E17.5 embryos were skinned and eviscerated, fixed in 100% ethanol overnight then in acetone overnight. Specimens were stained with alcian blue in a solution containing 15mg alcian blue (Alcian blue 8GX, Sigma, A5268), 80ml of 95% ethanol and 20ml of glacial acetic acid up to two days. The skeletons were rinsed in 100% ethanol overnight and cleared in 2% KOH for 3 hrs. The specimens were transferred into alizarin red staining solution with 50mg/L alizarin red (Alizarin Red S, Sigma, A5533) in 2% KOH for 3-5 hrs. The tissue was then cleared in 1% KOH with 20% glycerol and transferred through an increasing glycerol series (20%, 50%, 80%), finally into 100% for long-term storage.

qRT-PCR for Hoxd11 expression

To analyze deletion of Hoxd11 following recombination, control and Hox11 conditional mutant were collected after a 1-month chase. The soft tissue from both forelimb zeugopod skeletons were removed and the bone marrow was flushed from both the radius and ulna into 1ml of digestion buffer (2mg/ml of collagenase type IV (Thermo Scientific, 17104-019) and 3mg/ml of dispase II (Thermo Scientific, 17105-041) in 1X PBS) using a 30G needle. The bones were subsequently minced with a razor in a petri dish under a tissue culture hood and the resulting pulp was transferred into digestion buffer with the flushed bone marrow. Three digestion steps were carried out at 37°C with periodic agitation to obtain a single cell suspension. After each period of digestion, cells in suspension were collected into cell culture media containing DMEM with 4.5 g/L D-glucose (Gibco), 1X Glutamax (Gibco), 1mM sodium pyruvate, 15% fetal bovine serum (FBS), 100 mg/mL streptomycin, and 100 U/mL penicillin. Red blood cells were lysed on ice at a final concentration of 0.5X. The cells were then strained through a 100μM cell strainer and plated. The cells were expanded, passaged twice, then subsequently sorted by a MA900 (Sony) cell sorter to obtain Hoxa11eGFP-expressing cells. RNA was extracted using the Qiagen RNeasy micro kit (Qiagen, 74004) and cDNA was synthesized using Superscript™ (Thermo Fisher, 11904018). *Hoxd11* expression was measured relative to GAPDH. qPCR was performed with the following primer set using Roche PowerUp™ SYBR™ Green Mastermix: Hoxd11R AGTGAGGTTGAGCATCCGAG, Hoxd11F ACA CCAAGTACCAGATCCGC. ΔCt values were calculated relative to GAPDH.

CHAPTER IV

Conclusion

Summary of significant findings

The most significant finding in this work is the demonstration of the continued function of *Hox* genes beyond embryogenesis. Much previous work has focused on the role of *Hox* genes during skeletal development and their requirement after the skeleton is established was largely undetermined. This study, for the first time, show clear genetic and functional data regarding the continuing function of *Hox* genes in skeletal stem cells governing their differentiation towards the osteolineage. Adult conditional loss of *Hox11* function leads to an accumulation of a woven bone-like matrix that progressively replaces normal lamellar bone. This primarily stems from the inability of *Hox11* conditional mutant osteoblasts to fully differentiate and mature to produce a normal bone matrix. Lineage analysis clearly demonstrates that the cells downstream of the *Hox11*-expressing skeletal stem cells that lost *Hox* function constitute the abnormal bone matrix. Further, the osteocyte-like cells embedded in the abnormal matrix completely lack dendrites failing to establish a lacuna-canilicular network and exhibit maturation deficiencies.

The conditional deletion of *Hox* function in my study addresses the drawbacks of many models used to determine the role of *Hox* genes beyond their classic embryonic role.

Using engineered overexpression from retroviral vectors and transgenic knockout or knock-in mouse models it has been shown that abnormal *Hox* expression results in improper differentiation of hematopoietic stem cells leading to an imbalance of downstream blood lineages[166–168]. Further, deregulation of *Hox* genes have also been linked to the predisposition or progression of many different malignancies[66,70,169,170]. While important insight has been shed through these studies, an important fact to keep in mind is that most of these studies have been conducted *in vitro* using freshly isolated cells or established cells lines. It is known, especially in the context of stem cells, that their *in vitro* capacity does not faithfully reflect their *in vivo* behavior. Moreover, the vast majority of the studies use null mutants that harbor non-functional *Hox* genes from development. As mentioned previously, this obfuscates the phenotypes observed at later stages as it is challenging to distinguish which defects can be attributed to the loss of *Hox* function and which are secondary to the already abnormal physiology that manifest during embryogenesis. Therefore, using a conditional deletion allele that allows for temporal deletion of *Hox* function, I was able to control for normal development and growth subsequently deleting *Hox11* function at adult stages to interrogate the specific role *Hox* genes play during adult skeletal homeostasis.

Results from my work show that the conditional loss of *Hox11* leads to the perturbation of the osteolineage differentiation revealing definitive evidence for a continuing role for *Hox* genes in the adult skeleton. However, the specific molecular mechanism of how *Hox* genes exert their function is still unclear. It is critical to reiterate that *Hox* genes encode transcription factors and are expected to exert their function in a cell autonomous manner at the transcriptional level. One of the main functions of

osteoblasts is the secretion of a collagen matrix that subsequently become mineralized constituting the hard bony matrix of the skeleton. Therefore, a possible mechanism of *Hox11* function may involve the proper transcription of collagen chains, the transcription of enzymes involved in the post-translational modification or transcription of proteins involved in subsequent organization of the collagen in the extracellular space. The basic transcription, post-translational modification and organization of collagen are as follows: 1. The *Col1a1* and *Col1a2* genes are transcribed and the resulting mRNA is translated then transported to the endoplasmic reticulum (ER). 2. Once in the ER, the signal peptide is removed, the lysine and proline residues get additional hydroxyl groups added to them, glycosylation of selected hydroxyl groups on lysine occurs, and finally the collagen chains assemble into triple helices (termed pro-collagen) then secreted into the extracellular space. 3. Collagen peptidases cleave the ends of the non-helical ends of the procollagen molecule and lysyl oxidases act on certain amino acid groups on the collagen to form cross-links stabilizing the organization of the collagen matrix[171].

Multiple events during the transcription and post-translational modification of the collagen is confirmed by the use of the collagen mimetic peptide (CMP) used in my study. The CMP mimics the proline-hydroxyproline-glycine amino acid triplet motif present in the protein sequence. By the strong binding of the CMP to the abnormal bony matrix in the *Hox11* conditional mutants (**refer to Figure 3.4J**), I can confirm that a collagen matrix is being secreted by the mutant osteoblasts. This is further validated by the picrosirius red stain showing the haphazard organization of the collagen (**refer to Figure 3.4**). Due to the hydroxyproline motif in the CMP, the addition of the hydryoxyl groups is also confirmed. The CMP is only able to bind collagen strands and not to those assembled into triple

helices, which indicates that the collagen secreted by the mutant osteoblasts were either never assembled into normal triple helices or *Hox* genes facilitate the production of proteins that stabilize the organization of the collagen matrix (e.g. lysyl oxidase). In either case, further future investigation will be required to address these questions (explained in detail in *Future Directions* section below).

Another course of action *Hox11* may be involved in is the regulation of integrins. Integrins are the principle receptors for animal cells to facilitate binding to their extracellular surroundings. It has been shown that *Hoxa11* acts upstream to promote the expression of *Integrin α8* in the developing kidney[172] and expression of a dominant negative form of *Integrin β1* in mature osteoblasts show skeletal phenotypes reminiscent of our *Hox11* conditional mutant[173]. Blocking integrin-mediated adhesion of osteoblasts using mimetic peptides also led to abnormal bone formation[174]. A wide variety of integrins including *Integrin α1, α2, α3, α5, α6, αV, β1, β3, β4,* and *β5* have been identified to be expressed in MSCs and osteoblasts[175,176]. Matrix stiffness highly impacts the differentiation of MSCs indicating that the ability for cells to sense their environment plays a critical role in their differentiation (reviewed by [177]). Taken together, this supports the hypothesis that the MSCs' ability to bind to the extracellular matrix primarily through integrins highly influences the differentiation of progenitor cells. In-depth investigation into whether *Hox11* regulates integrin expression that in turn affects the differentiation of skeletal stem cells would be an interesting next step (detailed in *Future Directions* section below).

Overall, the definitive data presented in my study shifts the prevalent belief that

Hox gene function in the skeleton is largely restricted to developmental stages. Further, results from my study clearly demonstrate that *Hox* genes regulate the proper differentiation and subsequent maturation of osteoblasts *in vivo*. Future studies interrogating the specific mechanisms involved in *Hox* regulation of skeletal stem cell differentiation will reveal critical information to the still enigmatic molecular mechanism of *Hox* genes.

Future directions

Identifying downstream molecular targets of Hox11

Despite many decades since the discovery of *Hox* genes and the plethora of genetic studies revealing their critical function, their downstream targets still remain unclear. The lack of reliable Hox antibodies complicates this issue. Many studies have made an effort to interrogate this question by expressing tagged versions of Hox proteins into cells followed by chromatin immunoprecipitation (ChIP), performing microarrays, and utilizing enhancer-trap systems[125,178–181]. Many targets have been revealed by these endeavors, however the artificial nature of transfecting tagged Hox proteins complicates the interpretation of the results and targets identified by microarray may not necessarily be directly regulated by Hox proteins. Therefore, a comprehensive list of Hox protein targets are still lacking. The ideal system for identifying Hox downstream targets would involve the production of Hox proteins under their endogenous regulatory elements and their subsequent binding *in vivo.* To address this issue, I have generated two mouse models where a 3X FLAG peptide has been inserted into the 3' end of the *Hoxa11* and *Hoxd11* loci (refer to Appendix I). This allows for the identification of the downstream targets of

Hox11 in vivo with minimal disruption to their transcriptional regulatory machinery.

The expression of both genes has been verified by a FLAG antibody and the expression pattern recapitulates that seen by the *Hoxa11eGFP* reporter allele and *Hoxd11 in situ* hybridization in embryonic limbs (**Figure 4.1A-D**). The next imperative verification is proper function of the tagged Hox11 proteins. To that point, heterozygotes from the *Hoxa11-3XFLAG* and *Hoxd11-3XFLAG* colonies are currently being bred together to ultimately generate homozygotes for all four *Hox11* alleles. Animals with the genotype $Hoxa11^{3XFLAG/3XFLAG}$; $Hoxd11^{3XFLAG/3XFLAG}$ will be used to assess whether the insertion of the 3X FLAG peptide has negatively impacted the genes. If the 3X FLAG insertion rendered the alleles non-functional, then $Hoxa11^{3XFLAG/3XFLAG}$; $Hoxd11^{3XFLAG/3XFLAG}$ animals would be expected to display *Hox11* null phenotypes (i.e. malformation of zeugopod skeleton).

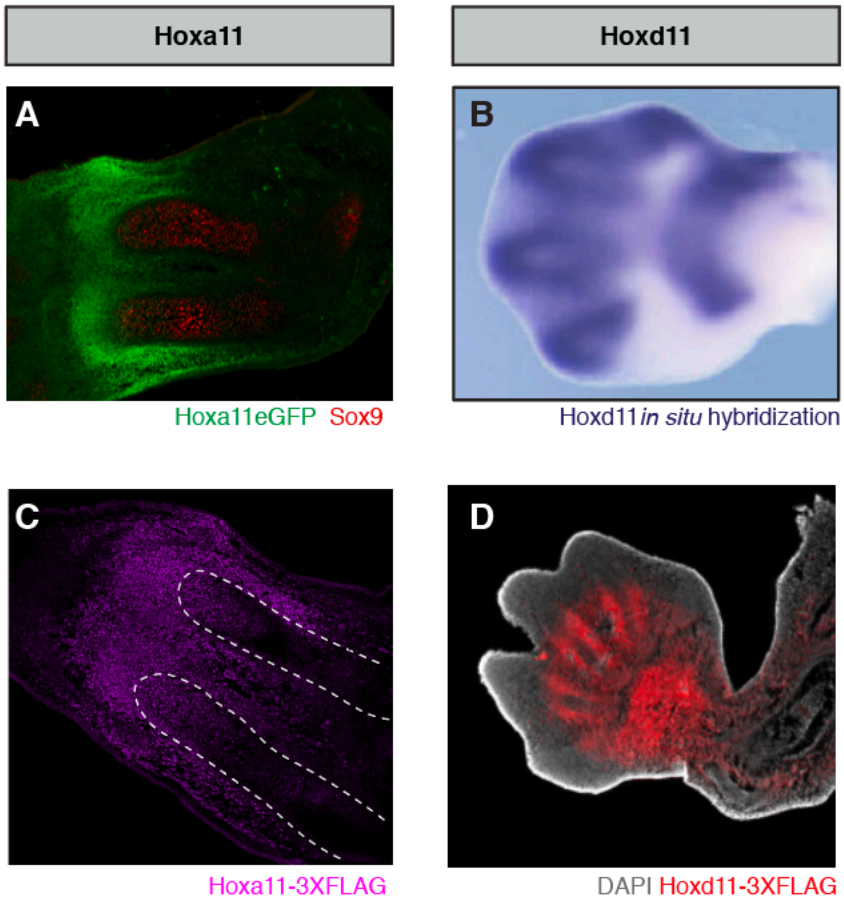

Figure 4.1. Expression pattern validation of *Hoxa11-3X FLAG* and *Hoxd11-3X FLAG* alleles. (A) Expression pattern of *Hoxa11* (green) at E13.5 is shown in the zeugopod region with the condensing cartilage anlage stained with Sox9 (red). Figure adapted from Swinehart *et al.* (2013)[88]. **(B)** *Hoxd11* expression pattern (blue color) is detected by *in situ* hybridization in E12.5 limbs. Figure adapted from Fabre *et al.* (2018)[182]. **(C)** Compare to Hoxa11eGFP expression pattern in (A) and note similar pattern. Expression pattern shown in E13.5 limbs from Hoxa11-3XFLAG animals detected by FLAG antibody (image courtesy of Lauren Koch). **(D)** Compare to *Hoxd11* expression pattern in (B) and note similar pattern. Expression pattern shown in E12.5 limbs from Hoxd11-3XFLAG animals detected by FLAG antibody (image courtesy of Lauren Koch).

Once proper function of the *Hox11* paralogs have been confirmed, subsequent ChIP experiments will identify DNA sites bound by the Hox11 proteins. However, the ChIP experiments alone will be insufficient to reveal targets of Hox11 proteins as mere binding

does not necessarily indicate transcriptional regulation. *Hox* genes have a rather generic TAAT core binding motif that has little specificity in binding DNA[183–185]. Therefore, performing RNA-sequencing of Hox11eGFP-expressing cells in control and Hox11 conditional mutants to identify differentially regulated mRNA and compare them to the bound sites from the ChIP experiments will reveal a more comprehensive list of downstream targets of Hox11 proteins.

Generating mouse models with different tags for the distinct *Hox11* paralogs will add more depth to understanding the downstream targets of Hox11. For example, one can generate a hemagglutinin (HA)-tagged *Hoxd11* and myc-tagged *Hoxc11* to use with the 3XFLAG-tagged *Hoxa11.* These animals can be generated using the same approach as the 3X FLAG-tagged *Hoxa11* and *Hoxd11* animals (refer to Appendix I). Both the HA and myc tag have a shorter peptide sequence compared to the 3X FLAG anticipating relatively simple generation of the animals. The different tags can be used in conjunction to interrogate whether *Hox* genes within the same paralogous group bind to the same or different targets. Intriguingly, *Hoxc11* is only expressed in the hindlimbs. Examining the differences in binding sites between *Hoxc11* compared to that of *Hoxa11* or *Hoxd11* would reveal interesting insights into the potential distinct mechanism of *Hoxc11* function in forelimbs and hindlimbs. Again, performing RNA-seq coinciding with the ChIP experiments will allow for the direct correlation of binding and transcriptional regulation.

As mentioned previously, the generic and simple binding motif of Hox proteins does not coincide with the highly specific functions they perform *in vivo*. The binding of co-factors have been found to increase Hox proteins' binding specificity. Extradenticle (Exd) and homothorax (Hth) in *Drosophila* and their vertebrate homologs Pbx and Meis

proteins, interact with Hox proteins to form a tripartite complex[186–189]. The presence of these cofactors confers longer binding consensus for Hox proteins and there is evidence for differential binding specificity of different Hox proteins[190–192]. In some cases, the Hox-cofactor complex can change the binding preference of Hox protein providing "latent specificity"[193]. These findings suggest that the binding of co-factors, establishing a complex is critical in DNA binding specificity. Therefore, in order to further comprehend the molecular mechanisms of Hox proteins, it would be important to identify co-factors that are part of the Hox-binding partner complex. To address this question, the 3X FLAG animals that are already available or the HA- or myc-tagged theoretical mouse models can be used to perform IP-mass spectrometry experiments to identify potential binding partners of Hox proteins.

Characterization of the potential targets of Hox11 could be identified by some follow-up studies from my work with the *Hox11* conditional mutant phenotype observed. As mentioned in the *Summary of significant findings* section, the mutant osteoblasts are capable of secreting a collagen matrix. However, whether the collagen that is secreted has a malformed structure or whether there is a lack of proteins that assist subsequent collagen organization and maturation was not determined. The structure of collagen molecules can be determined by Raman spectroscopy that uncovers biochemical information regarding the collagen molecules[194]. By comparing Raman spectroscopy results of collagen molecules from the control and *Hox11* conditional mutant bones may provide insight into pinpointing the defects found in the collagen molecules. Additionally, performing western blot analyses probing for proteins such as lysyl oxidases that are important in the organization of extracellular collagen would also offer further comprehension in potential

mechanisms of *Hox* function at the molecular level.

In regard to addressing *Hox11* regulation of integrins, the first experiment to perform would be an adhesion assay to determine whether cell adhesion is altered in the *Hox11* conditional mutant cells. Once an adhesion defect is confirmed, qRT-PCR as well as western blot analysis examining integrins that are known to be expressed in skeletal stem cells as well as osteoblasts that include *Integrin α1, α2, α3, α5, α6, αV, β1, β3, β4,* and *β5* will need to be examined to identify specific integrins molecule controlled by Hox11. These results can be verified by the RNA-seq and ChIP data, if available. Further, rescue experiments by either transfection or stimulatory antibodies[195] on the isolated *Hox11* mutant cells can be performed to validate these findings.

Hox function in mesenchymal stem cells (MSCs) or skeletal stem cells

An important function for adult MSCs is their ability to contribute to fracture repair. We have previously shown that the *Hox11*-lineage extensively contributes to the fracture callus[147]. Examining *Hox* requirement during adult fracture injury repair using the *Hox11* conditional mutant would provide further insight into adult *Hox* function in skeletal stem cells. Preliminary studies I have performed show that while the fracture callus forms and initial cartilage differentiation, identified by Sox9 expression, occurs in the *Hox11* conditional mutants at 10 days-post-fracture (DPF), there is a significant delay in fracture repair as the fracture gap has not been resolved even at 6 weeks-post-fracture (WPF) (Figure 4.1). As the timing of chondrocyte and osteoblast appearance within the fracture callus is well characterized, deleting *Hox* at various stages throughout the repair process would further refine *Hox*-mediated regulation of MSC differentiation at adult stages.

Scrutinizing stage-specific *Hox* function in the skeleton would be an interesting follow-up study to my work by using the conditional allele to delete *Hox* function during embryonic skeletal development and postnatal skeletal growth. While embryonic loss-of-function has clearly established that *Hox* genes impart region-specific function that differentially controls skeletal patterning and morphology, results from my study raise the question of whether differential *Hox* gene function continues to be conveyed in a region-specific manner or whether all *Hox* function is similar once the skeleton has been established. The experiment suggested above will further reveal intriguing information regarding the function of *Hox* genes in a stage-specific context.

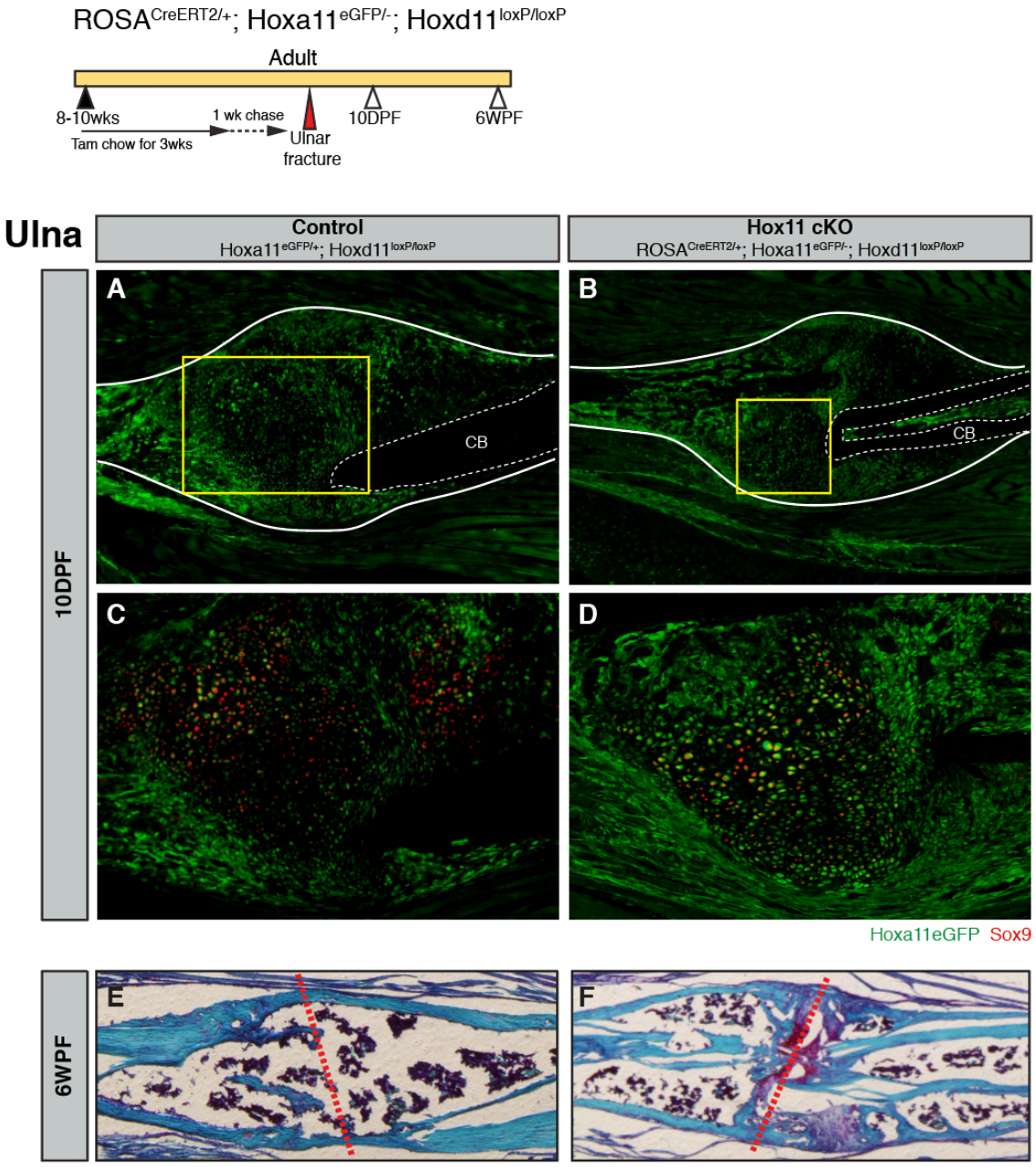

Figure 4.2. *Hox11* conditional mutants can initiate fracture repair but exhibit a significant lag in bridging the fracture gap. Controls (*Hoxa11$^{eGFP/-}$; Hoxd11$^{loxP/loxP}$*) and *Hox11* conditional mutants (*ROSA$^{CreERT2/+}$; Hoxa11$^{eGFP/-}$; Hoxd11$^{loxP/loxP}$*) animals were fed on tamoxifen chow at 8-10 weeks of age and their ulna were fractured after a 1-month chase starting from deletion. **(A, B)** At 10 days-post-fracture (10DPF) both control and *Hox11* conditional mutants form a fracture callus around the fracture site with an expansion of Hoxa11eGFP-expressing cells (green). Solid white line outlines the fracture callus. Dashed white lines outline the cortical bone (CB). **(C, D)** Sox9-expressing early cartilage cells (red) are present within both the control and *Hox11* conditional mutant fracture

calluses. **(E, F)** SafO-fast green stain that labels cartilage and bone, respectively, reveals that the fracture callus has not been resolved in the *Hox11* conditional mutants and the fracture gap has not been bridged. Red dashed line marks the fracture site.

Previous work from our lab suggests that the maintenance of skeletal stem cells is independent of *Hox* function as the Hoxa11eGFP-expressing MSCs are present in the *Hox11* compound mutant at comparable numbers to that of control[86] and Hoxa11eGFP-expressing cells are found in the zeugopod skeleton of the *Hox11* conditional mutant bones at 1-year of age (following a 10-month chase, refer to Sup Figure 3.3). However, a careful analysis has not been performed. Performing flow cytometry on the *Hox11* conditional mutant zeugopod bones and carefully quantifying the numbers of Hox11-expressing MSCs at various time points following the deletion of *Hox11* function, examining other sub-populations of MSCs (mentioned in Chapter II) and how they compare between control and conditional mutants may provide additional functions for *Hox* genes in MSCs such as maintenance of quiescence, promoting self-renewal, cross-talk with other MSC populations etc. Furthermore, the physical requirement for *Hox*-expressing cells within the skeleton has not been examined. DTR-mediated ablation of *Hox*-expressing cells at various time points throughout skeletal development, growth, and homeostasis may reveal unforeseen consequences that could provide intriguing insight into the function of *Hox*-expression cells.

To date, work in our laboratory has focused on *Hox11* as a model for global *Hox* function. This has led to intriguing and novel insights into *Hox* function. However, it still remains to be determined whether the findings from our laboratory using *Hox11* can be applied and broadened to other *Hox* paralogous groups. Several groups have reported that

fibroblasts extracted from distinct physiological locations retain region-specific *Hox* expression established during development[68,69,196]. Previous work from our lab extended these analyses to bone marrow stromal cells that were isolated from the adult zeugopod and stylopod to examine *Hox9-11* expression using qRT-PCR. It was confirmed that regional expression of *Hox* genes established during embryogenesis is maintained into adult stages, specifically in progenitor-enriched MSCs[86]. Generating a fluorescent reporter knock-in allele for a different *Hox* paralogs expressed at various axial levels followed by careful characterization mirroring that performed with the *Hoxa11eGFP* allele assessing the MSC characteristics of other *Hox*-expressing cells would broaden our findings. This can be taken further by generating inducible *CreERT2* alleles for the corresponding *Hox* paralogs to determine *in vivo* regional contribution to the skeleton and generating conditional alleles examining the consequences of conditional deletion of *Hox* function similar to that of my study in Chapter III. Information gathered from these kinds of future studies will determine whether other *Hox* paralogs share similar cellular mechanisms and functions.

Overall, these studies will provide unprecedented insight into the cellular function and molecular mechanism of *Hox* genes. These future directions will provide a strong foundation to address questions that are outside the current scope of this thesis including molecular targets of *Hox* genes and the global nature of *Hox* function in regional skeletal MSC populations. Results from these experiments will also have a significant impact on their potential therapeutic use considering the potential functional differences between region-specific MSC populations. Future studies will expand our understanding of *Hox* function in skeletal biology, broaden our knowledge regarding *Hox* function in

skeletal MSCs, and also contribute important new insight in skeletal MSC biology.

APPENDIX I

Generation of *Hoxa11-3XFLAG* and *Hoxd11-3XFLAG* by Cas9/CRISPR Genetic Engineering

Cas9/CRISPR genetic engineering was used to insert the synthetic 3X FLAG peptide into the 5' end of the *Hoxa11* and *Hoxd11* loci. We searched for guide RNAs that cut closest to the translational start site (ATG) with the minimum number of amino acids between the ATG and guide RNA cut site (Appx Figure 5.1A and 5.2A). The donor sequence was designed so that the 3X FLAG sequence was present between the guide RNA cut site and downstream PAM site eliminating the possibility of unwanted the Cas9 nuclease targeting to the donor sequence or recombined allele. This editing strategy was carefully designed not disrupt the surrounding sequence around both loci to keep all endogenous regulatory elements intact. Further, a Gly-Ser-Gly flexible bridge was inserted immediately downstream of the 3X FLAG sequence to relieve any conformation strain that may result from the FLAG peptide in the final protein product.

7 out of 85 live births for the *Hoxa11-3XFLAG* and 10 out of 61 live births for the *Hoxd11-3XFLAG* founder animals (F0) were confirmed to produce the correct size band for 3XFLAG insertion assessed by PCR (Appx Figure 5.1B and 5.2B). Precise and in-frame targeting was confirmed by sanger sequencing. 3 out of the 7 founders for the *Hoxa11-3XFLAG* and 4 out of the 10 for the *Hoxd11-3XFLAG* founders were confirmed

to have perfectly targeted insertion of the 3XFLAG peptide (Appx Figure 5.1C and 5.2C). Founder #541 for *Hoxa11-3XFLAG* and founder #23 for *Hoxd11-3XFLAG* were chosen to establish subsequent colonies. The founders were bred back to C57/Bl6 wildtype animals for two generations to generate heterozygotes.

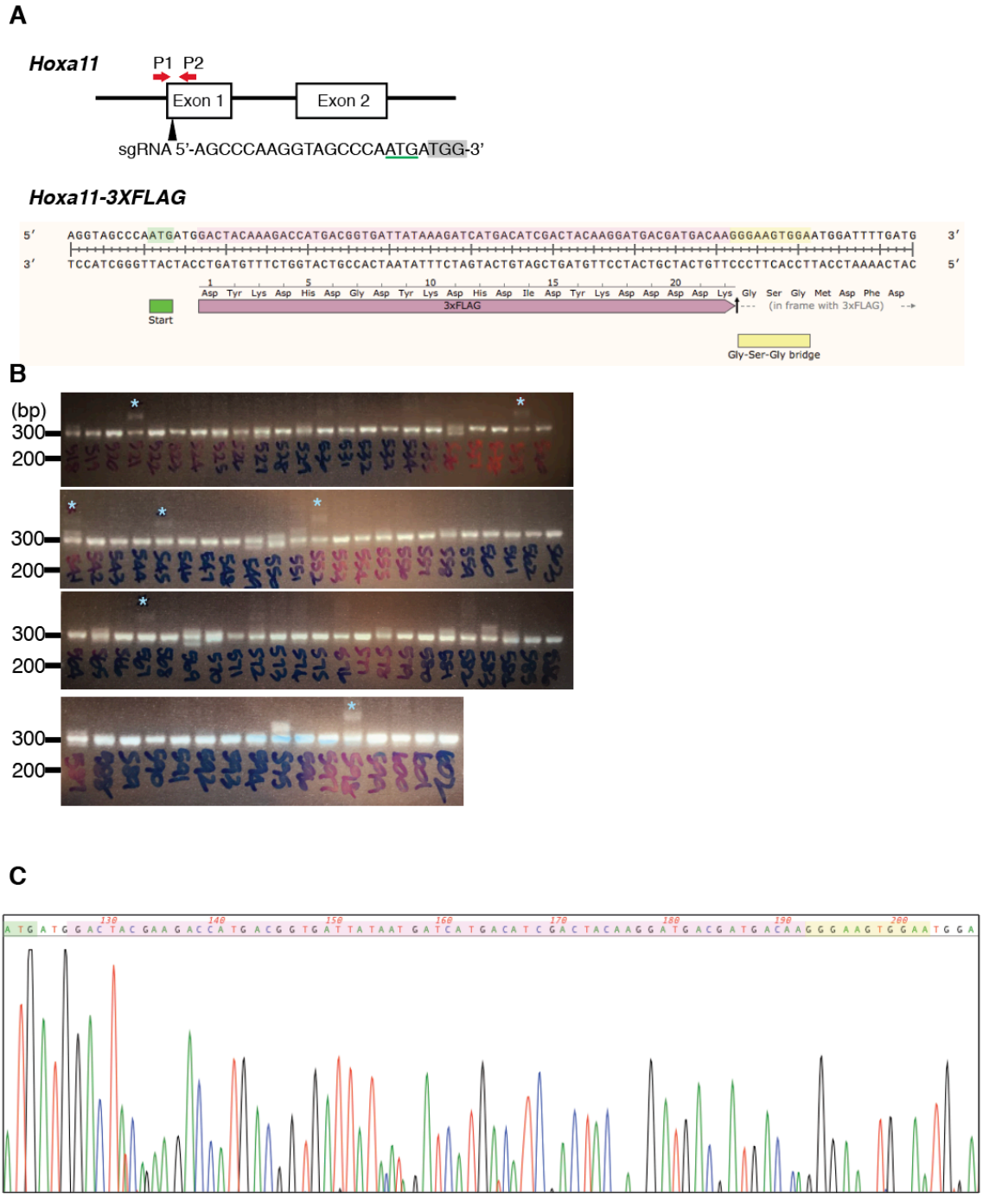

Appendix Figure 5.1. Generation of *Hoxa11-3XFLAG* allele *via* Cas9/CRISPR genetic engineering. (A) *Top panel:* cartoon schematic of the *Hoxa11* locus and approximate position of target guide RNA for 3XFLAG insertion. Green underline highlights transcription start site and gray highlight marks the PAM sequence of the guide RNA. *Bottom panel:* DNA sequence of the theoretical *Hoxa11-3XFLAG* allele. Green highlight: transcription start site (ATG). Pink highlight: 3X FLAG peptide sequence. Yellow

highlight: Gly-Ser-Gly flexible bridge sequence. **(B)** PCR analysis using P1 and P2 (red arrows) that are upstream and downstream from the gRNA cut site revealed 7 animals (blue asterisk) with the expected band size for a 3XFLAG insertion (317bp). **(C)** Sequence chromatogram from the #541 showing correct, in-frame insertion of the 3X FLAG peptide into the *Hoxa11* locus. Green highlight: transcription start site (ATG). Pink highlight: 3X FLAG peptide sequence. Yellow highlight: Gly-Ser-Gly flexible bridge sequence.

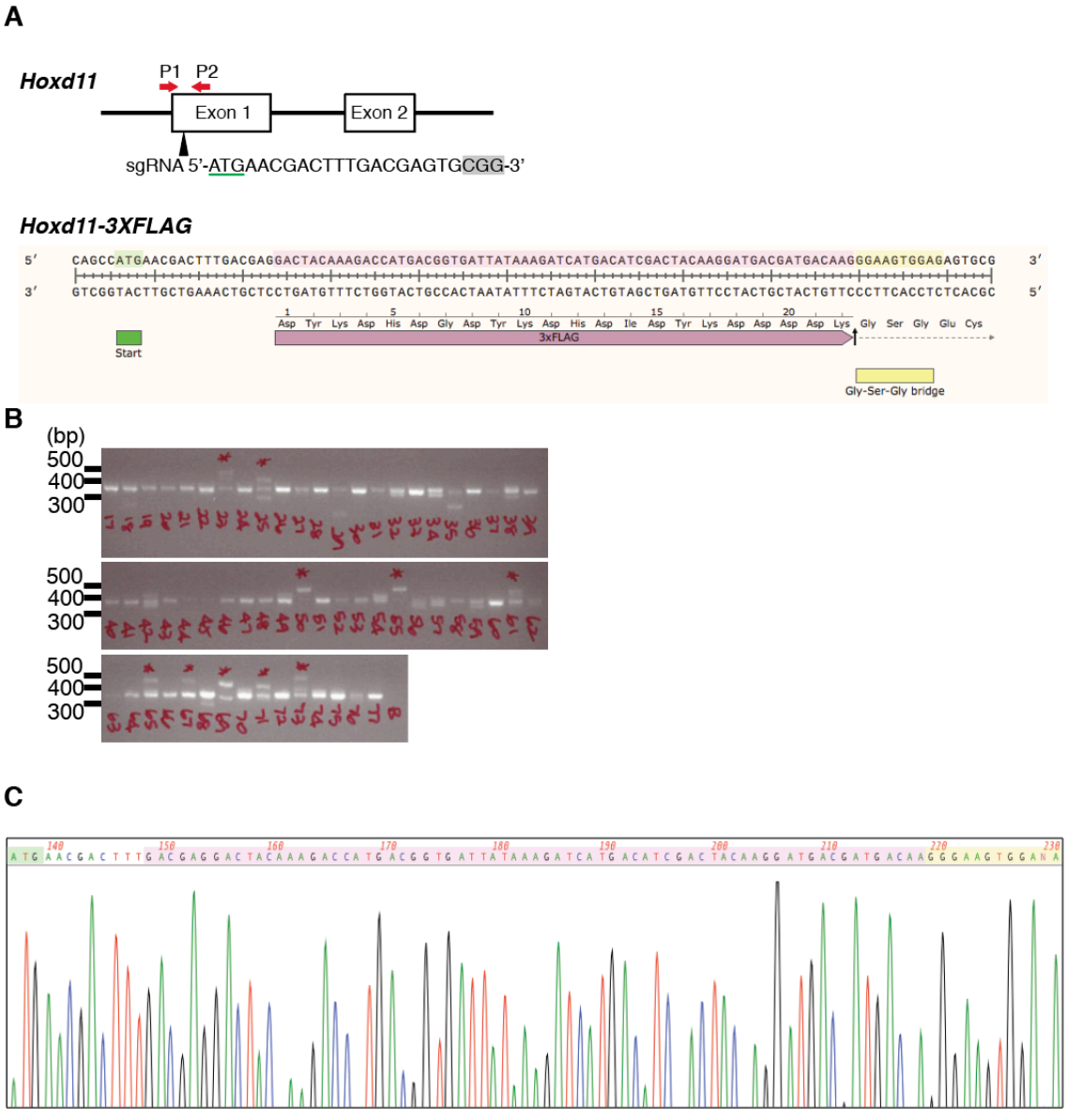

Appendix Figure 5.2. Generation of Generation of *Hoxd11-3XFLAG* allele *via* Cas9/CRISPR genetic engineering. (A) *Top panel:* cartoon schematic of the *Hoxd11*

locus and approximate position of target guide RNA for 3XFLAG insertion. Green underline highlights transcription start site and gray highlight marks the PAM sequence of the guide RNA. *Bottom panel:* DNA sequence of the theoretical *Hoxd11-3XFLAG* allele. Green highlight: transcription start site (ATG). Pink highlight: 3X FLAG peptide sequence. Yellow highlight: Gly-Ser-Gly flexible bridge sequence. **(B)** PCR analysis using P1 and P2 (red arrows) that are upstream and downstream from the gRNA cut site revealed 7 animals (blue asterisk) with the expected band size for a 3XFLAG insertion (450bp). **(C)** Sequence chromatogram from the #23 showing correct, in-frame insertion of the 3X FLAG peptide into the *Hoxa11* locus. Green highlight: transcription start site (ATG). Pink highlight: 3X FLAG peptide sequence. Yellow highlight: Gly-Ser-Gly flexible bridge sequence.

Materials and Methods

Production of sgRNAs and Cas9 mRNA

All guide sequences were cloned into the pT7-Guide Vector (Blue Heron Biotech, LLC). MEGAshortscript T7 kit (Life Technologies) was used to generate *in vitro* transcribed sgRNA's from the pT7-Guide Vector and products were subsequently purified using the MEGAclear kit (Life Technologies). Using the pT7-Cas9-Nuclease vector (gift from Dr. Moises Mallo), Cas9 mRNA was *in vitro* transcribed using the mMESSAGE mMACHINE T7 ULTRA kit (Life Technologies) and purified using the MEGAclear kit (Life Technologies).

Donor oligos

Donor oligos were purchased from Integrated DNA Technologies (IDT) as Megamer® Single-stranded DNA fragments. The total length of the donor oligo was kept at 200bp. Thus, the homology sequence on either side was approximately 50bp.

Zygote injection

Zygote injections were performed as previously described with minor modifications[145]. C57BL/6 female mice were super-ovulated and mated with C57Bl/6 male mice in order to

collect embryos of one-cell stage for microinjection. CRISPR reagents were microinjected at the following concentrations: Cas9 mRNA (100ng/μL), sgRNA (50ng/μL), and donor oligo (25ng/μL). Freshly injected eggs were transferred into pseudopregnant females and resulting progeny were initially screened for potential recombination events via PCR.

Confirmation of *Hoxa11-3XFLAG* targeting

85 live births were recovered from the microinjections and initial screening for 3XFLAG targeting was performed by PCR. Approximate location of all primers is indicated in Appx Figure 5.1A.

Primers (Wildtype 200bp, 3XFLAG targeted 317bp)

Forward: 5' – GTC ACA TGA CCA GCA CCT CC – 3'
Reverse: 5' – AGT ATG TCA TTG GGC GCG AA – 3'

Correct targeting was confirmed by sanger sequencing using the same primers used for PCR indicated above.

Confirmation of *Hoxd11-3XFLAG* targeting

61 live births were recovered from the microinjections and initial screening for 3XFLAG targeting was performed by PCR. Approximate location of all primers is indicated in Appx Figure 5.2A.

Primers (Wildtype 369bp, 3XFLAG targeted 450bp)

Forward: 5' – ACG TGA CAT AAT TAC CAC CAG AA – 3'
Reverse: 5' – CAG GCC GTA GTC GCG AAA – 3'

Correct targeting was confirmed by sanger sequencing using the same primers used for PCR indicated above.

References

1. Garcia-Fernàndez, J. The genesis and evolution of homeobox gene clusters. *Nat. Rev. Genet.* 881–892 (2005). doi:10.1038/nrg1723

2. Duboule, D. The rise and fall of Hox gene clusters. *Development* **134**, 2549–60 (2007).

3. Lewis, E. B. A gene controlling segmentation in Drosophila. *Nature* **276**, 565–570 (1978).

4. Kaufman, T. C., Lewis, R. & Wakimoto, B. Cytogenetic analysis of chromosome 3 in Drosophila melanogaster: The homoeotic gene complex in polytene chromosome interval 84A-B. *Genetics* **94**, 115–133 (1980).

5. Lewis, R. A., Kaufman, T. C., Denell, R. E. & Tallerico, P. Genetic analysis of the Antennapedia gene complex (ANT-C) and adjacent chromosomal regions of Drosophila melanogaster. *Genetics* **95**, 367–381 (1980).

6. Bateson, W. *Materials for the Study of Variation*. (Macmillan, 1984).

7. Harding, K., Wedeen, C., McGinnis, W. & Levine, M. Spatially regulated expression of homeotic genes in Drosophila. *Science (80-.).* 1236–1242 (1985). doi:10.1126/science.3898362

8. Akam, M. The molecular basis for metameric pattern in the Drosophila embryo. *Development* 1–22 (1987).

9. Rux, D. R. & Wellik, D. M. Hox Genes in the Adult Skeleton: Novel Functions Beyond Embryonic Development. *Dev. Dyn.* **007505**, 1–47 (2016).

10. Kmita, M., Fraudeau, N., Hérault, Y. & Duboule, D. Serial deletions and

duplications suggest a mechanism for the collinearity of Hoxd genes in limbs. *Nature* **420**, 145–150 (2002).

11. Marie Kmita and Denis Duboule. Organizing Axes in Time and Space; 25 years of colinear tinkering. *Science (80-.).* **301**, 331–333 (2003).

12. Kessel, M. & Gruss, P. Homeotic transformations of murine vertebrae and concomitant alteration of Hox codes induced by retinoic acid. *Cell* **67**, 89–104 (1991).

13. Burke, A. C., Nelson, C. E., Morgan, B. A. & Tabin, C. Hox genes and the evolution of vertebrate axial morphology. *Development* **121**, 333–346 (1995).

14. Nowicki, J. L. & Burke, A. C. Hox genes and morphological identity: axial versus lateral patterning in the vertebrate mesoderm. *Development* 4265–4275 (2000). doi:10.1038/NCHEM.1151

15. Burke, A. C. & Nowicki, J. L. Hox genes and axial specification in vertebrates. *Integr. Comp. Biol.* **41**, 687–697 (2001).

16. Mallo, M., Wellik, D. M. & Deschamps, J. Hox genes and regional patterning of the vertebrate body plan. *Dev. Biol.* **344**, 7–15 (2010).

17. Mallo, M. & Alonso, C. R. The regulation of Hox gene expression during animal development. *Development* **140**, 3951–3963 (2013).

18. Horan, G. S. B. *et al.* Compound mutants for the paralogous hoxa-4, hoxb-4, and hoxd-4 genes show more complete homeotic transformations and a dose-dependent increase in the number of vertebrae transformed. *Genes Dev.* **9**, 1667–XI (1995).

19. McIntyre, D. C. *et al.* Hox patterning of the vertebrate rib cage. *Development* **134**, 2981–2989 (2007).

20. Wellik, D. M. & Capecchi, M. R. Hox10 and Hox11 genes are required to globally

pattern the mammalian skeleton. *Science* **301**, 363–367 (2003).

21. Hrycaj, S. M. *et al.* Hox5 genes regulate the Wnt2/2b-Bmp4-signaling axis during lung development. *Cell Rep.* **12**, 903–912 (2015).

22. Chen, F. & Capecchi, M. R. Targeted mutations in hoxa-9 and hoxb-9 reveal synergistic interactions. *Dev. Biol.* **181**, 186–196 (1997).

23. Chen, F. & Capecchi, M. R. Paralogous mouse Hox genes, Hoxa9, Hoxb9, and Hoxd9, function together to control development of the mammary gland in response to pregnancy. *Dev. Biol.* **96**, 541–546 (1999).

24. Condie, B. G. & Capecchi, M. R. Mice with targeted disruptions in the paralogous genes hoxa-3 and hoxd-3 reveal synergistic interactions. *Nature* **370**, 304–307 (1994).

25. Davis, a P., Witte, D. P., Hsieh-Li, H. M., Potter, S. S. & Capecchi, M. R. Absence of radius and ulna in mice lacking hoxa-11 and hoxd-11. *Nature* **375**, 791–795 (1995).

26. Fromental-Ramain, C. *et al.* Hoxa-13 and Hoxd-13 play a crucial role in the patterning of the limb autopod. *Development* **122**, 2997–3011 (1996).

27. Fromental-Ramain, C. *et al.* Specific and redundant functions of the paralogous Hoxa-9 and Hoxd-9 genes in forelimb and axial skeleton patterning. *Development* **122**, 461–472 (1996).

28. Manley, N. R. & Capecchi, M. R. Hox group 3 paralogs regulate the development and migration of the thymus, thyroid, and parathyroid glands. *Dev. Biol.* **195**, 1–15 (1998).

29. Studer, M. *et al.* Genetic interactions between Hoxa1 and Hoxb1 reveal new roles in regulation of early hindbrain patterning. *Development* **125**, 1025–1036 (1998).

30. van den Akker, E. *et al.* Axial skeletal patterning in mice lacking all paralogous

group 8 Hox genes. *Development* **128**, 1911–1921 (2001).

31. Wahba, G. M., Hostikka, S. L. & Carpenter, E. M. The paralogous Hox genes Hoxa10 and Hoxd10 interact to pattern the mouse hindlimb peripheral nervous system and skeleton. *Dev. Biol.* **231**, 87–102 (2001).

32. Wellik, D. M., Hawkes, P. J. & Capecchi, M. R. Hox11 paralogous genes are essential for metanephric kidney induction. *Genes Dev.* 1423–1432 (2002). doi:10.1101/gad.993302.molecular

33. Gavalas, A., Trainor, P., Ariza-McNaughton, L. & Krumlauf, R. Synergy between Hoxa1 and Hoxb1: The relationship between arch patterning and the generation of cranial neural crest. *Development* **128**, 3017–3027 (2001).

34. Haack, H. & Gruss, P. The establishment of murine Hox-1 expression domains during patterning of the limb. *Developmental biology* **157**, 410–422 (1993).

35. Nelson, C. E. *et al.* Analysis of Hox gene expression in the chick limb bud. *Development* **122**, 1449–1466 (1996).

36. Tarchini, B. & Duboule, D. Control of Hoxd genes' collinearity during early limb development. *Dev. Cell* **10**, 93–103 (2006).

37. Zakany, J. & Duboule, D. The role of Hox genes during vertebrate limb development. *Current Opinion in Genetics and Development* **17**, 359–366 (2007).

38. Hostikka, S. L. & Capecchi, M. R. The mouse Hoxc11 gene: Genomic structure and expression pattern. *Mech. Dev.* 133–145 (1998). doi:10.1016/S0925-4773(97)00182-2

39. Xu, B. & Wellik, D. M. Axial Hox9 activity establishes the posterior field in the developing forelimb. *Proc. Natl. Acad. Sci. U. S. A.* **108**, 4888–91 (2011).

40. Xu, B. *et al.* Hox5 interacts with Plzf to restrict Shh expression in the developing forelimb. *Proc. Natl. Acad. Sci. U. S. A.* **110**, 19438–43 (2013).

41. Kmita, M. *et al.* Early developmental arrest of mammalian limbs lacking HoxA/HoxD gene function. *Nature* **435**, 1113–1116 (2005).

42. Thorogood, P. V & Hinchliffe, J. R. An analysis of the condensation process during chondrogenesis in the embryonic chick hind limb. *J. Embryol. Exp. Morphol.* **33**, 581–606 (1975).

43. Akiyama, H., Chaboissier, M. C., Martin, J. F., Schedl, A. & De Crombrugghe, B. The transcription factor *Sox9* has essential roles in successive steps of the chondrocyte differentiation pathway and is required for expression of *Sox5* and *Sox6*. *Genes Dev.* **16**, 2813–2828 (2002).

44. Bi, W., Deng, J. M., Zhang, Z., Behringer, R. R. & De Crombrugghe, B. *Sox9* is required for cartilage formation. *Nat. Genet.* **22**, 85–89 (1999).

45. Bi, W. *et al.* Haploinsufficiency of Sox9 results in defective cartilage primordia and premature skeletal mineralization. *Proc. Natl. Acad. Sci.* (2001). doi:10.1073/pnas.111092198

46. Akiyama, H. *et al.* Osteo-chondroprogenitor cells are derived from Sox9 expressing precursors. *Proc. Natl. Acad. Sci. U. S. A.* **102**, 14665–70 (2005).

47. Abad, V. *et al.* The role of the resting zone in growth plate chondrogenesis. *Endocrinology* **143**, 1851–1857 (2002).

48. Hunziker, E. B. Mechanism of longitudinal bone growth and its regulation by growth plate chondrocytes. *Microsc Res Tech* **28**, 505–519 (1994).

49. Beier, F. Cell-cycle control and the cartilage growth plate. *J. Cell. Physiol.* **202**, 1–8 (2005).

50. Cooper, K. L. *et al.* Multiple phases of chondrocyte enlargement underlie differences in skeletal proportions. *Nature* **495**, 375–8 (2013).

51. Rooney, P. & Archer, C. W. The development of the perichondrium in the avian

ulna. *J. Anat.* **181 (Pt 3**, 393–401 (1992).

52. Maes, C. *et al.* Osteoblast precursors, but not mature osteoblasts, move into developing and fractured bones along with invading blood vessels. *Dev. Cell* **19**, 329–344 (2010).

53. Karsenty, G. & Wagner, E. F. Reaching a genetic and molecular understanding of skeletal evelopment. *Dev. Cell* **2**, 389–406 (2002).

54. Kronenberg, H. M. The role of the perichondrium in fetal bone development. *Ann. N. Y. Acad. Sci.* **1116**, 59–64 (2007).

55. McKee, M. D. & Cole, W. G. *Chapter 2 Bone Matrix and Mineralization*. *Pediatric Bone* (Elsevier Inc., 2012). doi:10.1016/B978-0-12-382040-2.10002-4

56. Boyce, B. F., Rosenberg, E., de Papp, A. E. & Duong, L. T. The osteoclast, bone remodelling and treatment of metabolic bone disease. *European Journal of Clinical Investigation* (2012). doi:10.1111/j.1365-2362.2012.02717.x

57. Martin, T. J. & Seeman, E. Bone remodelling: its local regulation and the emergence of bone fragility. *Best Practice and Research: Clinical Endocrinology and Metabolism* (2008). doi:10.1016/j.beem.2008.07.006

58. Maes, C. & Kronenberg, H. M. Bone Development and Remodeling. in *Endocrinology: Adult and Pediatric* (2016). doi:10.1016/b978-0-323-18907-1.00060-3

59. Henriksen, K., Neutzsky-Wulff, A. V., Bonewald, L. F. & Karsdal, M. A. Local communication on and within bone controls bone remodeling. *Bone* (2009). doi:10.1016/j.bone.2009.03.671

60. Sims, N. A. & Gooi, J. H. Bone remodeling: Multiple cellular interactions required for coupling of bone formation and resorption. *Seminars in Cell and Developmental Biology* (2008). doi:10.1016/j.semcdb.2008.07.016

61. Xu, F. & Teitelbaum, S. L. Osteoclasts: New Insights. *Bone Res.* **1**, 11–26 (2013).

62. Dirckx, N., Van Hul, M. & Maes, C. Osteoblast recruitment to sites of bone formation in skeletal development, homeostasis, and regeneration. *Birth Defects Res. Part C - Embryo Today Rev.* **99**, 170–191 (2013).

63. Bonewald, L. F. Generation and function of osteocyte dendritic processes. *J. Musculoskelet. Neuronal Interact.* **5**, 321–324 (2005).

64. Turner, C. H., Robling, A. G., Duncan, R. L. & Burr, D. B. Do bone cells behave like a neuronal network? *Calcif. Tissue Int.* **70**, 435–442 (2002).

65. Klein-Nulend, J., Bacabac, R. G. & Mullender, M. G. Mechanobiology of bone tissue. *Pathol. Biol.* **53**, 576–580 (2005).

66. Takahashi, Y. *et al.* Expression profiles of 39 HOX genes in normal human adult organs and anaplastic thyroid cancer cell lines by quantitative real-time RT-PCR system. *Exp. Cell Res.* **293**, 144–153 (2004).

67. Rinn, J. L. *et al.* A dermal HOX transcriptional program regulates site-specific epidermal fate. *Genes Dev.* **22**, 303–307 (2008).

68. Ackema, K. B. & Charité, J. Mesenchymal stem cells from different organs are characterized by distinct topographic Hox codes. *Stem Cells Dev.* **17**, 979–991 (2008).

69. Liedtke, S. *et al.* The HOX Code as a 'biological fingerprint' to distinguish functionally distinct stem cell populations derived from cord blood. *Stem Cell Res.* **5**, 40–50 (2010).

70. Shah, N. & Sukumar, S. The Hox genes and their roles in oncogenesis. *Nat. Rev. Cancer* **10**, 361–371 (2010).

71. Sun, Y. *et al.* HOXA9 Reprograms the Enhancer Landscape to Promote Leukemogenesis. *Cancer Cell* (2018). doi:10.1016/j.ccell.2018.08.018

72. Mohr, S. *et al.* Hoxa9 and Meis1 Cooperatively Induce Addiction to Syk Signaling by Suppressing miR-146a in Acute Myeloid Leukemia. *Cancer Cell* (2017). doi:10.1016/j.ccell.2017.03.001

73. Van Scherpenzeel Thim, V. *et al.* Mutation analysis of the HOX paralogous 4-13 genes in children with acute lymphoid malignancies: Identification of a novel germline mutation of HOXD4 leading to a partial loss-of-function. *Hum. Mutat.* (2005). doi:10.1002/humu.20155

74. Hoffmann, T. J. *et al.* Imputation of the Rare HOXB13 G84E Mutation and Cancer Risk in a Large Population-Based Cohort. *PLoS Genet.* (2015). doi:10.1371/journal.pgen.1004930

75. Pilié, P. G. *et al.* Germline genetic variants in men with prostate cancer and one or more additional cancers. *Cancer* (2017). doi:10.1002/cncr.30817

76. Alanee, S., Couch, F. & Offit, K. Association of a HOXB13 variant with breast cancer. *New England Journal of Medicine* (2012). doi:10.1056/NEJMc1205138

77. Akbari, M. R. *et al.* Germline HOXB13 p.Gly84Glu mutation and risk of colorectal cancer. *Cancer Epidemiol.* (2013). doi:10.1016/j.canep.2013.03.003

78. Pfaltzgraff, E. R. *et al.* Anatomic origin of osteochondrogenic progenitors impacts sensitivity to EWS-FLI1-Induced Transformation. *Cancers (Basel).* (2019). doi:10.3390/cancers11030313

79. Svoboda, L. K. *et al.* Overexpression of HOX genes is prevalent in Ewing sarcoma and is associated with altered epigenetic regulation of developmental transcription programs. *Epigenetics* (2014). doi:10.4161/15592294.2014.988048

80. Raman, V. *et al.* Compromised HOXA5 function can limit p53 expression in human breast tumours. *Nature* **405**, 974–978 (2000).

81. Ventura, A. *et al.* Restoration of p53 function leads to tumour regression in vivo. *Nature* **445**, 661–665 (2007).

82. Harris, S. L. & Levine, A. J. The p53 pathway: Positive and negative feedback loops. *Oncogene* (2005). doi:10.1038/sj.onc.1208615

83. Saldaña-Meyer, R. & Recillas-Targa, F. Transcriptional and epigenetic regulation of the p53 tumor suppressor gene. *Epigenetics* (2011). doi:10.4161/epi.6.9.16683

84. Chen, H., Chung, S. & Sukumar, S. HOXA5-Induced Apoptosis in Breast Cancer Cells Is Mediated by Caspases 2 and 8. *Mol. Cell. Biol.* (2004). doi:10.1128/mcb.24.2.924-935.2004

85. Pineault, K. M. *et al.* Hox11 genes regulate postnatal longitudinal bone growth and growth plate proliferation. *Biol. Open* 1538–1548 (2015). doi:10.1242/bio.012500

86. Rux, D. R. *et al.* Regionally Restricted Hox Function in Adult Bone Marrow Multipotent Mesenchymal Stem/Stromal Cells. *Dev. Cell* 1–14 (2016). doi:10.1016/j.devcel.2016.11.008

87. Rux, D. R. *et al.* Hox11 Function Is Required for Region-Specific Fracture Repair. *J. Bone Miner. Res.* **32**, 1750–1760 (2017).

88. Swinehart, I. T., Schlientz, A. J., Quintanilla, C. a, Mortlock, D. P. & Wellik, D. M. Hox11 genes are required for regional patterning and integration of muscle, tendon and bone. *Development* **140**, 4574–82 (2013).

89. McCulloch, E. A. & Till, J. E. The Radiation Sensitivity of Normal Mouse Bone Marrow Cells , Determined by Quantitative Marrow Transplantation into Irradiated Mice Author. *Radiat. Res.* **13**, 115–125 (1960).

90. Till, J. E. & McCulloch, E. A. A Direct Measurement of the Radiation Sensitivity of Normal Mouse Bone Marrow Cells. *Radiat. Res. Soc.* **14**, 213–222 (1961).

91. Siminovitch, L., McCulloch, E. A. & Till, J. E. The distribution of colony-forming cells among spleen colonies. *J. Cell. Comp. Physiol.* **62**, 327–336 (1963).

92. Friedenstein, A. J., Gorskaja, J. F. & Kulagina, N. N. Fibroblast precursors in

normal and irradiated mouse hematopoietic organs. *Exp. Hematol.* (1976).

93. Friedenstein, A. J., Chailakhyan, R. K. & Gerasimov, U. V. Bone marrow osteogenic stem cells: in vitro cultivation and transplantation in diffusion chambers. *Cell Tissue Kinet.* **20**, 263–272 (1987).

94. Friedenstein, A. J., Petrakova, K. V., Kurolesova, A. I. & Frolova, G. P. Heterotopic Transplants of Bone Marrow. *Transplantation* **6**, 230–247 (1968).

95. Friedenstein, A. J., Latzinik, N. W., Grosheva, A. G. & Gorskaya, U. F. Marrow microenvironment transfer by heterotopic transplantation of freshly isolated and cultured cells in porous sponges. *Exp. Hematol.* (1982).

96. Caplan, A. Mesenchymal stem cells. *J. Orthop. Res.* **9**, 641–50 (1991).

97. Sacchetti, B. *et al.* Self-renewing osteoprogenitors in bone marrow sinusoids can organize a hematopoietic microenvironment. *Cell* **131**, 324–36 (2007).

98. Morrison, S. J. & Scadden, D. T. The bone marrow niche for haematopoietic stem cells. *Nat. Rev. Mol. Cell Biol.* **505**, 327–3334 (2014).

99. Méndez-Ferrer, S. *et al.* Mesenchymal and haematopoietic stem cells form a unique bone marrow niche. *Nature* **466**, 829–834 (2010).

100. Omatsu, Y. *et al.* The Essential Functions of Adipo-osteogenic Progenitors as the Hematopoietic Stem and Progenitor Cell Niche. *Immunity* **33**, 387–399 (2010).

101. Sugiyama, T., Kohara, H., Noda, M. & Nagasawa, T. Maintenance of the Hematopoietic Stem Cell Pool by CXCL12-CXCR4 Chemokine Signaling in Bone Marrow Stromal Cell Niches. *Immunity* (2006). doi:10.1016/j.immuni.2006.10.016

102. Roberts, E. W. *et al.* Depletion of stromal cells expressing fibroblast activation protein-α from skeletal muscle and bone marrow results in cachexia and anemia. *J. Exp. Med.* (2013). doi:10.1084/jem.20122344

103. Ding, L. & Morrison, S. J. Haematopoietic stem cells and early lymphoid

progenitors occupy distinct bone marrow niches. *Nature* **495**, 231–235 (2013).

104. Ding, L., Saunders, T. L., Enikolopov, G. & Morrison, S. J. Endothelial and perivascular cells maintain haematopoietic stem cells. *Nature* **481**, 457–62 (2012).

105. Koide, Y. *et al.* Two distinct stem cell lineages in murine bone marrow. *Stem Cells* **25**, 1213–1221 (2007).

106. Dominici, M. *et al.* Minimal criteria for defining multipotent mesenchymal stromal cells. The International Society for Cellular Therapy position statement. *Cytotherapy* **8**, 315–317 (2006).

107. Kfoury, Y. & Scadden, D. T. Mesenchymal Cell Contributions to the Stem Cell Niche. *Cell Stem Cell* **16**, 239–253 (2015).

108. Pinho, S. *et al.* PDGFRα and CD51 mark human nestin+ sphere-forming mesenchymal stem cells capable of hematopoietic progenitor cell expansion. *J. Exp. Med.* **210**, 1351–1367 (2013).

109. Ono, N. *et al.* Vasculature-Associated Cells Expressing Nestin in Developing Bones Encompass Early Cells in the Osteoblast and Endothelial Lineage. *Dev. Cell* **29**, 330–339 (2014).

110. Park, D. *et al.* Endogenous bone marrow MSCs are dynamic, fate-restricted participants in bone maintenance and regeneration. *Cell Stem Cell* **10**, 259–272 (2012).

111. Worthley, D. L. *et al.* Gremlin 1 Identifies a Skeletal Stem Cell with Bone, Cartilage, and Reticular Stromal Potential. *Cell* **160**, 269–284 (2015).

112. Zhou, B. O., Yue, R., Murphy, M. M., Peyer, J. G. & Morrison, S. J. Leptin-receptor-expressing mesenchymal stromal cells represent the main source of bone formed by adult bone marrow. *Cell Stem Cell* **15**, 154–168 (2014).

113. Martin, J. F. & Olson, E. N. Identification of a prx1 limb enhancer. *Genesis* **26**,

225–229 (2000).

114. Liu, Y. *et al.* Osterix-Cre Labeled Progenitor Cells Contribute to the Formation and Maintenance of the Bone Marrow Stroma. *PLoS One* **8**, (2013).

115. Mizoguchi, T. *et al.* Osterix marks distinct waves of primitive and definitive stromal progenitors during bone marrow development. *Dev. Cell* **29**, 340–349 (2014).

116. Zhou, X. *et al.* Multiple functions of Osterix are required for bone growth and homeostasis in postnatal mice. *Proc. Natl. Acad. Sci.* **107**, 12919–12924 (2010).

117. Yuan, X., Caron, A., Wu, H. & Gautron, L. Leptin receptor expression in mouse intracranial perivascular cells. *Front. Neuroanat.* **12**, 1–17 (2018).

118. Suzuki, S., Namiki, J., Shibata, S., Mastuzaki, Y. & Okano, H. The neural stem/progenitor cell marker nestin is expressed in proliferative endothelial cells, but not in mature vasculature. *J. Histochem. Cytochem.* **58**, 721–730 (2010).

119. Kunisaki, Y. *et al.* Arteriolar niches maintain haematopoietic stem cell quiescence. *Nature* **502**, 637–643 (2013).

120. Morikawa, S. *et al.* Prospective identification, isolation, and systemic transplantation of multipotent mesenchymal stem cells in murine bone marrow. *J. Exp. Med.* **206**, 2483–2496 (2009).

121. Chan, C. K. F. *et al.* Identification and Specification of the Mouse Skeletal Stem Cell. *Cell* **160**, 285–298 (2015).

122. Nusspaumer, G. *et al.* Ontogenic Identification and Analysis of Mesenchymal Stromal Cell Populations during Mouse Limb and Long Bone Development. *Stem Cell Reports* **9**, 1–15 (2017).

123. Debnath, S. *et al.* Discovery of a periosteal stem cell mediating intramembranous bone formation. *Nature* **562**, 133–139 (2018).

124. Duchamp de Lageneste, O. *et al.* Periosteum contains skeletal stem cells with high bone regenerative potential controlled by Periostin. *Nat. Commun.* **9**, 773 (2018).

125. Bradaschia-Correa, V. *et al.* Hox gene expression determines cell fate of adult periosteal stem/progenitor cells. *Sci. Rep.* **9**, 1–13 (2019).

126. Logan, M. *et al.* Expression of Cre Recombinase in the developing mouse limb bud driven by a Prxl enhancer. *Genesis* **33**, 77–80 (2002).

127. Ono, N., Ono, W., Nagasawa, T. & Kronenberg, H. M. A subset of chondrogenic cells provides early mesenchymal progenitors in growing bones. *Nat. Cell Biol.* **16**, 1157–1167 (2014).

128. Mizuhashi, K. *et al.* Resting zone of the growth plate houses a unique class of skeletal stem cells. *Nature* **563**, 254–258 (2018).

129. Shi, Y. *et al.* Gli1 identifies osteogenic progenitors for bone formation and fracture repair. *Nat. Commun.* **8**, 2043 (2017).

130. Kawanami, A., Matsushita, T., Chan, Y.Y., and Murakami, S. Mice expressing GFP and CreER in osteochondro progenito cells in the periosteum. *Biochem. Biophys. Res. Commun.* **4**, 477–482 (2009).

131. Siclari, V. A. *et al.* Mesenchymal progenitors residing close to the bone surface are functionally distinct from those in the central bone marrow. *Bone* **53**, 575–586 (2013).

132. Matsuda, T. & Cepko, C. L. Controlled expression of transgenes introduced by in vivo electroporation. *Proc. Natl. Acad. Sci. U. S. A.* **104**, 1027–1032 (2007).

133. Nelson, L. T., Rakshit, S., Sun, H. & Wellik, D. M. Generation and expression of a Hoxa11eGFP targeted allele in mice. *Dev. Dyn.* **237**, 3410–3416 (2008).

134. Jilka, R. L., Weinstein, R. S., Bellido, T., Parfitt, A. M. & Manolagas, S. C. Osteoblast Programmed Cell Death (Apoptosis): Modulation by Growth Factors

and Cytokines. *J. Bone Miner. Res.* **13**, 793–802 (1998).

135. Matic, I. *et al.* Quiescent bone lining cells are a major source of osteoblasts during adulthood. *Stem Cells* 2930–2942 (2016). doi:10.1634/stemcells.2007-0439

136. OWEN, M. CELL POPULATION KINETICS OF AN OSTEOGENIC TISSUE. I. *J. Cell Biol.* **19**, 19–32 (1963).

137. Ono, N. & Kronenberg, H. M. Mesenchymal Progenitor Cells for the Osteogenic Lineage. *Curr. Mol. Biol. Reports* 95–100 (2015). doi:10.1007/s40610-015-0017-z

138. Méndez-Ferrer, S., Scadden, D. T. & Sánchez-Aguilera, A. Bone marrow stem cells: current and emerging concepts. *Ann. N. Y. Acad. Sci.* **1335**, 32–44 (2015).

139. Chen, G., Deng, C. & Li, Y. TGF-β and BMP signaling in osteoblast differentiation and bone formation. *Int. J. Biol. Sci.* **8**, 272–88 (2012).

140. Lai, L. P. & Mitchell, J. Indian hedgehog: Its roles and regulation in endochondral bone development. *Journal of Cellular Biochemistry* (2005). doi:10.1002/jcb.20635

141. Yoon, B. S. & Lyons, K. M. Multiple functions of BMPs in chondrogenesis. *J. Cell. Biochem.* (2004). doi:10.1002/jcb.20211

142. Kronenberg, H. M. Developmental regulation of the growth plate. *Nature* **423**, 332–6 (2003).

143. DeFalco, J. *et al.* Virus-assisted mapping of neural inputs to a feeding center in the hypothalamus. *Science (80-.).* (2001). doi:10.1126/science.1056602

144. Madisen, L., Zwingman, T.A., Sunkin, S.M., Oh, S.W., Zariwala, H.A., Gu, H., Ng, L.L., Palmiter, R.D., Hawrylycz, M.J., Jones, A.R., Lein, E.S.& Zeng, H. A robust and high-throughout Cre reporting and characterization system for the whole mouse brain. *Nat. Neurosci.* **13**, 133–140 (2010).

145. Wu, Y. *et al.* Correction of a genetic disease in mouse via use of CRISPR-Cas9.

Cell Stem Cell (2013). doi:10.1016/j.stem.2013.10.016

146. Kawamoto, T. & Shimizu, M. A method for preparing 2-to 50-μm-thick fresh-frozen sections of large samples and undecalcified hard tissues. *Histochem. Cell Biol.* **113**, 331–339 (2000).

147. Pineault, K. M., Song, J. Y., Kozloff, K. M., Lucas, D. & Wellik, D. M. Hox11 expressing regional skeletal stem cells are progenitors for osteoblasts, chondrocytes and adipocytes throughout life. *Nat. Commun.* **10**, 1–15 (2019).

148. Leucht, P. *et al.* Embryonic origin and Hox status determine progenitor cell fate during adult bone regeneration. *Development* **135**, 2845–54 (2008).

149. Hernandez, C. J., Majeska, R. J. & Schaffler, M. B. Osteocyte density in woven bone. *Bone* **35**, 1095–1099 (2004).

150. van Oers, R. F. M., Wang, H. & Bacabac, R. G. Osteocyte Shape and Mechanical Loading. *Curr. Osteoporos. Rep.* **13**, 61–66 (2015).

151. Lattouf, R. *et al.* Picrosirius Red Staining: A Useful Tool to Appraise Collagen Networks in Normal and Pathological Tissues. *J. Histochem. Cytochem.* **62**, 751–758 (2014).

152. Junqueira, L. C. U., Bignolas, G. & Brentani, R. R. Picrosirius staining plus polarization miscroscopy, a specific method for collagen detection in tissue sections. *Histochem. J.* 447–455 (1979).

153. Dones, J. M. *et al.* Optimization of interstrand interactions enables burn detection with a collagen-mimetic peptide. *Org. Biomol. Chem.* **17**, (2019).

154. Ljusberg, J. *et al.* Proteolytic excision of a repressive loop domain in tartrate-resistant acid phosphatase by cathepsin K in osteoclasts. *J. Biol. Chem.* **280**, 28370–28381 (2005).

155. Lian, J. B. & Stein, G. S. *Osteoporosis: Chapter 6 Osteoblast Biology*. *Elsevier*

Inc. (Elsevier Inc., 2008). doi:10.1016/B978-0-12-370544-0.50008-2

156. Rutkovskiy, A., Stensløkken, K.-O. & Vaage, I. J. Osteoblast Differentiation at a Glance. *Med. Sci. Monit. Basic Res.* **22**, 95–106 (2016).

157. Pavalko, F. M. *et al.* A model for mechanotransduction in bone cells: The load-bearing mechanosomes. *J. Cell. Biochem.* **88**, 104–112 (2003).

158. Lindahl, A. *et al. Cartilage and Bone Regeneration*. *Tissue Engineering: Second Edition* (Elsevier Inc., 2014). doi:10.1016/B978-0-12-420145-3.00016-X

159. Reznikov, N., Shahar, R. & Weiner, S. Bone hierarchical structure in three dimensions. *Acta Biomater.* **10**, 3815–3826 (2014).

160. Gross, S., Krause, Y., Wuelling, M. & Vortkamp, A. Hoxa11 and hoxd11 regulate chondrocyte differentiation upstream of Runx2 and Shox2 in mice. *PLoS One* **7**, 1–10 (2012).

161. Zhao, W., Byrne, M. H., Wang, Y. & Krane, S. M. Osteocyte and osteoblast apoptosis and excessive bone deposition accompany failure of collagenase cleavage of collagen. *J. Clin. Invest.* **106**, 941–949 (2000).

162. Bachmanov, A. A., Reed, D. R., Beauchamp, G. K. & Tordoff, M. G. Food intake, water intake, and drinking spout side preference of 28 mouse strains. *Behav. Genet.* **32**, 435–443 (2002).

163. Mangiavini, L., Merceron, C. & Schipani, E. *Analysis of Mouse Growth Plate Development*. *Current protocols in mouse biology* **6**, (2016).

164. Jáuregui, E. J. *et al.* Parallel mechanisms suppress cochlear bone remodeling to protect hearing. *Bone* (2016). doi:10.1016/j.bone.2016.04.010

165. Dempster, D. W. *et al.* Histomorphometry Nomenclature: A 2012 Update of the Report of the ASBMR Histomorphometry Nomenclature David. *J. Bone Miner. Res.* **28**, 2–17 (2014).

166. Abramovich, C., Pineault, N., Ohta, H. & Humphries, R. K. Hox genes: From leukemia to hematopoietic stem cell expansion. *Ann. N. Y. Acad. Sci.* **1044**, 109–116 (2005).

167. Fischbach, N. A. *et al.* HOXB6 overexpression in murine bone marrow immortalizes a myelomonocytic precursor in vitro and causes hematopoietic stem cell expansion and acute myeloid leukemia in vivo. *Blood* (2005). doi:10.1182/blood-2004-04-1583

168. Argiropoulos, B. & Humphries, R. K. Hox genes in hematopoiesis and leukemogenesis. *Oncogene* **26**, 6766–6776 (2007).

169. Bhatlekar, S., Fields, J. Z. & Boman, B. M. Role of HOX genes in stem cell differentiation and cancer. *Stem Cells Int.* **2018**, (2018).

170. Li, B., Huang, Q. & Wei, G. H. The role of hox transcription factors in cancer predisposition and progression. *Cancers (Basel).* **11**, 1–25 (2019).

171. Nimni, M. E. & Harkness, R. D. Molecular structure and functions of collagen. *Collagen Vol. I Biochem.* **I**, 1–77 (2018).

172. Valerius, M. T., Patterson, L. T., Feng, Y. & Potter, S. S. Hoxa 11 is upstream of Integrin 8 expression in the developing kidney. *Proc. Natl. Acad. Sci.* **99**, 8090–8095 (2002).

173. Zimmerman, D., Jin, F., Leboy, P., Hardy, S. & Damsky, C. Impaired bone formation in transgenic mice resulting from altered integrin function in osteoblasts. *Dev. Biol.* **220**, 2–15 (2000).

174. Gronowicz, G. A. & Derome, M. E. Synthetic peptide containing Arg-Gly-Asp inhibits bone formation and resorption in a mineralizing organ culture system of fetal rat parietal bones. *J. Bone Miner. Res.* **9**, 193–201 (1994).

175. Bennett, J. H., Moffatt, S. & Horton, M. Cell adhesion molecules in human osteoblasts: Structure and function. *Histol. Histopathol.* **16**, 603–611 (2001).

176. Marie, P. J., Haÿ, E. & Saidak, Z. Integrin and cadherin signaling in bone: Role and potential therapeutic targets. *Trends Endocrinol. Metab.* **25**, 567–575 (2014).

177. Lv, H. *et al.* Mechanism of regulation of stem cell differentiation by matrix stiffness. *Stem Cell Res. Ther.* **6**, 1–11 (2015).

178. Sánchez-Herrero, E. Hox Targets and Cellular Functions. *Scientifica (Cairo).* **2013**, 1–26 (2013).

179. Agrawal, P., Habib, F., Yelagandula, R. & Shashidhara, L. S. Genome-level identification of targets of Hox protein Ultrabithorax in Drosophila: Novel mechanisms for target selection. *Sci. Rep.* **1**, 1–10 (2011).

180. Pearson, J. C., Lemons, D. & McGinnis, W. Modulating Hox gene functions during animal body patterning. *Nat. Rev. Genet.* **6**, 893–904 (2005).

181. Hueber, S. D. & Lohmann, I. Shaping segments: Hox gene function in the genomic age. *BioEssays* (2008). doi:10.1002/bies.20823

182. Fabre, P. J. *et al.* Heterogeneous combinatorial expression of Hoxd genes in single cells during limb development. *BMC Biol.* **16**, 1–15 (2018).

183. Rezsohazy, R., Saurin, a. J., Maurel-Zaffran, C. & Graba, Y. Cellular and molecular insights into Hox protein action. *Development* **142**, 1212–1227 (2015).

184. Pellerin, I., Schnabel, C., Catron, K. M. & Abate, C. Hox proteins have different affinities for a consensus DNA site that correlate with the positions of their genes on the hox cluster. *Mol. Cell. Biol.* **14**, 4532–4545 (1994).

185. Mann, R. S. & Affolter, M. Hox proteins meet more partners. *Curr. Opin. Genet. Dev.* **8**, 423–429 (1998).

186. Jacobs, Y., Schnabel, C. A. & Cleary, M. L. Trimeric Association of Hox and TALE Homeodomain Proteins Mediates Hoxb2 Hindbrain Enhancer Activity . *Mol. Cell. Biol.* **19**, 5134–5142 (1999).

187. Ryoo, H. D., Marty, T., Casares, F., Affolter, M. & Mann, R. S. Regulation of Hox target genes by a DNA bound homothorax/Hox/extradenticle complex. *Development* **126**, 5137–5148 (1999).

188. Shen, W.-F. *et al.* HOXA9 Forms Triple Complexes with PBX2 and MEIS1 in Myeloid Cells. *Mol. Cell. Biol.* **19**, 3051–3061 (1999).

189. Longobardi, E. *et al.* Biochemistry of the tale transcription factors PREP, MEIS, and PBX in vertebrates. *Dev. Dyn.* **243**, 59–75 (2014).

190. Chan, S. K., Jaffe, L., Capovilla, M., Botas, J. & Mann, R. S. The DNA binding specificity of ultrabithorax is modulated by cooperative interactions with extradenticle, another homeoprotein. *Cell* **78**, 603–615 (1994).

191. Chang, C. P. *et al.* Pbx proteins display hexapeptide-dependent cooperative DNA binding with a subset of Hox proteins. *Genes Dev.* **9**, 663–674 (1995).

192. van Dijk, M. A. & Murre, C. extradenticle Raises the DNA binding specificity of homeotic selector gene products. *Cell* **78**, 617–624 (1994).

193. Slattery, M. *et al.* Cofactor binding evokes latent differences in DNA binding specificity between hox proteins. *Cell* **147**, 1270–1282 (2011).

194. Martinez, M. G., Bullock, A. J., MacNeil, S. & Rehman, I. U. Characterisation of structural changes in collagen with Raman spectroscopy. *Appl. Spectrosc. Rev.* **54**, 509–542 (2019).

195. Byron, A. *et al.* Anti-integrin monoclonal antibodies. *J. Cell Sci.* **122**, 4009–4011 (2009).

196. Chung, N. *et al.* HOX gene analysis of endothelial cell differentiation in human bone marrow-derived mesenchymal stem cells. *Mol. Biol. Rep.* **36**, 227–235 (2009).